Aus dem Fachbereich Medizin
der Johann Wolfgang-Goethe-Universität
Frankfurt am Main

betreut am
Zentrum der Molekularen Medizin
Institut für Vaskuläre Signaltransduktion
Direktorin: Prof. Dr. Ingrid Fleming

The Role of Soluble Epoxide Hydrolase in Macrophage and Astrocyte Polarization

Thesis
zur Erlangung des Grades Doctor of Philosophy (PhD)
des Fachbereichs Medizin
der Johann Wolfgang-Goethe-Universität
Frankfurt am Main

vorgelegt von
Xiaoming Li

aus Guangzhou, China

Frankfurt am Main, 2023

Dekan:	Prof. Dr. Stefan Zeuzem
Referentin:	Prof. Dr. Ingrid Fleming
Korreferent/in:	Prof. Dr. Denisa Bojkova
	Prof. Dr. Nina Wettschureck
	Dr. Dmitry Namgaladze
Tag der mündlichen Prüfung:	May 6th, 2024

Table of contents

1. Introduction

1.1 Cytochrome P450 and sEH

Fatty acids are carboxylic acids with an aliphatic chain that can be either saturated or unsaturated [1]. Saturated fatty acids have no double bonds between carbon atoms while polyunsaturated fatty acids (PUFAs) do contain one or more double bonds [1]. PUFAs can be further characterized as ω-3 or ω-6 fatty acids. The ω-3 PUFAs have a double bond at carbon 3 while ω-6 have one at position 6. A typical ω-3 fatty acid is α-linolenic acid (18:3) from which docosahexaenoic acid (DHA, 22:6) and eicosatetraenoic acid (EPA, 20:5) are generated [1,2]. The ω-6 fatty acid includes arachidonic acid (AA, 20:4) and linoleic acid (LA, 18:2). PUFAs, exemplified by AA, LA, DHA and EPA have been implicated in pathophysiological conditions, such as cancer and cardiovascular diseases, particularly those that involve inflammatory processes [3–8]. The biological activities of these PUFAs are largely attributed to their biologically activate metabolites produced by three distinct enzyme systems: cyclooxygenases (COX), lipoxygenases (LOX) and cytochrome P450 (CYP) enzymes (ω-hydroxylases and epoxygenases), which generate an array of bioactive fatty acid mediators that exerts a broad range of physiological and pathological effects [9].

AA is a well-studied PUFA (for review see [10]). COX, which generate prostaglandins (PGs) and thromboxane (TX), were the first enzymes reported to metabolize AA [11]. Numerous studies have found that the COX and LOX derived AA metabolites are active players in inflammation and immune responses [9]. However, the enzymes of the CYP system, which are often referred as a third pathway in AA metabolism, is less well understood [9,12]. The ω-hydroxylase activity of CYP enzymes converts AA to hydroxyeicosatetraenoic acids (HETEs) (Figure 1) [13]. 11,12- epoxyeicosatrienoic acids (EET) is one of best-studied metabolites in this context and has been shown to possess pro-inflammatory effects in addition to the regulation of vascular tone [13].

In comparison, LA can be oxidized by CYP enzymes to its respective 9,10- or 12,13-epoxyoctadecenoic acid (EpOME), DHA to 19,-20-dihydroxydocosapentaeonic acid

(EDP), and eicosapentaenoic acid (EPA) to epoxyeicosatetraenoic acid (EEQ) [10] (Figure 2).

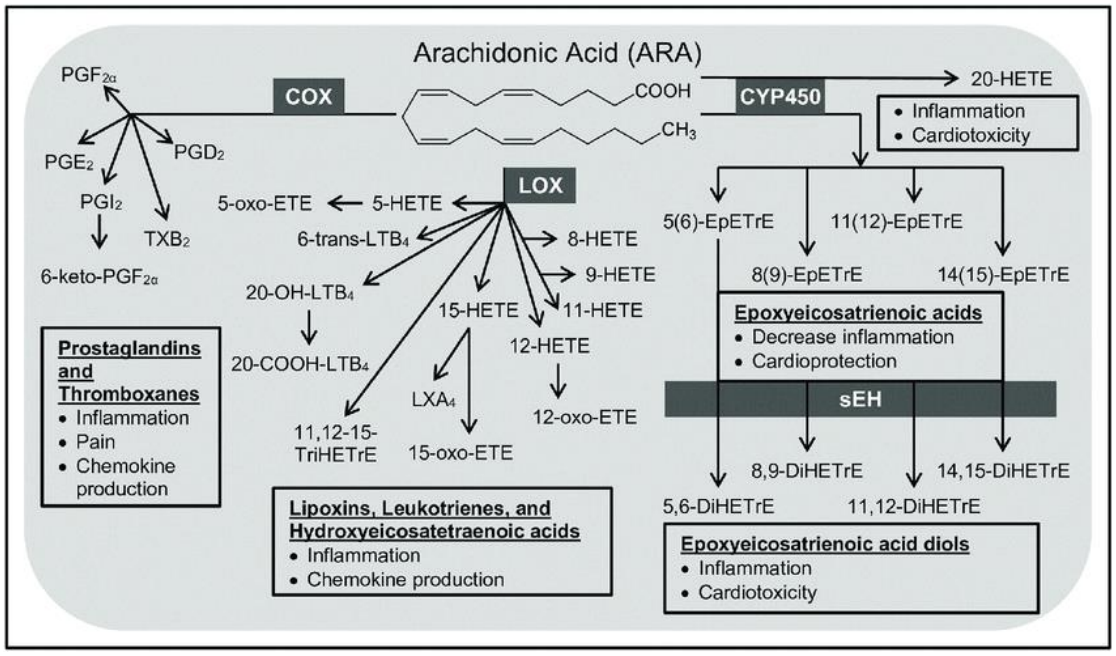

Figure 1. Metabolism of arachidonic acid (AA) via COX, LOX and CYP450 (modified from [14]). The metabolism of arachidonic acid (AA) involves various enzymatic pathways. Phospholipase A (PLA), phospholipase C (PLC), and phospholipase D (PLD) release AA from membrane-bound phospholipids by breaking specific covalent bonds [15]. COX enzymes (PGHSs) convert AA to protanoids, prostacyclin, and thromboxane, while LOX enzymes metabolize AA to leukotrienes and Hydroxyeicosatetraenoic acids (HETEs) [15]. Additionally, cytochrome P450 (CYP450) epoxygenases metabolize AA to midchain (HETE) and four different regioisomers of EETs [10]. Finally, soluble epoxide hydrolase (sEH) further metabolizes all EETs to less active dihydroxyeicosatrienoic acids (DHETs). The figure was taken from [15].

The epoxygenase activity of CYP enzymes, such as the CYP2J and 2C families, generates AA epoxides eg. EETs including 5,6-EET, 8,9-EET, 11,12-EET, and 14,15-EET [16–18]. EETs have various effects in different cell types and tissues. In vascular system EETs have anti-inflammatory, pro-angiogenic, and Ca^{2+} signaling properties in endothelial cells, and they are also able to trigger vasodilation and inhibit vascular smooth muscle cell migration [18–22]. In addition, EETs also have mitogenic effects in renal tubules and mesangial cells, result in bronchodilation, and have anti-adhesive effects on platelets [23–28]. The receptors for EETs have not yet been identified, making it

challenging to distinguish between primary and secondly events in the cellular actions initiated by EETs (for review see [15]) (Figure 2).

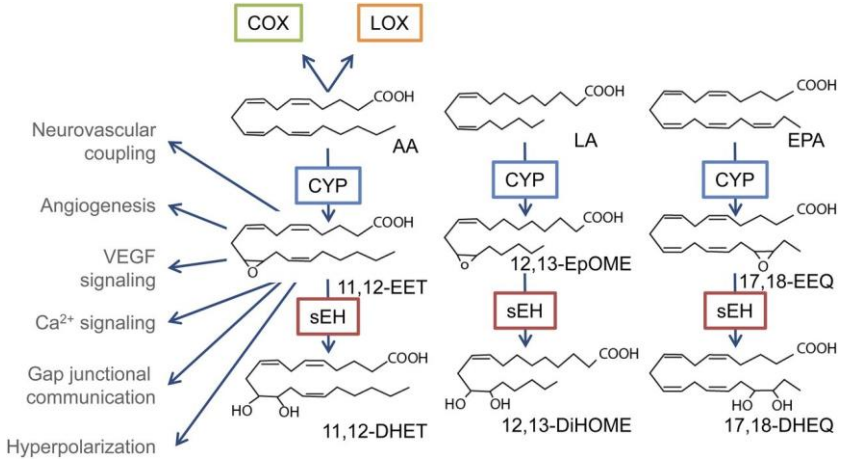

Figure 2. Cytochrome P450 (CYP) and soluble epoxide hydrolase (sEH)-mediated metabolism of polyunsaturated fatty acids. AA, LA and EPA are metabolized by three different enzyme systems namely COX, LOX and CYP. CYP metabolizes the lipids to their corresponding epoxide fatty acids. sEH further metabolizes the epoxide fatty acids to their corresponding diols.11,12-EET has been shown be associated with neurovascular coupling [29], angiogenesis [30], VEGF signaling [31], calcium signaling [32,33], gap junction communication [34] and hyperpolarization [35–37]. The figure is taken from [38]

The soluble epoxide hydrolase (sEH) is a bifunctional enzyme that is encoded by the Ephx2 gene and belongs to the epoxide hydrolase (EH) family, which also includes Ephx1, Ephx3, and Ephx4 [39,40]. This enzyme plays a crucial role in metabolizing primary substrates such as endogenous EETs, as well as other epoxides like EDPs, EpOMEs and EDQs (Figure 2). By adding a water chemical group, sEH converts these epoxides into their corresponding diols [39,40]. The sEH enzyme functions as a homodimer, with two distinct activities present in separate structural domains of each monomer [39,40]. The C-terminus contains epoxide hydrolase activity, while the N-terminus exhibits lipid-phosphate phosphatase activity [38,39]. Through its enzymatic conversion, sEH reduces the biological activity of EETs and other substrates, leading to alterations in their physiological effects.

Although sEH is primarily expressed in the liver, it is also found in various other tissues throughout the body [38, 41] . These include the vascular endothelium, leukocytes, red blood cells, smooth muscle cells, adipocytes, and the kidney proximal tubule (for review

see [38]). Notably, in the human brain, sEH exhibits a widespread distribution [41]. It is prominently expressed in neuronal cell bodies and is also present in astrocytes and oligodendrocytes, indicating its involvement in multiple cell types within the central nervous system [41].

1.2 Inflammation and resolution of inflammation

Inhibition or genetically deletion of sEH has been correlated with anti-inflammatory effects in many studies including liver injury, cancer, Alzheimer's diseases and renal fibrosis [52,53]. Increased levels of epoxides for example 11,12-EET by depletion or inhibition of sEH, which is able to activate peroxisome proliferator-activated receptors (PPAR)-γ or inactivate nuclear factor-κB (NF-κB) signaling has been proposed as one of the underline mechanisms [54,55]. Lipid mediators play critical roles in mediating chronic inflammation and resolution of inflammation mediated by monocytes and monocyte-derived macrophages [56]. The role of LOX and COX enzymes in mediating the inflammation and inflammatory resolution has been extensively investigated [57]. However, the role of CYP and sEH axis mediating epoxides and diols generation and their respective role in inflammatory resolution remains largely unclear.

Inflammation is a response to danger and usually initiates after an injury or infection [42,43]. The functions of inflammatory responses are to eliminate the infection or injury, thereby promoting tissue repair and healing, and subsequently establish immune memory and assist the host system to respond more rapidly and effectively to local and systemic stimulus for the future events [43]. The acute inflammatory response is a complex event coordinated with cellular, molecular and physiological processes [42,44]. It begins with the secretion of soluble mediators, such as complement, chemokines, cytokines and eicosanoids by resident macrophages, neutrophils, endothelial cells, fibroblasts and mast cells [43]. The resolution of inflammation is no longer considered to be a passive process, but rather linked to the clearance of inflammatory cells from the inflamed areas [43,45]. Initially, the focus is on eliminating the harmful factors that triggered the inflammatory response [45]. This involves halting the production of pro-inflammatory mediators and breaking down any remaining mediators to prevent further recruitment of immune cells and the formation of swelling [46]. Subsequently, immune cells, whether they are

polymorphonuclear cells, eosinophils, or lymphocytes responding to a recalled antigen, are removed from the tissues [47]. While some inflammatory cells can re-enter the bloodstream, many of the infiltrating polymorphonuclear cells, eosinophils, and lymphocytes undergo apoptosis or necrosis and are subsequently cleared by recruited macrophages derived from monocytes [46]. Multiple complexes signaling mechanisms and factors, including intercellular receptor interactions and bioactive lipids, regulate these processes and the delicate balance between them. Once the clearance of inflammatory cells is complete, macrophages can exit the inflammation site through lymphatic drainage [46]. However, there is also evidence suggesting that a small fraction of macrophages may undergo apoptosis [47].

Dysregulated inflammation occurs in many disease states [43]. Historically, therapies aimed to modulate the production of pro- or anti-inflammatory mediators have yielded mixed results [43]. However, the resolution of inflammation is a tightly regulated process that is essential for maintaining tissue homeostasis [46]. Failure to resolve inflammation triggers chronic inflammatory diseases, i.e. arthritis, colitis or asthma, resulting in irreversible tissue damage and an increased risk of cardiovascular disease and cancer [48]. Thus, insights into the signaling pathways associated with the inflammatory resolution have highlighted new opportunities for pharmacological interventions, which may represent a complementary (and perhaps even superior) therapeutic approach. In humans and animals, billions of cells die every day due to apoptosis or infection. In normal conditions, the clearance of apoptotic cells or pathogenic microorganisms by phagocytosis is generally enough to reduce tissue necrosis and eliminate the consequent release of cell contents that could induce inflammation, autoimmunity and disrupt tissue hemostasis[47]. This helps preserve tissue integrity.

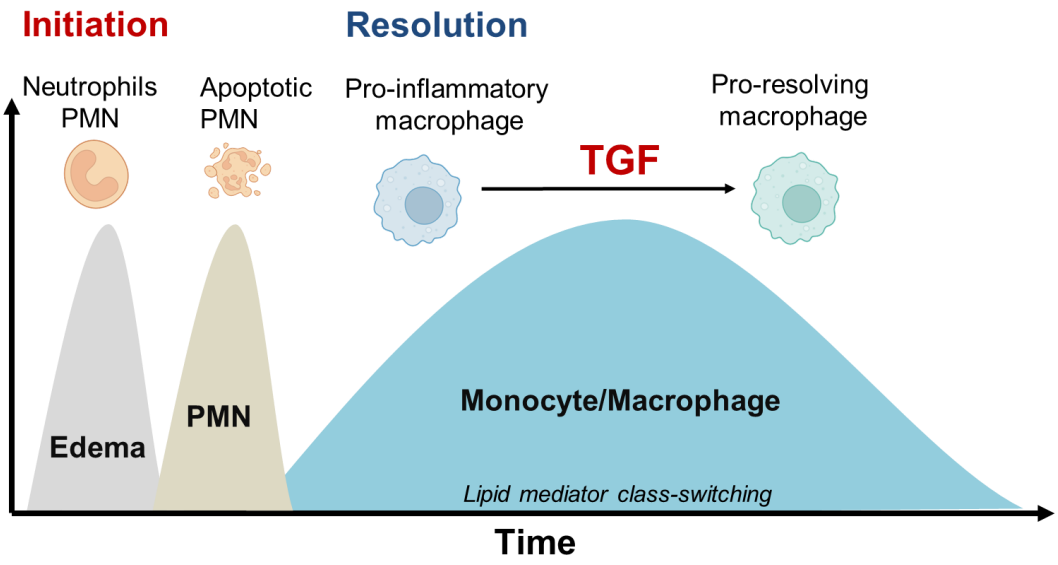

Figure 3. Overview of the events from onset of inflammation to resolution of inflammation, post-resolution and recovery with respect to time, figure was adapted from [43]. Inflammation is initiated by an irritant or vaccine, triggering resident cells to produce inflammatory mediators that initiate the inflammatory response. The resolution of inflammation involves the clearance of inflammatory stimuli, the apoptosis of polymorphonuclear cells (PMNs), and efferocytosis [47]. Post-resolution of inflammation is characterized by the influx of adaptive immune cells and the reconstitution of tissue-resident macrophages and dendritic cells. The role of resolution serves as a bridge between innate and adaptive immunity, encompassing a distinct phase known as post-resolution. The resolution of inflammation does not mark the end of the immune response but rather represents a crucial step that influences the development of adaptive immunity. Furthermore, chronic inflammation can contribute to the pathogenesis of certain diseases. Diseases characterized by "inflammation gone wrong" may result from incomplete resolution of the initial acute response, which fails to activate an appropriate adaptive immune response for complete resolution. The persistence of early-phase T helper 1-type cytokines, such as interferon (IFN), interleukin-6 (IL-6), polymorphonuclear cells (PMNs), and tumor necrosis factor (TNF), can impede antigen clearance and lead to the development of maladaptive immunity [for review see [43]. The figure is modified from [43]

1.3Macrophage heterogeneity

Macrophages are the key mediators for the inflammation and resolution of inflammation [50]. Macrophages have diverse functions that are critical for immune defense and tissue maintenance that play roles in inflammation, host defense, tissue homeostasis, and tissue regeneration (for review see [49,50]). Phagocytic macrophages are capable of initiating inflammatory resolution by releasing anti-inflammatory cytokines such as transforming

growth factor (TGF)-β and interleukin (IL)-10 which facilitate the clearance of apoptotic cells [49]. Studies of the role of TGF-β has revealed multiple mechanisms underlying the anti-inflammatory processes triggered by apoptosis [49]. The mechanisms include the release of anti-inflammatory molecules from apoptotic cells, activation of immediate anti-inflammatory signaling pathways through phagocyte receptors interacting with apoptotic cell surface molecules, activation of phagocyte nuclear receptors upon uptake, and stimulation of phagocytes to produce anti-inflammatory soluble mediators [60]. These soluble mediators may act through paracrine or autocrine mechanisms to amplify and sustain the anti-inflammatory state [50].

Macrophages are highly plastic and exhibit significant heterogeneity in their phenotypes and functions, reflecting their ability to adapt to different stimuli and microenvironments [49,50]. Macrophages can be classified into several subpopulations, including tissue-resident macrophages, monocyte-derived macrophages, and inflammatory macrophages with distinct gene expression profiles, indicating the diversity in function [51]. Tissue-resident macrophages, such as Kupffer cells in the liver, microglia in the brain, and alveolar macrophages in the lung, are derived from embryonic precursors and maintained independently of circulating monocytes [52,53]. In contrast, monocyte-derived macrophages are recruited to inflamed tissues, from the circulation s and are characterized by high plasticity and functional diversity [49,50]. Inflammatory macrophages, which are induced by microbial products, cytokines or danger signals, exhibit potent pro-inflammatory responses and are involved in host defense and tissue damage [49,50] .

Macrophages are classified into two broad activation states: classically activated (M1) macrophages and alternatively activated (M2) [54]. M1 macrophages are generally activated by pro-inflammatory stimuli such as interferon-gamma (IFN-γ) and lipopolysaccharide (LPS) induced by T-helper 1 (Th-1) cytokines [55,56]. They exhibit enhanced microbicidal activity, produce pro-inflammatory cytokines (e.g., interleukin-1 beta, tumor necrosis factor-alpha), and play a role in defense against pathogens [56]. M2 macrophages, on the other hand, are alternatively activated by anti-inflammatory cytokines, such as interleukin-4 (IL-4) and interleukin(IL)-13 [56]. They can be further

subdivided into more refined phenotypes: M2a, M2b, M2c, and M2d depending on the use of different stimuli such as interleukin IL-4 (M2a) [56], immune complexes and IL-R (M2b) [57], transforming growth factor (TGF)-β/IL-10 (M2c) [58] and toll-like receptor (TLR) agonist (M2d) [55]. However, the phenotypic characterization of macrophages is highly complicated and there are many more distinct genetic fingerprints and metabolic states than are reflected in a basic M0/M1/M2 classification [55].

1.4 TGF-β signaling

TGF-β has been recognized as the key mediator for the resolution of inflammation [58]. TGF-β stimulates macrophages to differentiate into an M2c phenotype and is considered as a macrophage “deactivation factor” as it reduces nitric oxide production and inducible oxide synthase expression [58]. Therefore, the generation of TGF-β by macrophages acts as a critical feedback loop that promotes inflammatory resolution [58]. Although the cellular and molecular mechanisms of M2c macrophages polarization is not totally understood, M2c polarization contributes significantly to the clearance of cellular debris and resolution of inflammation [59].

TGF-β signaling pathway is involved in a wide range of cellular processes in maintaining organism function and embryo development, as well as cellular homeostasis processes including cell differentiation, cell proliferation, cell migration, apoptosis and other cellular functions [58]. The canonical pathway of TGF-β is activated by homodimer TGF-β ligands binding to serine-threonine kinase receptors such as activin receptor-like kinase 1 or 5 (ALK1 or ALK5), which in turn activate the downstream signaling cascade mediated by small mothers against decapentaplegic protein (SMADs) family.

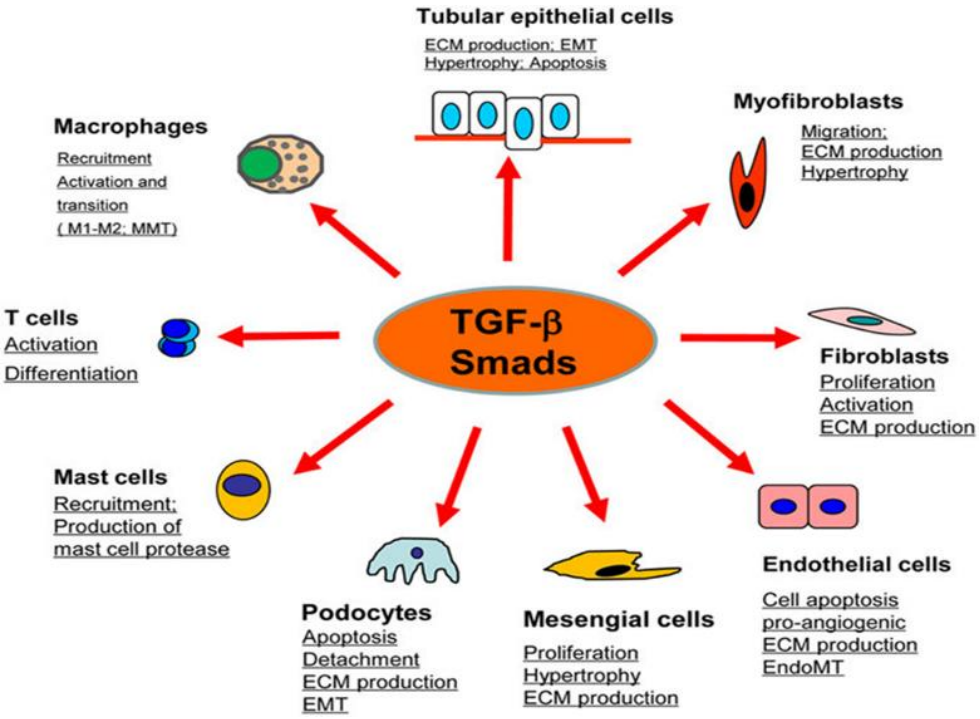

Figure 4. TGF-β in multiple cell function adapt from [59]. The involvement of TGF-β/Smad signaling in various cell functions. TGF-β/Smads play roles in tubular epithelial cells, including ECM production, EMT, hypertrophy, and apoptosis. Additionally, TGF-β/Smads regulate macrophage functions such as recruitment, activation, and transition. In T cells, TGF-β/Smads are involved in activation and differentiation. Mast cells are affected by TGF-β/Smads, leading to recruitment and production of mast cell protease. Podocytes exhibit TGF-β/Smad-mediated apoptosis, detachment, ECM production, and EMT. TGF-β/Smads influence mesangial cell proliferation, hypertrophy, and ECM production. Endothelial cells undergo cell apoptosis, pro-angiogenesis, ECM remodeling, and EndoMT under the control of TGF-β/Smads. Fibroblasts are influenced by TGF-β/Smads, resulting in proliferation, activation, and ECM production. Lastly, myofibroblasts demonstrate TGF-β/Smad-regulated migration, ECM production, and hypertrophy (for review see [59]). (ECM: extracellular matrix, EMT: endothelial mesenchymal transition). The picture is taken from [59]

1.4.1 Ligands, receptors and SMADs

The TGF-β superfamily, including TGF-βs, activin, nodal, and BMPs, activates a complex of type 1 and type 2 TGF-β receptors [11,60–62]. There are three isoforms of TGF-β (TGF-β1, TGF-β2, and TGF-β3) produced by different cell types. Type II receptors bind to TGF-β ligands and phosphorylate type I receptors [61,62]. Mammals have five type I receptors (ALK1, ALK2, ALK3, ALK4, and ALK5) and two type II receptors (TGFBR2 and

BMPR2) that bind to multiple type I receptors [11,60–62]. Ligand binding initiates signaling, with specific ligands binding to specific type II receptors. There are seven type I receptors and five type II receptors. Activin binds to ACVR2B or ACVR1B/ACVR1C, while BMPs bind to BMPR2. TGF-β receptor III (TβRIII) and endoglin act as co-receptors, enhancing ligand-receptor interactions [61,62]. SMAD proteins (R-SMADs, Co-SMAD, and I-SMADs) transduce signals, regulating gene expression and cellular processes [61,62]. Dysregulation of SMAD signaling is associated with diseases like cancer, fibrosis, and cardiovascular diseases for review see [59].

Molecular category	TGFβ pathway*	Activin/inhibin/Nodal pathway*	BMP pathway*
Ligands	TGFβ1, TGFβ2, TGFβ3	Activin A, activin B, inhibin A, inhibin B, Nodal	BMP2, BMP4, BMP5, BMP6, BMP7, BMP8A, BMP8B, BMP9, BMP10
Type I receptors	TβRI (ALK5), ALK1 (ACVRL1 or SKR3)	ALK4 (ACVR1B or ACTRIB), ALK7 (ACVR1C or ACTRIC)	ALK1 (ACVRL1, SKR3), ALK2 (ACVR1, ACTRI), ALK3 (BMPR1A), ALK6 (BMPR1B)
Type II receptors	TβRII	ACTRIIA, ACTRIIB	BMPR2, ACTRIIA, ACTRIIB
Type III receptors	TβRIII (betaglycan), endoglin, CRIPTO3 (TDGF1P3)	CRIPTO1 (TDGF1), CRIPTO3 (TDGF1P3), TβRIII (betaglycan)	RGMA, RGMB (DRAGON), RGMC (HJV or HFE2), endoglin
R-SMADs	SMAD2, SMAD3	SMAD2, SMAD3	SMAD1, SMAD5, SMAD8
Co-SMAD	SMAD4	SMAD4	SMAD4
I-SMADs	SMAD7	SMAD7	SMAD6, SMAD7

*Alternative protein names are listed in brackets. ACTR, activin receptor; ALK, activin receptor-like kinase; BMP, bone morphogenetic protein; BMPR, BMP receptor; RGM, repulsive guidance molecule; TβR, TGFβ receptor; TDGF, teratocarcinoma-derived growth factor.

Figure 5. TGF-β signal superfamily ligands (TGF-βs, Activin/inhibin/Nodal and BMPs), receptors (Type I, Type II and Type III), SMADs (R-SMADs, Co-SMAD, I-SMADs) [11,60–62]. The major pathways of the TGF-β superfamily signaling include the TGF-β pathway, activin/inhibin/nodal pathway, and BMP pathway. The respective ligands for these pathways include TGF-β1 to TGF-β, activin A and B, inhibin A and B, and BMP2 to BMP10 from the BMP pathway family. The type I receptors involved are ALK1, ALK2, ALK3, ALK4, ALK5, ALK6, and ALK7. The type II receptors include TβRII, ACTRIIA, ACTRIIB, BMPR2, ACTRIIA, and ACTRIIB [63]. The type III receptors are beta-glycan, endoglin, and CRIPTO3[64] . The regulatory SMADs (R-SMADs) consist of SMAD1, SMAD2, SMAD3, SMAD5, and SMAD8. The co-SMAD is SMAD4. The inhibitory SMADs (I-SMADs) are SMAD6 and SMAD7 [61,62]. The figure is taken from [61,62]

1.4.2 Transcriptional regulation of TGF-β

SMAD2 and SMAD3 are transcription factors that play critical roles in the TGF-β signaling pathway [61,62]. Upon activation of the TGF-β receptor complex, SMAD2 and SMAD3 are phosphorylated and form complexes with SMAD4, which then translocate to the nucleus to regulate gene expression [60,62]. SMAD2/3 regulate gene expression by binding to specific DNA sequences known as SMAD binding elements (SBEs) located in the promoter regions of target genes [65,66]. These SBEs typically contain a conserved sequence motif that allows SMAD2/3 to bind with high affinity [65,66]. SMAD2/3 binding to SBEs can lead to both activation and repression of target genes, depending on the presence of co-factors and co-regulators[67–69]. SMAD2/3 complexes can interact with co-activators, such as p300/CBP and MED1, to activate gene transcription [67–69]. Conversely, SMAD2/3 can also interact with co-repressors, such as TGIF and SKI, to repress gene transcription [69,70]. Another pathway is via ALK/pSMAD1/5, which in turn to activate the target gene for SMAD1/5 such as ID3.

In addition to their direct regulation of gene expression, SMAD2/3 also interact with other transcription factors and co-regulators to modulate gene expression [71,72]. For example, SMAD2/3 can interact with the ETS-family transcription factor PU.1 to regulate the expression of genes involved in immune functions [71,72]. SMAD2/3 can also interact with the transcriptional co-activator YAP1 to regulate the expression of genes involved in cell proliferation and differentiation [71,72].

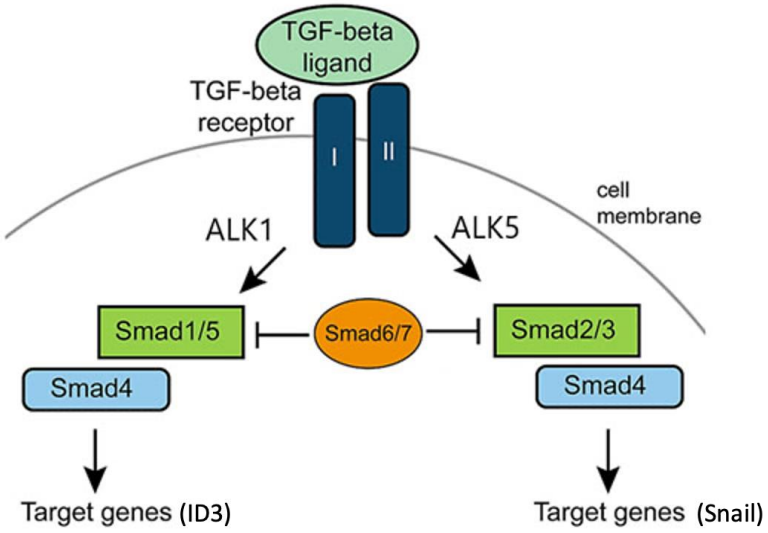

Figure 6. Transcriptional regulation of TGF-related target gene expression. The TGF-β ligand, such as TGF-β1, binds to the TGF-β receptor 2 and induces the phosphorylation of TGF-β receptor 1 (ALK5 or ALK1). This phosphorylation, in turn, triggers the phosphorylation of Smad2/3 or Smad1/5. Consequently, the target gene of SMAD2/3, Snail, or the SMAD1/5 target gene, ID3, is activated. The figure was generated via from Biorender (https://www.biorender.com/).

1.5 Alzheimer's diseases and astrocyte polarization

1.5.1 Astrocyte polarization

Astrocytes are the most abundant cells in the brain and play essential roles in maintaining the brain's overall health and function [73]. In the context of Alzheimer's disease, astrocytes have been implicated in both protective and detrimental processes [74]. One aspect of the relationship between Alzheimer's disease and astrocytes involves their role in regulating the clearance of beta-amyloid (Aβ) plaques [74], helping to remove these toxic protein aggregates from the brain [75]. However, in Alzheimer's disease, this clearance mechanism can become overwhelmed or impaired, leading to the accumulation of Aβ plaques [76]. Additionally, astrocytes are involved in modulating the inflammatory response in the brain [77]. In Alzheimer's disease, the chronic activation of inflammatory processes contributes to neuroinflammation, which can further exacerbate neuronal

damage [78]. Astrocytes can release inflammatory mediators and cytokines in response to the presence of Aβ and neuroinflammatory signals, potentially contributing to the progression of the disease [78]. Furthermore, astrocytes provide support to neurons by maintaining the brain's energy metabolism, regulating neurotransmitter balance, and promoting synapse formation and function [78,79]. In Alzheimer's disease, astrocyte dysfunction can disrupt these supportive functions, compromising neuronal health and contributing to cognitive impairment [78].

Similar to macrophages, astrocytes also undergo polarization/differentiation in response to physiological and pathological stimuli [73]. Under certain conditions, such as lipopolysaccharide (LPS) or disease states, microglia become activated and secrete pro-inflammatory cytokines, including interleukin 1α (IL-1α), tumor necrosis factor (TNFα), and complement component (C1q), which can reprogram a non-reactive A0 astrocyte into a toxic A1 astrocyte, contributing to neurodegeneration, neurotoxicity, and synaptic impairments [80]. The reverse transition from A1 astrocytes to A0 astrocytes is regulated by signaling pathways involving TGF-β and Fibroblast Growth Factor (FGF) [80]. Additionally, the transition from A0 astrocytes to A2 astrocytes occurs under the conditions of ischemia or hypoxia and is associated with neuroprotection and neural repair [80,81]. Liddelow et al. demonstrated that A1 astrocytes can exacerbate disease pathogenesis by killing both neurons and oligodendrocytes and losing the ability to promote neural outgrowth, synaptogenesis, and phagocytosis [80,82,83]. Conversely, A2 astrocytes appear to upregulate neurotrophic genes that promote neuronal survival [80]. Moreover, A1 astrocytes are enriched in multiple neurodegenerative diseases, such as Alzheimer's, Parkinson's, and Huntington's diseases [80].

sEH has been shown to be highly expressed in astrocytes and is involved in the process of Alzheimer's disease (AD) [84]. The survival of astrocytes in retinopathy is promoted by sEH [85]. However, the role of sEH in astrocyte polarization is still unknown. Inhibition of sEH can promote the expression of anti-inflammatory and neurotrophic factors, such as IL-10 and brain-derived neurotrophic factor (BDNF), in astrocytes [86]. It can also suppress the expression of pro-inflammatory cytokines, including tumor necrosis factor-alpha (TNF-α) and IL-1β [86]. Furthermore, sEH inhibition can also protect astrocytes

from apoptosis induced by oxidative stress, such as hyperoxia [85]. In a mouse model of retinopathy of prematurity, a condition characterized by abnormal blood vessel growth and neuronal damage in the retina, sEH deletion or inhibition can prevent the loss of astrocytes [85]. By preventing the dissociation of presenilin-1 and presenilin-1–associated protein, which are involved in mitochondrial calcium homeostasis, sEH inhibition can preserve the mitochondrial function and integrity of astrocytes [85]. Therefore, sEH plays a crucial role in regulating astrocyte polarization and survival, and sEH inhibition may serve as a potential therapeutic strategy for neurodegenerative diseases.

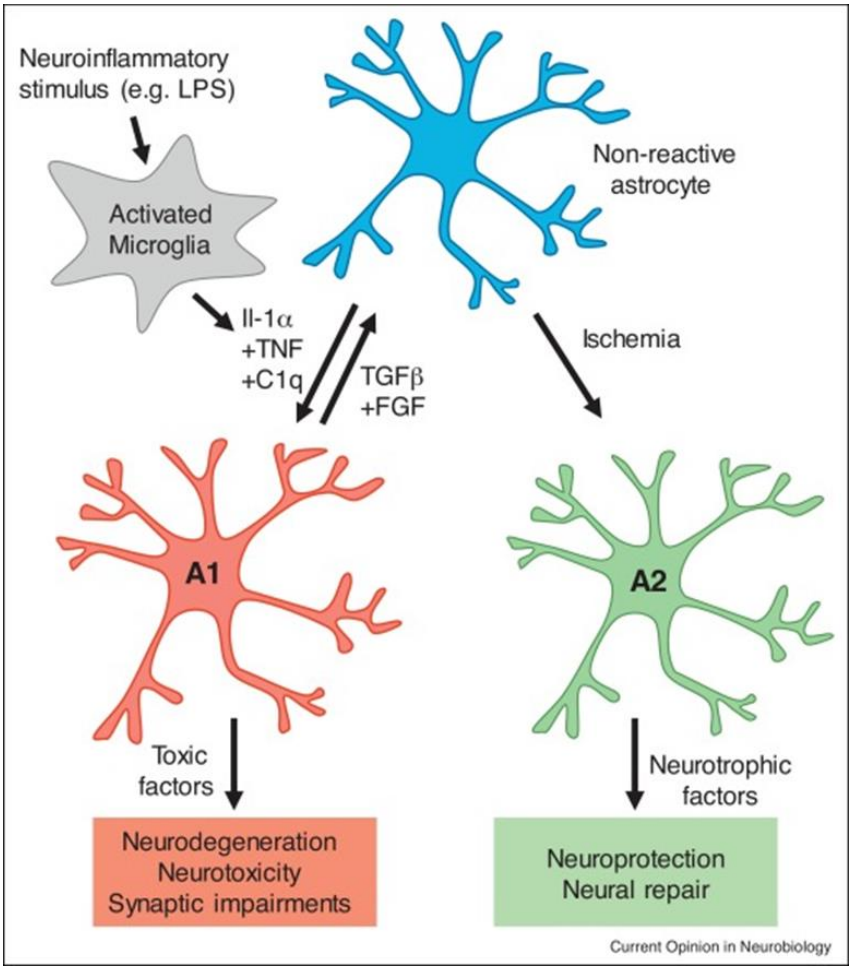

Figure 7. Astrocytes heterogeneity adapted from [87]. Astrocytes can be classified into three states, including non-reactive A0, reactive A1, and protective A2 astrocytes [80]. Non-activated microglia were activated under neuroinflammatory stimulus (e.g., LPS). The activated microglia secreted interleukin 1α (Il-1α), tumor necrosis factor (TNF) and complement component (C1q) to induce the transformation of non-reactive astrocyte (A0) to toxic A1 astrocyte (A1) and exert neurodegeneration, neurotoxicity and synaptic impairments [80]. A2 astrocyte was activated under ischemia condition to exert the neural repair function [81]. The picture is taken from [87].

1.5.2 Alzheimer's diseases

Mounting evidence suggests a role of sEH in neurodegenerative diseases[84,88]. It has been implicated that sEH is a novel target for treatment of AD, genetic deletion of sEH delays the onset of Alzheimer's diseases-like memory impairments in mice [88]. The inhibitor of sEH has been shown to reduce the neuroinflammation in a mouse model of

AD [84]. The epoxy lipids produced from AA have anti-inflammatory properties and exert the anti-inflammatory effects in the mouse model of AD [84].

AD is a progressive and irreversible neurodegenerative disease that affects the function of the brain, memory, and behaviors [89,90]. It is the most common cause of dementia, accounting for up to 70%, and mainly affects older adults [90]. AD is characterized by the accumulation of abnormal protein deposits in the brain, including amyloid plaques and neurofibrillary tangles, which cause brain cells to break down and stop communicating with each other [89,90]. APP/PS1 are double transgenic mice expressing a chimeric mouse/human amyloid precursor protein (Mo/HuAPP695swe) and a mutant human presenilin 1 (PS1-dE9), both directed to CNS neurons [91,92]. Both mutations are associated with early-onset AD [91,92]. These mice are useful in studying neurological disorders of the brain, specifically AD, amyloid plaque formation and aging [91,92]. The APP/PS1 mouse model is a transgenic mouse model that overproduces amyloid-beta (Aβ) and is often used to study the mechanisms of neuropathology of AD and the therapeutic effects of drugs on AD [93]. The model is characterized by developing neuropathological as well as AD-like behavioral alterations [93]. Aβ is a peptide that is produced when the amyloid precursor protein (APP) is cleaved by enzymes called β-secretase and γ-secretase [91,92]. Aβ peptides are classified based on their length, with Aβ42 and Aβ40 being the most common subtypes [94]. Aβ42 is more prone to aggregation than Aβ40 and is considered more toxic [94]. It is also the primary component of amyloid plaques in Alzheimer’s disease [90].

2. Aim of the study

Therefore, the aims of this study are:

- To investigate the role of sEH in macrophage polarization.
- To investigate the role of sEH in the resolution of inflammation.
- To identify the sEH-related bioactive lipid mediators in the resolution of inflammation.
- To investigate the role of sEH and TGF-β signaling in astrocyte heterogeneity.

3. Material and Methods

3.1 Materials.

Roswell Park Memorial Institute (RPMI) 1640 cell culture medium (Cat. # 2242222), Minimum Essential Medium (MEM,Cat. # 2209288), MEM Non-Essential Amino Acids Solution (Cat. # 11140050), MEM Vitamin Solution (Cat. # 11120052), Fetal bovine serum (FBS,Cat. #10270-106) were purchased from Gibco (Invitrogen; Darmstadt, Germany). 11, 12-EET (Cat. #50511),11, 12-DHET (Cat. # 51511), 9, 10-EpOME (Cat. # 52400), 9,10-DiHOME (Cat. #53400) and all other epoxide and diol standards for liquid chromatography–tandem mass spectrometry were obtained from Cayman Chemical (Tallinn, Estonia). Macrophage colony-stimulating factor (M-CSF, Cat. # 315-02), granulocyte macrophage colony-stimulating factor (GM-CSF, Cat.# 315-03), hIFN-γ (Cat. #300-02), murine IFNγ (Cat. #315-05), murine IL-4 (Cat. #214-14), human IL-4 (Cat. #200-04), human TGF-β1 (Cat. #100-21) were from peprotech (Hamburg, Germany). pHrodo™ Red Zymosan Bioparticles (Cat. #P35364) was from Invitrogen (Darmstadt, Germany), DiI-oxLDL (Cat. #L34358) was from Invitrogen (Darmstadt, Germany). The sEH inhibitor trans-4-[4-(3-adamantan-1-ylureido) cyclohexyloxy]-benzoic acid (t-AUCB) was kindly provided by Bruce D. Hammock (UC Davis, Davis, California, USA). All other chemicals (unless otherwise specified) were from Merck (Darmstadt, Germany).

Animals. C57BL/6 mice (6-8 weeks old) were purchased from Charles River (Sulzfeld, Germany). Floxed sEH mice ($Ephx2^{tm1.1Arte}$) were generated in the C57BL/6N background by TaconicArtemis GmbH (Cologne, Germany) as described (15), and crossed with Gt(ROSA)26Sortm16(Cre)Arte mice (TaconicArtemis) expressing Cre under the control of the endogenous Gt(ROSA)26Sor promoter to generate mice globally lacking sEH ($sEH^{-/-}$). All animals were housed in conditions that conform to the Guide for the Care and Use of Laboratory Animals published by the U.S. National Institutes of Health (NIH publication no. 85-23). Age- and strain-matched animals (littermates) of both genders were used throughout. Experiments involving mice were approved by and followed the guidelines of the Hessian animal care and use committee (FU2009, 2021).

3.2 Zymosan-induced peritonitis and fluorescence-activated cell sorting (FACS).

To induce a self-resolving inflammation, zymosan-A (10 mg/kg in 200 µL PBS, Intraperitoneal injection) was injected in female and male wild-type and $sEH^{-/-}$ mice (8 to 12 weeks old). One, 3, and 6 days after zymosan injection, chemokines and cells in the peritoneum were isolated via lavage using 3 mL ice-cold PBS, as described. For determination of the composition of immune cells in the lavage, cells were stained with different antibodies and analyzed using flow cytometry (BD, LSRFortessa). Data were analyzed using FlowJo Software (version 10.6.2). Gating strategies was shown in Figure 8.

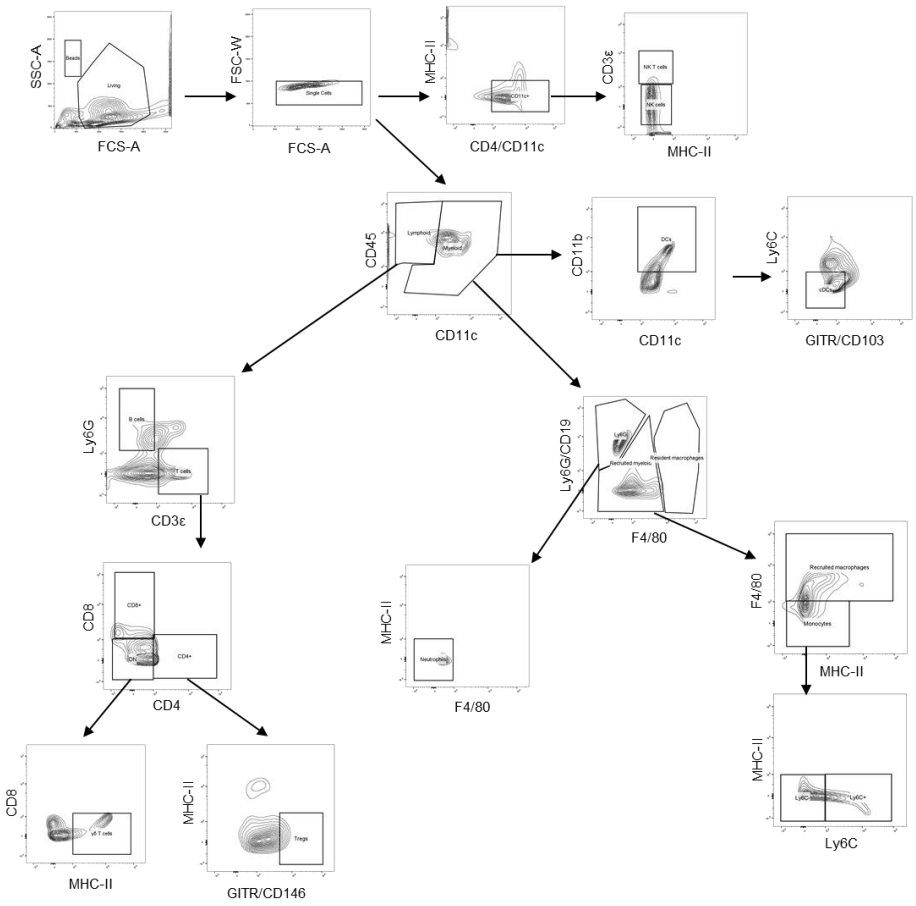

Figure 8. Gating strategy of intraperitoneal cell population's identification (Example from day 1). Peritoneal lavage obtained from the wild-type and sEH-/- was evaluated by flow cytometry. The analysis to evaluate immune populations was performed using the indicated gating strategy. Leucocyte categories were defined as the following subtypes: Neutrophils (CD11b+ Ly6G+), monocytes (CD11b+ F4/80low Ly6G- Ly6C+/-), macrophages (CD11b+ F4/80+Ly6G-), NK Cells (CD11c+ CD3ε+), NK T cells (CD11c+ CD3ε), dendritic cells (CD11c+ CD11b+), C dendritic cells (CD11c+ CD11b+ Ly6C-), T cells (CD11b-, CD3ε+), B cells (Ly6G+CD11b- CD3ε-).

3.3 Monocyte isolation and culture

Human monocytes were isolated from peripheral blood from healthy donors (DRK-Blutspendedienst Baden-Württemberg-Hessen, Frankfurt) as described before [95] and further differentiated to naïve (M0) macrophages in RPMI supplement with 3% human plasma for 7 days. Macrophages were polarized to M1 macrophages (100 ng/ml LPS and 20 ng/ml hIFNγ,12 hours), M2a macrophages (20 ng/ml IL-4, 24 hours) and M2c

macrophages from M1 macrophages by TGF-β1 (10 ng/ml) for 48 hours. Cultures were kept in a humidified incubator at 37°C containing 5% CO_2.

Murine monocytes were isolated from bone marrow of 8–10-week-old mice. Monocytes were differentiated to naïve (M0) macrophages in RPMI 1640 medium containing 8% heat inactivated FCS supplemented with M-CSF (15 ng/ml) and GM-CSF (15 ng/ml) for 7 days. Thereafter M0 macrophages were polarized to M1 macrophages (10 ng/ml LPS and 1 ng/ml IFNγ, 12 hours), M2a macrophages (20 ng/ml IL-4, 24 hours) and M2c macrophages from M1 macrophages by TGF-β1 (10 ng/ml) for 48 hours. Cultures were kept in a humidified incubator at 37°C containing 5% CO_2.

Cell culture. HEK-293 cells were obtained from the American Type Culture Collection (LGC Standards, Wesel, Germany) and cultured in MEM containing 8% heat inactivated FCS, gentamycin (Cat. 15710064, 25 µg/mL), non-essential amino acids (Cat. 11140068, MEM NEAA) and sodium pyruvate (Cat. #11360070) were obtained from Thermo Fisher Scientific (Schwerte, Germany). Cultures were kept in a humidified incubator at 37°C containing 5% CO_2. Experiments were performed in a total of 4-6 independent cell passages.

3.4 Immunoblotting.

Cells or tissue were lysed in RIPA lysis buffer (50 mM Tris/HCL pH 7.5, 150 mM NaCl, 10 mM NaPPi, 20 mM NaF, 1% sodium deoxycholate,1% Triton and 0.1% SDS) enriched with protease and phosphatase inhibitors and detergent-soluble proteins were resuspended in SDS-PAGE sample buffer. Samples were separated by SDS-PAGE and subjected to Western blotting as described [96]. Membranes were blocked in 3% BSA in TBST or ROTI-Block (Cat. # No. A151.1, ROTH), incubated with primary antibodies in the blocking solution and horseradish peroxidase-conjugated secondary antibodies in TBST, and detection was performed with a Lumi-Light plus western blotting substrate (Roche, Mannheim, Germany). Antibodies against sEH (1:2000, s4737-2, specifically designed by ProteinTech, Planegg-Martinsried, Germany), p-SMAD2 (Ser465/467, 1:1000, CST, CST, Massachusetts, USA), SMAD2 (1:1000, 5339 P, CST, Massachusetts, USA), p-SMAD1/5 (1:1000, 9516, CST, Massachusetts, USA), SMAD1 (1:1000, 6944, CST CST,

Massachusetts, USA), ALK5 (1:500, ab31013, abcam), ALK1 (1:500, AP01172-PU-N, Acris), TGFRII (1:1000, ab 186838, abcam), TLR2 (1:1000, ab16894, abcam), MRC1 (1:1000, NBP1-90020, Novus), NLRP3 (1:1000, NBP2-12446SS, Novus), PPAR-γ (1:1000, sc-7196, Santa Cruz), β-actin (1:3000, MAK6019, Linaris) were used in this study. The secondary antibodies were used: a goat anti-mouse IgG, H and L chain specific peroxidase conjugate, goat anti-rabbit IgG H and L chain specific peroxidase conjugate (both 1:20,000; Cat. # 401393, Cat. # 401253, Merck).

3.5 RNA isolation and real time quantitative PCR (RT-qPCR)

Total RNA was extracted from cells and tissues using QIAgen RNeasy kits (Invitrogen, Carlsbad, CA, USA) according to the manufacturer's protocol and RNA (1 µg) was used for reverse transcription (RTase SuperScript IV, Invitrogen). Primers (BioSpring GmbH, Germany) were designed using an online tool, primer3 (https://primer3.ut.ee), and the cDNA was amplified using SensiFAST SYBR No-ROX kit (GENTAUR GmbH, Aachen, Germany) and a real-time thermal cycler (BMS, Queensland, Australia). All RNAs were normalized to 18s rRNA.

Table 1. PCR primers used in the thesis

Gene	Forward	Reverse
18S	ctttggtcgctcgctcctc	ctgaccgggttggttttgat
Nos2	gtggtgacaagcacatttgg	gttcgtccccttctcctgtt
Tnfa	ggccttcctaccttcagacc	ccggccttccaaataaatac
Il1b	caggcaggcagtatcactca	agctcatatgggtccgacag
Arg1	gtgaagaacccacggtctgt	ctggttgtcaggggagtgtt
Ym-1	ctggaattggtgcccctacaa	tcataaccaacccactcattacc
Fizz	cccttctcatctgcatctcc	cagtagcagtcatcccagca
Mrc1	tggatggatgggagcaaagt	gctgctgttatgtctctggc
Vctn1	aaagacgacctctcacagca	catactgaaggctccggtct
Snai1	tggctgatggagtgcctttgta	agccagtgggttggctttagtt
Id3	cctgcagcgtgtcatagactacat	agatcacaagttccggagtgag
Tlr2	ccctgtgccaccatttcc	ccacgcccacatcattctc
Mertk	tcggaatgagattggctggt	tcccacacgtgagatatccg
Cd36	gttgatactatgcccgcctct	gtttcccacactcctttctcc
Dectin	tctcagccttgccttcctaa	catggcccttcactctgatt
Tlr4	cagcaaagtccctgatgaca	agaggtggtgtaagccatgc
Ephx2	acgaccgtgctgagagagat	ttcagattagccccgatgtc
Pparg	acaagagctgacccaatggt	tgaggcctgttgtagagctg
Nlrp3	aaggcttgtgtgggaccaaa	aggaggggcaggagtaagag
Alk5	accttctgatccatcggttg	ttcctgttggctgagttgtg
Cxcr4	atggaaccgatcagtgtgagt	tagatggtgggcaggaagatc
Ptgs2	gctgtacaagcagtggcaaa	ccccaaagatagcatctgga
Ptx3	cctgctttgtgctctctggt	tctccagcatgatgaacagc

3.6 RNA sequencing

Total RNA was isolated from macrophages using the RNeasy Micro kit (Qiagen, Hilden, Germany) according to the manufacturer's instructions. The concentration of RNA was determined using the NanoDrop ND-1000 (TFS, USA; 600 nm). Total RNA (1 µg) was used as input for the SMARTer Stranded Total RNA Sample Prep Kit - HI Mammalian (Takara Bio, Kyoto, Japan). Trimmomatic version 0.39 was used to trim the reads after mass reduction. In a window of 20 nucleotides, Trimmomatic version 0.39 was used to trim reads when the mass dropped below the mean of Q20 and only filtered reads longer than 15 nucleotides were retained.

The filtered reads were longer than 15 nucleotides. Reads were compared to Ensembl mouse genome version mm10 (Ensembl version 101) using STAR 2.7.10a. The compared reads were filtered with Picard 2.25.5 (Picard A) to remove duplicates. A set of tools for processing next-generation sequencing data in BAM format (Java)), multi-graph, ribosomal or mitochondrial reads. Gene counts were built using feature Counts 2.0.2 to exclude those multiple genes that overlap by aggregating reads for overlapping exons on the correct strand. The raw count matrix was normalized using DESeq2 version 1.30.1. Based on the raw count matrix, comparisons were established using DESeq2. Genes were classified as significantly differentially expressed at mean counts >5, multiple test adjusted P values <0.05, and log2FC >0.585 or <-0.585. Ensemble annotations were enriched with UniProt data.

Heatmap, volcano plot, pathway and KEGG analysis were generated with an online tools SRPLOT (http://www.bioinformatics.com.cn/en). String analysis was generated with an online tool (https://cn.string-db.org/).

3.7 Phagocytosis assay

Zymosan. Murine macrophages were incubated with 10 µg/ml pHrodo Red Zymosan Bioparticles Conjugate (Thermo Fisher Scientific, Schwerte, Germany) in RPMI basal medium supplemented with 0.1% BSA at 37°C and 5% CO2 for 20 minutes. After 30 minutes, the cells were washed to remove non-phagocytosed material. Automated

microscopy (Incucyte, Sartorius, Göttingen, Germany) was used to track and monitor phagocytosis.

Oxidized LDL. Murine macrophages were incubated with 2.5 µg/ml oxo-LDL in RPMI medium supplement with 0.1% BSA for 20 minutes (37°C, 5% CO_2). Cells were washed 3 times with cold PBS and fixed in 4% PFA for 15 min and oxo-LDL uptake was visualized in microscope.

3.8 Luciferase activity assay.

HEK cells were seeded at a density of 5x104 cells/well in 24-well plates (Falcon). After 24 hours, the cells were transfected with 200 ng of each human sEH promoter plasmid (-374/+28, -974/+28, -1474/+28, -2974/+28, -4174/+28, -4774/+28, -5974/+28 bp) using Lipofectamine 2000, according to the manufacturer's instructions. A control plasmid, pRL-CMV, expressing renilla luciferase (4 ng) was included as an internal control for each transfection. After 24 hours, the cells were treated with either solvent or 10 ng/ml TGF-β1 for an additional 24 hours. The cells were then lysed using 100 µl of Triton Lysis Buffer (TLB: 100 mM potassium phosphate, pH 7.8; containing 0.2% Triton X-100), and luciferase activities were measured using the Dual-Glo Luciferase Reporter assay (Promega) and a microplate reader. Firefly luciferase activity was normalized to renilla luciferase activity, and the results were presented as relative luciferase activity (relative luciferase activity = firefly luciferase activity/renilla luciferase activity).

3.9 sEH activity assay

sEH activity was determined using cytosolic cell lysates as described (109). Briefly, reactions were performed with 5 µg protein at 37 °C for 10 minutes in 100 µL of potassium phosphate buffer (100 mmol/L, pH 7.2) containing 0.1% BSA and fresh 0.25 mmol/L phenylmethylsulfonylfluorid, were added in a 96 well plate and then mixed with 50 µL of 40 µM (3-phenyl-oxiranyl)-acetic acid cyano-(6-methoxy-naphthalen-2-yl)-methyl ester (PHOME) at 37 °C. The mixture was recorded at excitation and emission of 330 nm and 465 nm for 1 hour. The fluorescent intensity was measured in Perkin Elmer 2104 EnVision Multilabel Plate Readers (Waltham, MA, USA).

3.10 PPAR-γ activity assay

PPAR-γ activity was assessed using PPRE-X3-Luc Luciferase construct (Addgene No. 1015) that harbors 3 response elements (AGGACAAAGGTCA) upstream of a luciferase reporter gene [97]. For transfection, M0 macrophages were first incubated in RPMI medium supplemented with 0.1% BSA for 2 hours before transfection with plasmid (100 ng/mL per well of a 96 well plate) and Lipofectamine 3000 Transfection Reagent (ThermoFischer Scientific, Karlsruhe, Germany) following the manufacturer's instructions. After 24 hours, the cells were polarized into M1 and M2c macrophages and stimulated as details in the results section. Luciferase activity was measured 48 hours after cell polarization or stimulation with 11,12-EET (1 µmol/L, Cayman Europe, Tallinn, Estonia), using a commercially available kit (ONE-Glo Luciferase Assay System, Promega, Walldorf, Germany). For transfection, HEK-293 cells at 80% confluence were transfected with lipofectamine 2000 Transfection Reagent (ThermoFischer Scientific, Karlsruhe, Germany) following the manufacturer's instructions.

3.11 Chromatin immunoprecipitation (CHIP-qPCR)

CHIP-PCR was performed using a Magna chip protein A/G beads kit from Millipore (Merck, Darmstadt, Germany). Firstly, cells were fixed with 0.1% paraformaldehyde to crosslink DNA-protein interactions in the nucleus. Secondly, the isolated nucleus was sheared into small fragments, allowing for subsequent immunoprecipitation of specific protein-DNA complex. Thirdly, the sheared chromatin was immunoprecipitated with a Smad2 antibody (5339P, CST, Massachusetts, USA) using the protein A/G beads. This allowed for the isolation of DNA fragments bound specifically to SMAD2 protein. Then, the DNA-protein complexes were eluted from the beads and the DNA was purified with DNA was purified with the commercial kit (Cat. #56304, QIAGEN). The binding of SMAD2 to the sEH promoter was monitored via quantitative PCR (qPCR) using primers listed in Table 1. Finally, the enrichment of SMAD2 binding to the sEH promoter was normalized with the anti-IgG group to account for any non-specific binding that may have occurred during the immunoprecipitation step.

3.12 Epoxide/diol profiling.

Samples of human and murine macrophages were mixed with 100 µL potassium phosphate buffer (100 mM, pH 7.2) and subjected to 3 cycles of freezing and thawing. Samples were spiked with a deuterated internal standard mix (8,9-DHET-d11, 11,12-DHET-d11, 14,15-DHET-d11, 9,10-DiHOME-d4, 12,13-DiHOME-d4, 5,6-EET-d11, 8,9-EET-d8, 11,12-EET-d8, 14,15-EET-d8, 9.10-EpOME-d4, 12,13-EpOME-d4, 5S-HETE-d8, 12S-HETE-d8, 15S-HETE-d8, 20-HETE-d6, 9S-HODE-d4, 13S-HODE-d4) and 500 µL ethyl acetate was added. The samples were vortexed, placed on ice for 10 minutes, vortexed again and then centrifuged at 10,000 g for 5 min at 4°C. The upper phase samples were combined and evaporated to dryness in a vacuum manifold under a continuous nitrogen stream. The residues were reconstituted with 50 µL of methanol: water (50:50, v/v, containing 100 ng/mL flufenamic acid as internal control) and analyzed with a Sciex QTrap5500 mass spectrometer in negative ionization mode operating in multiple reaction monitoring (MRM) mode. ESI parameters were set to CUR: 24 psi, IS: -4500 V, TEM: 600°C, GS1: 45 psi, GS2: 60 psi. The chromatographic separation was carried out on an Agilent 1290 Infinity LC system (Agilent, Waldbronn, Germany) using a Gemini C18 column (150 x 2 mm I.D., 5 µm particle size; Phenomenex, Aschaffenburg, Germany). The mobile phase consisted of (A) water + 0.0125% ammonia and (B) acetonitrile + 0.0125% ammonia. Elution of analytes was carried out under gradient conditions at a flow rate of 0.5 mL/min going from 15% B to 40% B in 10 min, increasing to 90% B in 2 min, hold 90% B for 1 min, and equilibrated in 15% B for 5.5 min. 10 µL of each sample was injected onto the column. The column temperature was kept at 40 °C. Samples were kept in the autosampler at 6 °C until analysis. Calibration curves were performed with authentic standards. All samples and dilutions of the standards were spiked with internal deuterated standards: Metabolite concentrations were determined by reference to the standards. Analyst 1.6.2 and MultiQuant 3.0 (both Sciex, Darmstadt, Germany), were used for data acquisition and analysis, respectively.

3.13 sEH overexpression

Adenoviral mediated expression of the sEH was performed as described [98]. Briefly, wild-type or a catalytically inactive sEH mutants were overexpressed in either macrophages from wild-type or $sEH^{-/-}$ mice. To generate the sEH mutate in epoxide hydrolase activity ($sEH^{\Delta EH}$), tyrosine residues Tyr383 and Tyr466 were mutated to phenylalanine in the pAd-shuttle sEH vector using the following primers (Biospring GmbH: Y381F: 5'-GCCAACCCAGTATTTGATTTCCAGCTCTACTTCCAAGAACCAGG-3', Y465F:5'-GTCCTCTAAACTGGTTCCGAAACATGGAAAGGAACTGGAAGTGG-3').
After DpnI restriction enzyme digestion, the DNA was transformed in Escherichia coli and the mutations were confirmed by sequencing (Eurofins MWG Operon). After overnight transduction cells were washed with medium and treated as described in the results section.

3.14 siRNA induced gene silencing

siRNA induced gene silencing was performed according to the protocol described based on manual provides. Briefly, M0 macrophages were starved in RPMI medium containing 0.1%BSA for 2 hours. siRNA was transfected into cells using Lipofectamine™ RNAiMAX Transfection Reagent (Cat. #13778075, Thermo Fisher). The cell culture medium was changed overnight, and the macrophages were then polarized into different stages of macrophages.

3.15 Immunostaining

Polarized M2c macrophages were incubated with dil-oxLDL 1:200 (Cat. # L34358, Thermo Fischer Scientific) for 15 minutes. The cells were washed three times with ice-cold PBS, fixed with 4% Rotifix, and blocked with 10% horse serum for 1 hour. Following this, primary antibodies were added and incubated overnight at 4°C on a shaker, and then washed 3 times with 1X PBS. The macrophages were then incubated with secondary antibodies for two hours on a shaker, washed three times with phosphate-buffered saline, and incubated with DAPI (1:1000). Images were captured using a confocal microscope (LSM-780; Zeiss, Jena, Germany) with ZEN software (Zeiss).

3.16 Astrocyte isolation

Astrocyte isolation was performed according to a previously described protocol [99]. Briefly, cortex from P1 to P4 mouse pups was used for isolation, with 4 mouse pup cortices required to achieve proper astrocyte density per T75 tissue culture flask. Therefore, the volumes in the following protocol are calculated for a cell preparation using 4 murine pups. The cerebral cortex was then placed in 50 mL of Hanks' Balanced Salt solution (HBSS) Falcao and spun at 900 rpm for 5 minutes, meanwhile the flask was coated with poly-l-lysin for 30 minutes. The buffer was removed, and the cortex was washed with 15 mL of HBSS. Next, trypsin was added (in 50 ml of falcon) to cover the brain (2 mL/5 mice) along with 100 µl of DNase I. The tissue was incubated at room temperature for 5 min until the tissue was flaky or at 37°C for 2-5 min (water bath). The digestion was stopped by adding 10 ml of medium, and the supernatant was removed. Fresh medium (8 ml) and 100 µL DNase I was added, and the tissue was separated with a 5 ml pipette until no large pieces of tissue remained. The cells were then spun at 900 rpm for 12 minutes, and the flask coated with poly-l-lysin was washed with PBS to resuspend the cells in 10 ml of medium. If single cells were not readily available, 50 µL of DNase I was added, and the cells were resuspended and centrifuged again. The cells were seeded (2 mice/1 T25 flask or 4 mice/1 T75 flask) and washed once the next day with 10x PBS to remove non-adherent material. Medium was changed after 2 days. After culturing the cells for 7 days, they were purified with a Percoll gradient as described previously (104). Confluent astrocytes were harvested with 0.05% Trypsin-EDTA for 10 minutes, and the cells were resuspended with 6 mL of 70% Percoll, 3 ml of 50% Percoll, 3 ml of 35% Percoll, and 2 ml of PBS from bottom to top. The falcons were centrifuged at a speed of 2000 g for 20 minutes with acceleration and break. The myelin present in the top layer was removed from the top layer, and astrocytes in the middle layer were collected layer and centrifuged for another 10 minutes. The cells obtained were then used for culture in DMEM/F12 medium supplemented with 10% FCS.

3.17 Statistical analyses.

The data are presented as mean ± SEM. Statistical analysis was performed using Prism 9.0.2 (GraphPad Software Inc.). Unpaired data were analyzed using Student's t-test, one-way ANOVA followed by Bonferroni's or Tukey's multiple comparisons test, or two-way ANOVA with a Tukey's or Sidak's post-test, where appropriate. Normalized data were compared using the Kruskal-Wallis's rank sum test or Kruskal-Wallis test, followed by Dunn's multiple comparison test (using Prism 9.0.2, GraphPad Software Inc.), as indicated in the figure legends. The statistical tests used for each experiment are described in the figure legend. A P value of less than 0.05 was considered statistically significant

4. Results

4.1 Expression of the sEH in different cell lines and cell types

The sEH is expressed in numerous organs i.e., liver, heart, kidney and brain (for review see [100]). However, the expression of sEH in different cell lines or cell types in vitro remains poorly characterized. To address this gap in knowledge, we investigated the expression of sEH in various cell lines and primary isolated cell types. Our findings revealed that sEH expression was either undetectable or low in cell lines such as HepG2 and HEK293 cells (Figure 9a). However, sEH was highly expressed in isolated primary murine hepatocytes, although its expression decreased during culture (Figure 9b). Additionally, sEH was highly expressed in murine astrocytes and murine M0 or M1 macrophages either in culture or after passage (Figure 9c and d).

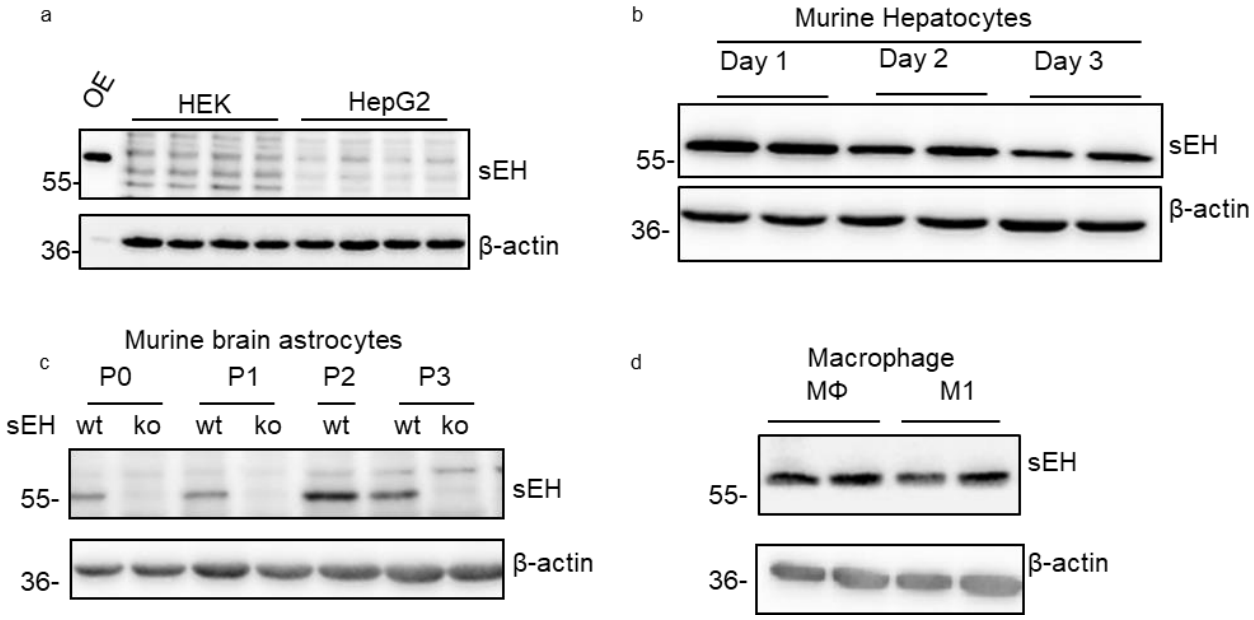

Figure 9. Expression of sEH in different cell lines and cell types. (a) sEH expression in HEK293 and HepG2 cells, OE represents sEH overexpressing cell samples; (b) sEH expression in isolated murine hepatocytes at different days of culture after isolation; (c) sEH expression in isolated murine astrocytes at different passages; d. sEH expression in murine macrophages (M0, M1).

4.2 Expression of soluble epoxide hydrolase in macrophages

To investigate the expression of sEH in macrophage polarization, we first isolated monocytes from murine bone marrow and differentiated to naïve (M0) macrophages by adding murine M-CSF (15 ng/ml) and murine GM-CSF (15 ng/ml) for 7 days. Following this, M0 macrophages were either polarized into classically activated (M1) macrophages by adding LPS, 10 ng/ml and murine IFN-γ (1 ng/mL) for 12 hours or into pro-resolving M2c by treating M1 macrophages with TGF-β1 (10 ng/ml) for another 48 hours. Additionally, M2a macrophages were generated by adding 20 ng/ml murine IL-4 for 24 hours, as illustrated in (Figure. 10a). We examined the expression pattern of sEH in these different macrophages types and found similar levels of sEH expression in M0, M1 and M2a macrophages (Figure. 10 b-c). However, significantly increased mRNA, protein, and sEH activity were observed in M2c macrophages (Figure. 10 b-c), indicating that TGF-β1 can induce sEH expression during M2c macrophage polarization.

The standard M1 macrophages polarization protocol requires only 12 hours of stimulation, whereas M2c macrophages require 48 hours. To investigate whether the difference in sEH expression between M1 and M2c macrophages was attributable to the time difference, we treated M1 macrophages with LPS and IFN-γ for either 12 or 48 hours. Our results indicated that sEH expression levels were similar in M1 macrophages treated with LPS and IFN-γ for either 12 or 48 hours (Figure. 11), suggesting that the differences in sEH expression between M1 and M2c macrophages were not due to the duration of the stimulation protocol.

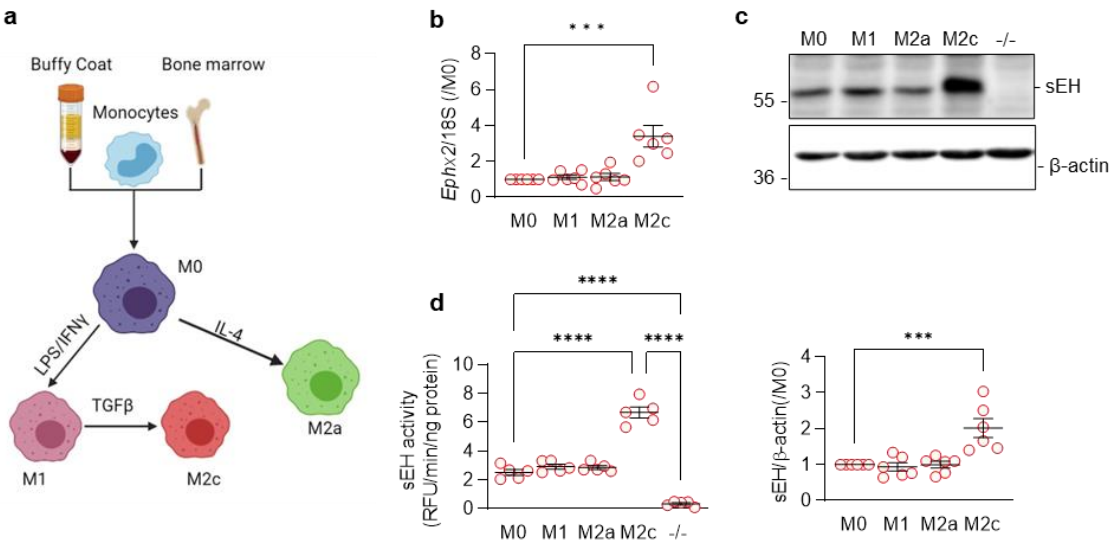

Figure 10. Expression of sEH in murine macrophages. (a) scheme indicating the isolation and polarization of macrophages. (b&c) Expression of sEH mRNA (b) and protein (c) in murine bone marrow-derived macrophages under basal conditions M0 (Sol, PBS) and after polarization to the M1, M2a or M2c; n=6 batches from different mice (Kruskal-Wallis test followed by Dunn's multiple comparison test). M2c macrophages from sEH-/- mice were included as a negative control; (d) sEH activity in polarized macrophages assessed using Phome and the florescent product 6-methoxy-2-naphthaldehyde was measured (relative fluorescence units λ_{ex} 350 nm and λ_{em} 485 nm); n=5 independent experiments (one way ANOVA followed by Turkey's multiple comparisons). M2c polarized macrophages from sEH-/- mice were included as a negative control. *P<0.05, **P<0.01, ***P<0.001, ****P<0.0001.

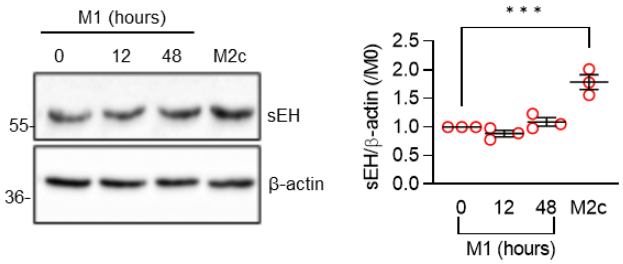

Figure. 11. Expression of sEH during M1 polarization at different time point in comparison with M2c (48 hours). Impact of M1 polarized at different time (0, 12 hours and 48 hours), n=3 independent experiments (Kruskal-Wallis test followed by Dunn's multiple comparisons test). ***P<0.001

Differential regulation of sEH expression between males and females has been previously reported [101]. Males exhibits higher levels of sEH than females in different tissues such as brain endothelial cells [102], and the heart [103]. To assess gender-specific differences

in sEH expression, we compared macrophages from male and female mice. Indeed, our results showed that macrophages from female mice expressed less than male mice (Figure. 13). Furthermore, we found that TGF-β1 induced a greater increase in sEH expression in macrophages from female mice (approximately 2.2 folds over basal) compared to those from male mice (approximately 1.3 folds to basal), suggesting that macrophages from females are much more responsive to TGF-β1 stimulation (Figure. 13).

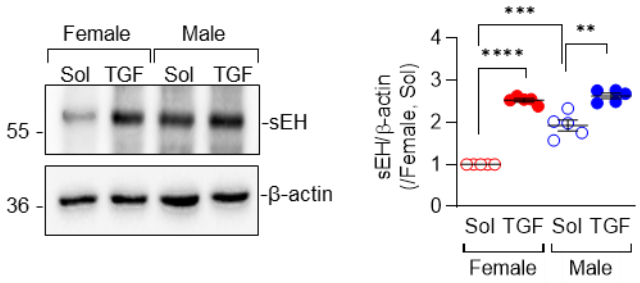

Figure 12. Expression of sEH in murine macrophages between different genders. Effect of solvent (Sol) and TGF-β1 (10 ng/mL, 48 hours) on sEH expression in M1 polarized macrophages from female and male mice; n=5 mice per group (two-way ANOVA followed by Sidak's multiple comparisons test). **P<0.01, ***P<0.001, ****P<0.0001.

Next, we also generated macrophages from human monocytes as indicated in Figure 10.a, to compare the similarity between human and mouse samples. Similar to the findings from murine macrophages, sEH expression was significantly increased in human M2c macrophages compared to M0, M1, and M2a macrophages (Figure 13a). Interestingly, the sEH expression was lower in human macrophages from female donors (M0, M1 and M2a) and significantly increased in M2c macrophages (Figure 13b).

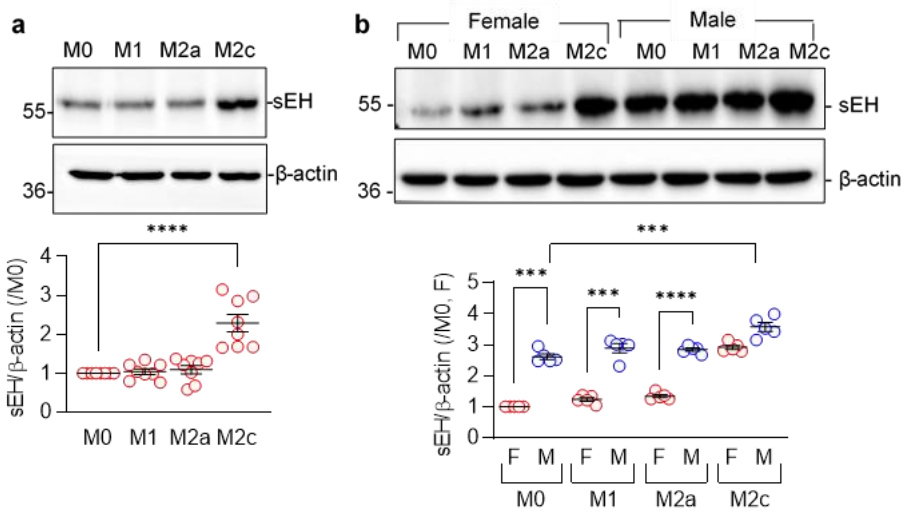

Figure 13. Expression of sEH in human macrophages between different genders. (a) Expression of sEH in M0, M1, M2a and M2c macrophages from human female donors. (b) Expression of sEH in M0, M1, M2a and M2c macrophages from human male and female donors. a: one way ANOVA and Sidak's multiple comparison test, b: two-way ANOVA and Sidak's multiple comparison test. ***P<0.001, ****P<0.0001.

4.3 TGF-β increased the sEH expression

To study the relationship between TGF-β and sEH expression, a dose-response experiment was carried out. Increasing concentrations of TGF-β led to a corresponding increase in sEH mRNA and protein expression which indicates that TGF-β regulates the sEH expression in transcriptional level (Figure 14a and b). Based on these results, a concentration of TGF-β at 10 ng/ml was selected for subsequent experiments.

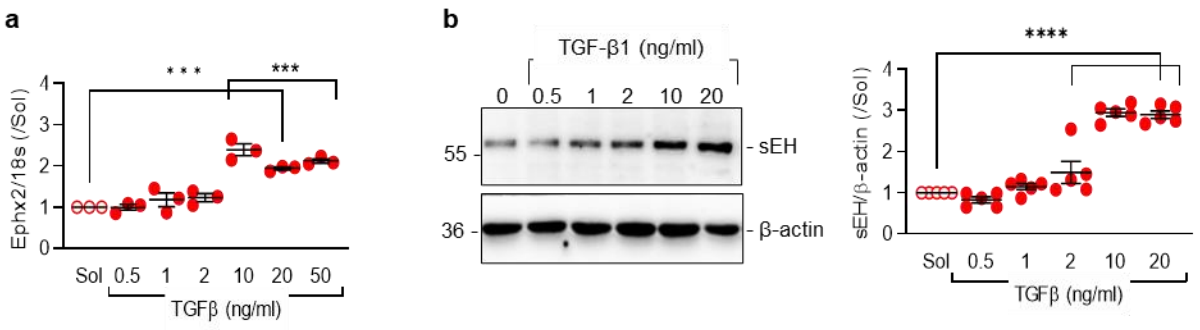

Figure 14. TGF-β1 increased the sEH expression in a dose-dependent manner**.** M1 macrophages were stimulated with different dose of TGF-β1 for 48 hours. mRNA (n=3) and protein (n=5) levels were assessed with q-PCR and Western Blotting, respectively. (Kruskal-Wallis test followed by Dunn's multiple comparisons test). ***P<0.001, ****P<0.0001.

4.4 TGF-β increased the sEH expression is mediated via Alk5/Smad2 activation

In response to TGF-β stimulation, two distinct pathways can be activated. The activation of ALK5 pathway leads to SMAD2/3 phosphorylation while via ALK1 pathway it activates SMAD1/5 phosphorylation via ALK1 pathway. To test which pathway was activated in M1 macrophages, we examined SMAD2 and SMAD1/5 phosphorylation and observed that TGF-β stimulation resulted in SMAD2 phosphorylation but did not affect SMAD1/5 phosphorylation (Figure 15a). This was also evidenced by the increase of ALK5 target gene Snai1 in M1 macrophages treating with TGF-β (Figure 15b). And again, the expression of ALK1 target gene Id3 was not affected (Figure 15b).

We used ALK5 and ALK1-specific inhibitors to examine their impact on TGF-β induced sEH expression. To confirm the selectivity of ALK5 inhibitor SD208 and ALK1 inhibitor LDN193189, we examined the ALK5-target gene Snai1 and ALK1-target gene Id3. We found that inhibition of ALK5 by the ALK5 inhibitor attenuated TGF-β induced Snail1 expression but not Id3 expression (Figure 16a). Similarity, inhibition of ALK1 by the ALK1 inhibitor attenuated TGF-β induced Id3 expression but not Snai1 expression (Figure 16b). More importantly, the inhibition of ALK5 attenuated the effect of TGF-β on sEH expression in polarized M1 macrophages, not that of ALK1 inhibitor (Figure 16c).

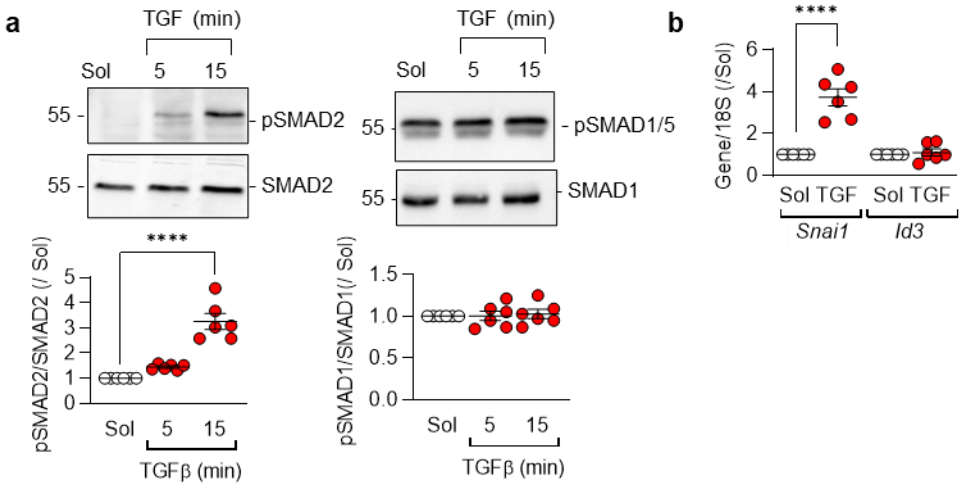

Figure 15. Role of ALK5-Smad2 pathway in the regulation of sEH expression by TGF-β1. (a) Effect of TGF-β1 (10 ng/mL) on the phosphorylation of SMAD2 (p-SMAD2) and SMAD1/5 (p-SMAD1/5) in M1 polarized murine macrophages; n=5-6 mice per group (n=5 independent experiments, Kruskal-Wallis test followed by Dunn's multiple comparison test). (b) Expression of Snail and Id3 in M2c polarized macrophages; n=5-6 mice per group (n=5 independent experiments, Kruskal-Wallis test followed by Dunn's multiple comparison test).

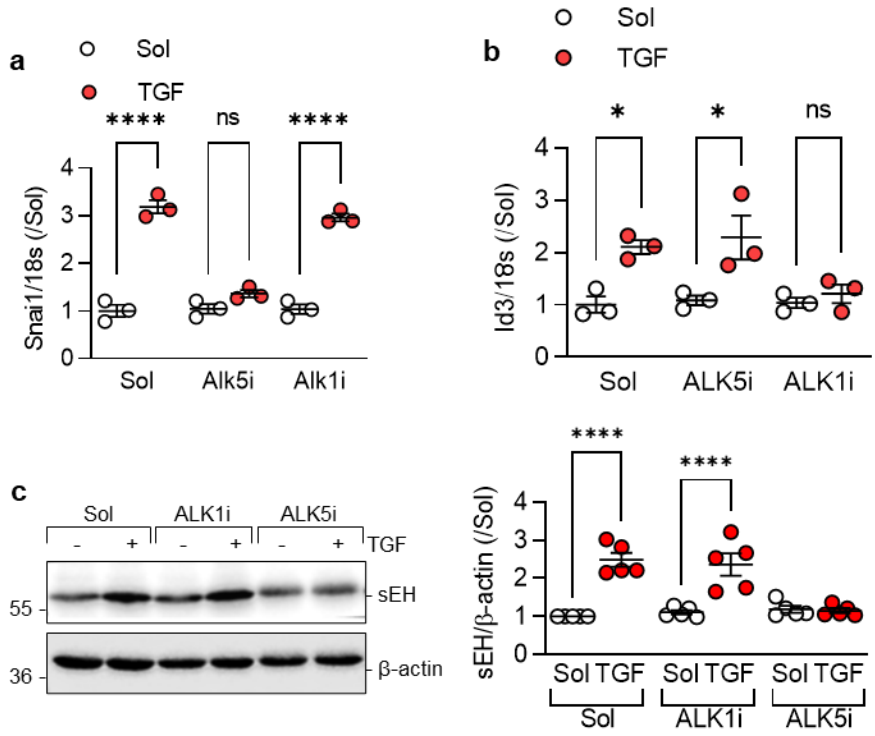

Figure 16. Effects of Alk5 and Alk1 inhibitors on TGF-induced gene expression, Snai1 and Id3 in macrophages. Macrophages were treated with ALK1 inhibition (ALK1i) using LDN193189 (100 nmol/L) and ALK5 inhibition (ALK5i) using SD208 (500 nmol/L) two hours before adding TGF-β1. After 48 hours, the cells were harvested and the expression of Snai1 and Id3 was quantified using RT-PCR (n=3 mice per group). two-way ANOVA and Sidak's multiple comparison test. ***P<0.001, ****P<0.0001. (c) (c) Consequence of ALK1 inhibition (ALK1i) with LDN193189 (100 nmol/L) and ALK5 inhibition (ALK5i) with SD208 (500 nmol/L) on the TGF-β1-induced increase in sEH expression in murine macrophages; n=5-6 mice per group (two-way ANOVA followed by Turkey's multiple comparison). *P<0.05, **P<0.01, ***P<0.001, ****P<0.0001.

It has been previously reported that SMOC1 functions as an antagonist of ALK5 signaling [104]. In line with this, heterozygous SMOC1 mice display increased levels of both mRNA and protein expression of sEH (Figure 17 a and b). These findings suggest that the activation of the ALK5 pathway may play a crucial role in the upregulation of sEH expression in macrophages.

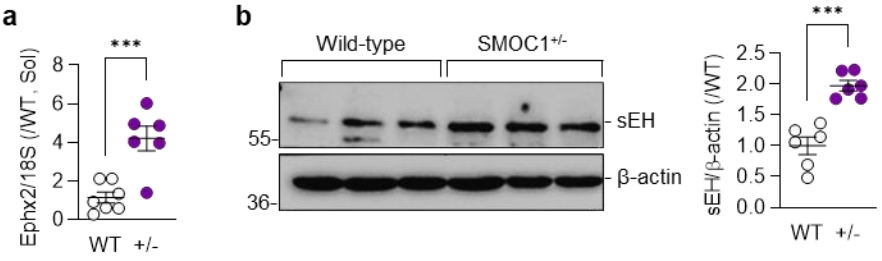

Figure 17. Consequences of SMOC1-deficiency on sEH expression. Expression of sEH mRNA (a) and protein (b) in M2c polarized macrophages from wild-type (WT) and SMOC1$^{+/-}$ (+/-) littermates; n=6 (Student's t test). *P<0.05, **P<0.01, ***P<0.001, ****P<0.0001.

Similarity, siRNA-mediated silencing of Endoglin, which has been implicated in the activation of ALK5 [104], also resulted in the increased expression of sEH in human macrophages (Figure 18). Altogether, these data demonstrate that TGF-β was able to induce sEH expression in an ALK5 dependent manner.

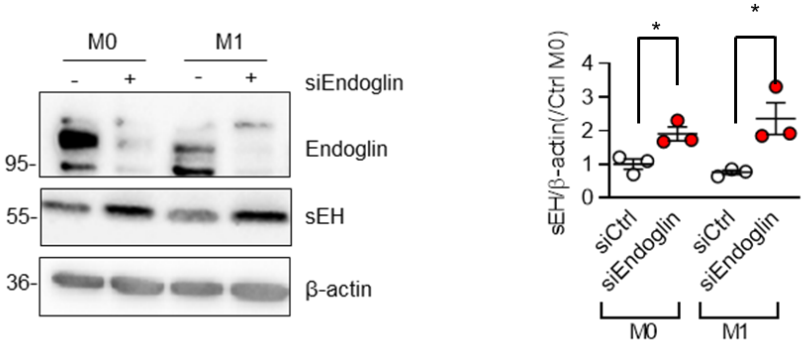

Figure 18. Consequences of Endoglin defiency on sEH in human macrophages. M0 macrophages were transfected with siRNA to induce the silencing of Endoglin. 48 hours after transfection, M0 macrophages were further polarized to M1 by adding LPS/IFNγ for additional 24 hours. n=3 (Student's t test). *P<0.05.

4.5 TGF-β increased the sEH promoter activity

To verify the transcriptional regulation of sEH following TGF-β stimulation, the activity of sEH promoter constructs of different lengths were tested. The promoter activity of all plasmid constructs was increased under TGF-β stimulation. The shortest lengths (-370 to +28 bp) showed the maximum fold change of promoter activity by TGF-β stimulation (Figure 19a). Additionally, promoter analysis revealed the presence of multiple SMAD2 binding elements in the shortest promoter region of sEH (Figure 20).

To further confirm the binding of potential SMADs to the Ephx2 promoter region, Chip-PCR combined with primers for specific regions was applied. This indicated increased binding of SMAD2 on the promoter region (-370 to +28 bp) of sEH (Figure 19b). SP1 was previously identified as an important transcription factor for the regulation of Ephx2 expression [105]. Oligonucleotides targeting SMAD2 and SP1 were applied to validate the potential role of SMAD2 and SP1 binding in the TGF-β-induced regulation of EPHX2 expression (Figure 19c). Only SMAD2-binding antagonists but not SP1-binding antagonists attenuated the effect of TGF-β-induced sEH gene expression (Figure 19c).

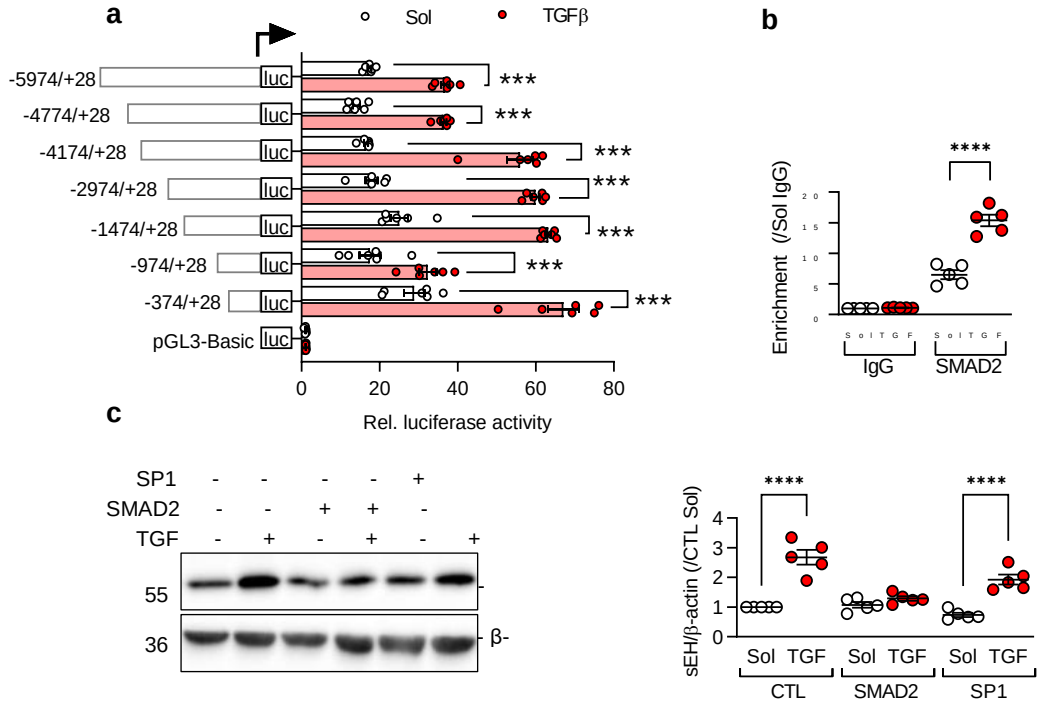

Figure 19. TGF-β increased sEH promoter activity. HEK cells at 70% confluence were transfected with human sEH promoter constructs and after 24 hours, transfected cells were administrated with 10 ng/ml of TGF-β1 for 24 hours and the luciferase activity was measured and normalized against rellina activity (a). (b) Evaluation of SMAD2 binding to sEH promoter region using CHIP-PCR by specific primer targeting the promoter region using SMAD2 antibody, IgG was used as negative control (n=5 independent experiments, two-way ANOVA followed by Turkey's multiple comparisons). (c) Effects of SP1 and SMAD2 oligonucleotides against SP1 and SMAD2 binding on the effects of TGF on sEH expression in M1 macrophages. *P<0.05, **P<0.01, ***P<0.001, ****P<0.0001.

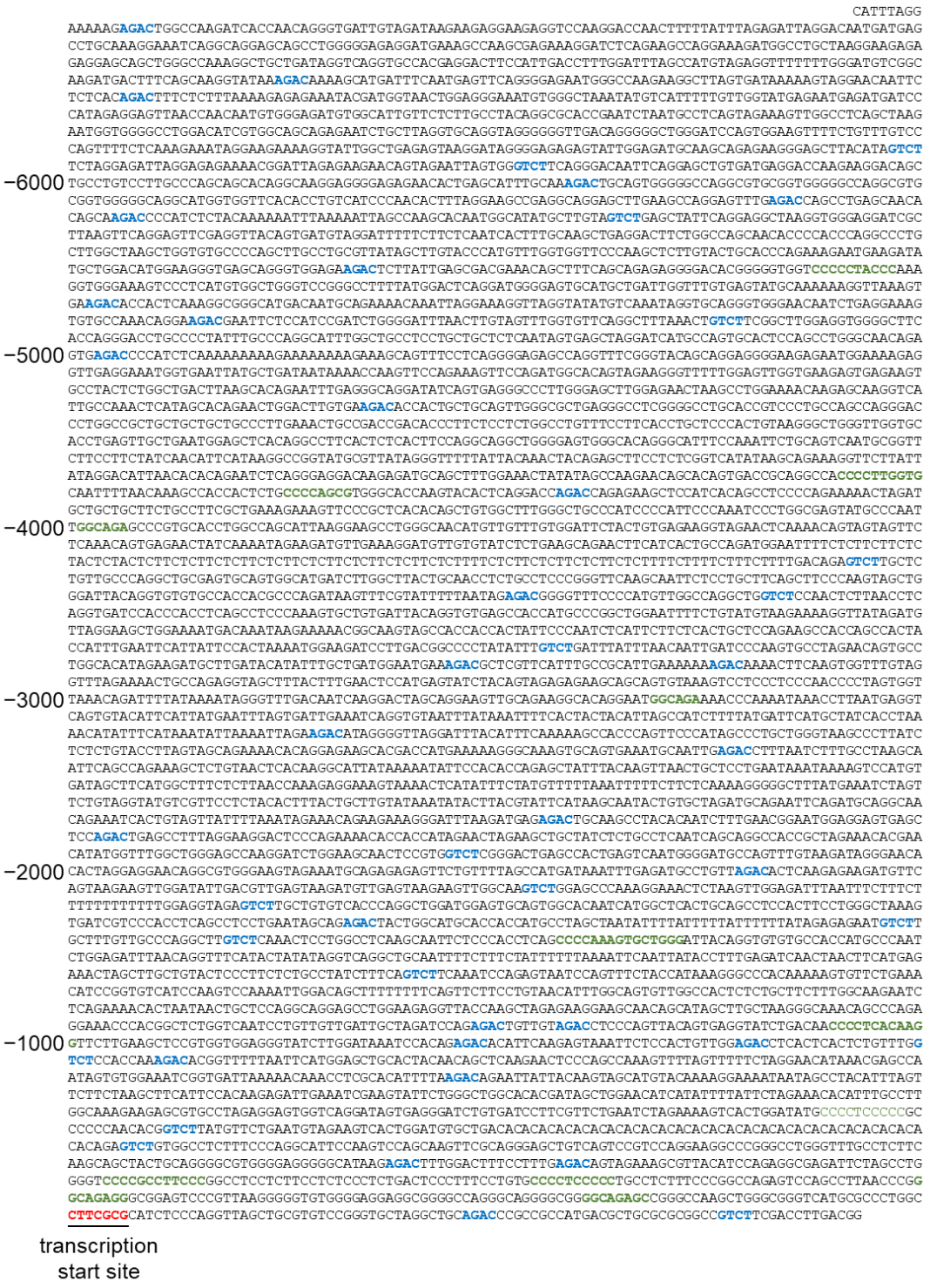

Figure 20. The potential binding element of SMAD2 in the human sEH promoter (approximately 7 kb). SMAD binding elements (AGAC/GTCT) are highlighted in blue, SP1 binding element in green, transcriptional start site (defined as +1) in red.

4.6 sEH deletion caused a deficiency in M2c macrophages polarization

The increased expression of sEH in M2c macrophages suggests that sEH may play a role in M2c macrophage polarization. To examine the potential role of sEH in the macrophage polarization, monocytes from wild-type (WT) and $sEH^{-/-}$ (-/-) mice were polarized into M1, M2a and M2c macrophages, and the expression of phagocytic markers. As previously reported [106], sEH deficiency resulted in a slight reduction in M1 polarization, as evidenced by lower expression of Tnfa, Il1b, and Nos2 (Figure 21). However, no significant difference was observed in alternate M2a macrophages polarization (Figure 21). The most notable difference was observed in M2c macrophages, which displayed incomplete M2c polarization, as reflected by lower expression of M2 markers such as Mrc1, Tlr2, and Actn1, as well as higher expression of M1 markers such as Tnfa, Il1b, Nlrp3, and Nos2 in sEH-/- macrophages (Figure 21). These findings indicate that sEH is required for M2c macrophage polarization.

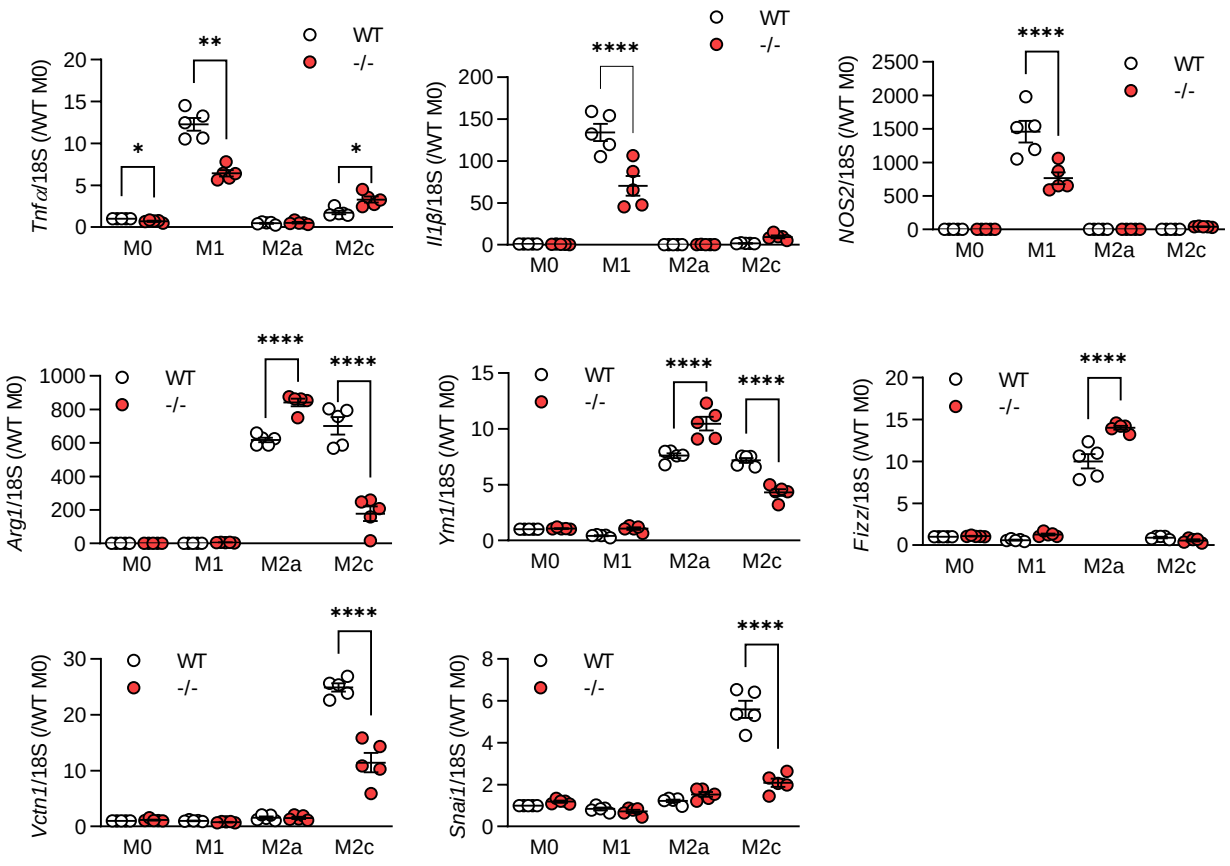

Figure 21. Effect of sEH deletion on macrophage polarization. Expression of a panel of marker genes in bone marrow-derived macrophages from wild-type (WT) and sEH-/- (-/-) mice under basal conditions (M0) and following M1, M2a and M2c polarization; n=5-6 mice per group (two-way ANOVA followed by Sidak's multiple comparisons test). *P<0.05, **P<0.01, ***P<0.001, ****P<0.0001.

4.7 sEH deficiency impaired M2c macrophage function

In the resolution of inflammation, M2c macrophages play a critical role by regulating the phagocytosis and efferocytosis processes [107]. In order to investigate the potential impact of sEH deficiency on the function of M2c macrophages, we monitored its ability to takeup fluorescent-labeled zymosan particles and dil-ox-LDL. Our results showed that disruption of sEH functions, either by inhibiting sEH or deleting it, impaired the uptake of zymosan particles and dil-ox-LDL by M2c macrophages (Figure 22 a, b and c).

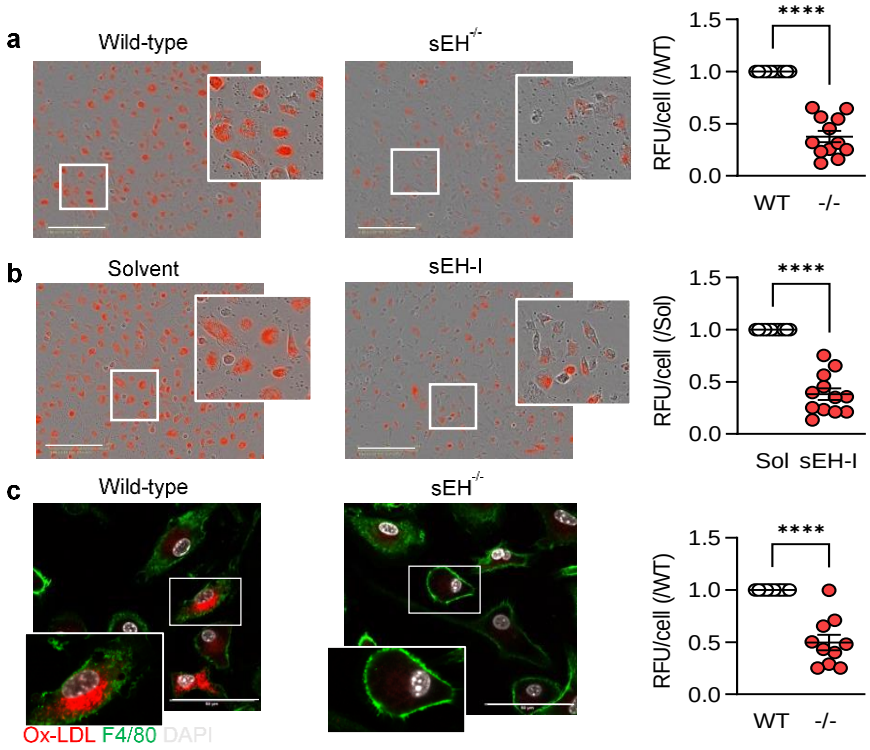

Figure 22. Uptake of zymosan and ox-LDL by M2c macrophages. (a) pHrodo Red Zymosan uptake by M2c polarized macrophages from (a) wild-type (WT) and sEH$^{-/-}$ (-/-) mice, or (b) from WT M2c macrophages treated with solvent or a sEH inhibitor (sEH-I, *t*-AUCB, 5 µmol/L, Kruskal-Wallis rank sum test), bar= 200 µm; n=12 mice per group (Kruskal-Wallis rank sum test). (c) Oxidized LDL (ox-LDL) uptake by M2c polarized macrophages from WT and sEH$^{-/-}$ mice, bar= 50 µm; n=10 mice per group (Kruskal-Wallis rank sum test). *P<0.05, **P<0.01, ***P<0.001, ****P<0.0001.

4.8 sEH deletion attenuated the resolution of inflammation in in vivo

As M2c macrophages are crucial for the clearance of apoptotic cells and the promotion of inflammation resolution and healing, we next examined the impact of sEH deficiency on the resolution of inflammation *in vivo*. Zymosan-induced peritonitis, which is a self-resolution model, was used. To evaluate the effect of sEH deficiency on the resolution of inflammation *in vivo*, 8–12-week-old mice were challenged with zymosan. Peritoneal lavage fluid was collected at different days (1, 3 and 6 days) after zymosan injection to investigate the immune cell profile during the acute inflammatory and inflammatory resolution phases.

In wild-type mice, a rapid increase in neutrophil infiltration was detected on day 1 after zymosan injection, defining as the acute inflammatory phase, which is the onset of inflammation (Figure 23a). The number of neutrophils decreased rapidly on day 1 and decreased to almost basal levels on day 6, which is defined as the resolution of inflammation phase (Figure 23a). The proportion of neutrophils in the $sEH^{-/-}$ group was lower than that detected in wild-type mice, indicating an anti-inflammatory effect of sEH depletion (Figure 23a) as previously reported [108]. The number of resident macrophages (Res. MΦ) (Figure 23b), conventional dendritic cells (cDCs) (Figure 23d), T cells (Figure 24f) and B cells decreased on day 1 and increased on day 3 and day 6, which are both defined as the resolution of inflammation phase. Among these, recruited macrophages (Rec. MΦ) (Figure 23c) and natural killer T cells (NKT cells) (Figure 23j) increased from day 1 to day 6 compared to day 0. The absence of sEH affected the increase in Resident. MΦ, Rec. MΦ, DCs and cDCs, Res. MΦ, Rec. MΦ, dendritic cells (DCs) and cDCs are associated with efflux cells and phagocytosis in several studies [109–112]. These data indicate an impaired resolution of inflammation in sEH-/- mice.

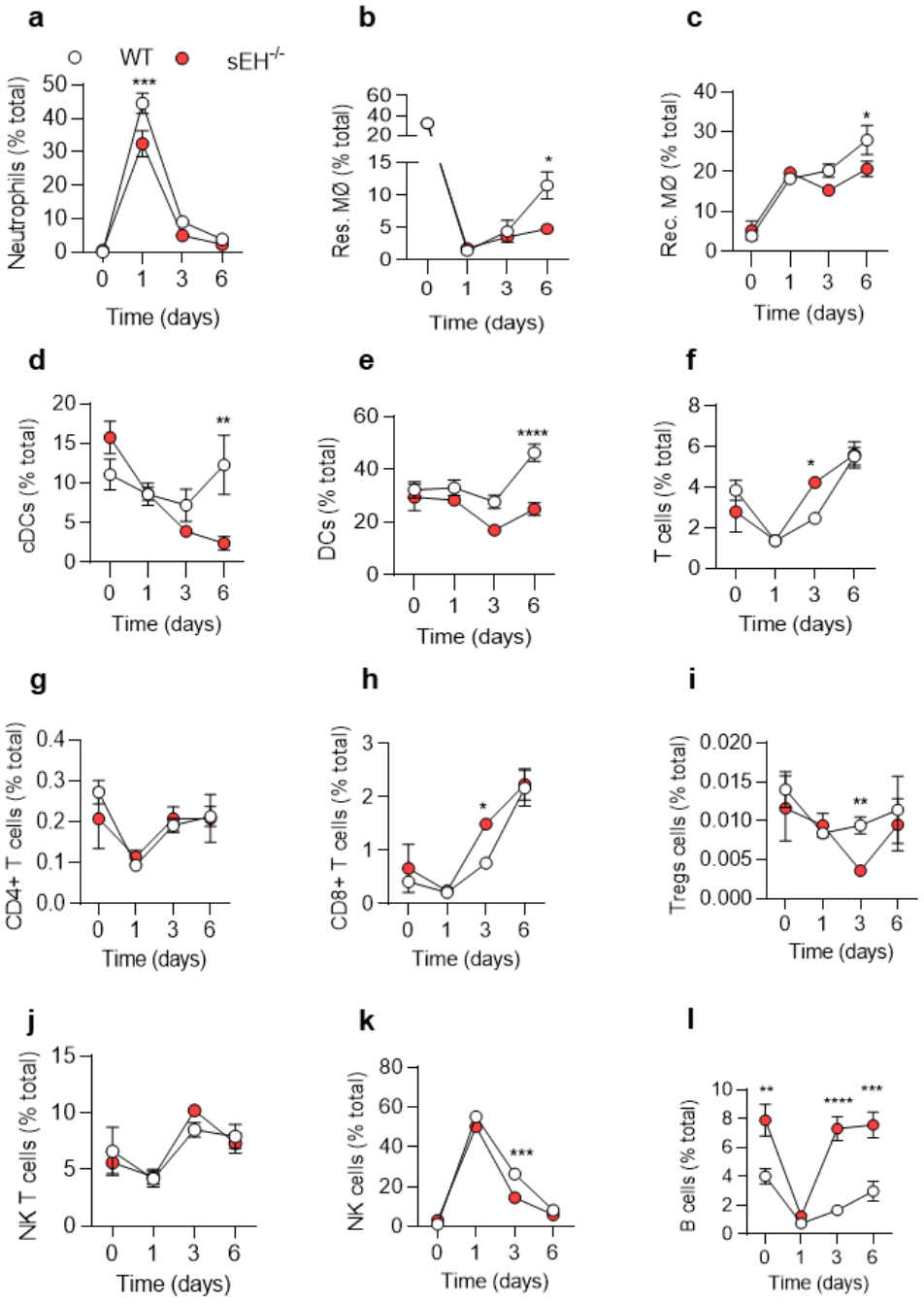

Figure 23. Immune cell profiling of peritoneal lavage from wild-type and sEH$^{-/-}$ mice up to 6 days after a single intraperitoneal injection of zymosan A (10 mg/kg). Neutrophils (a), Res. MØ: resident macrophages (b), Rec. MØ: recruited macrophages (c), cDCs: conventional dendritic cells (d), DCs: dentritic cells (e), T cells (f). CD4+ T cells (g), CD8+ T cells (h), Tregs: regulatory T cells (i), NKT cells: natural killer T cells (j). NK cells: natural killer cells (k) and B cells (i). n=5-6 animals per group (two-way ANOVA and Sidak's multiple comparisons test). *P<0.05, **P<0.01, ***P<0.001, ****P<0.0001

4.9 RNA-seq analysis

Next, we conducted bulk RNA sequencing of M0, M1 and M2c macrophages from wild-type (WT) and sEH$^{-/-}$ mice. As indicated in the principal component analysis (PCA) plot, there was a clear difference between M0, M1 and M2c, indicating the successful polarization from M0 to M1 and M1 to M2c polarization (Figure 24).

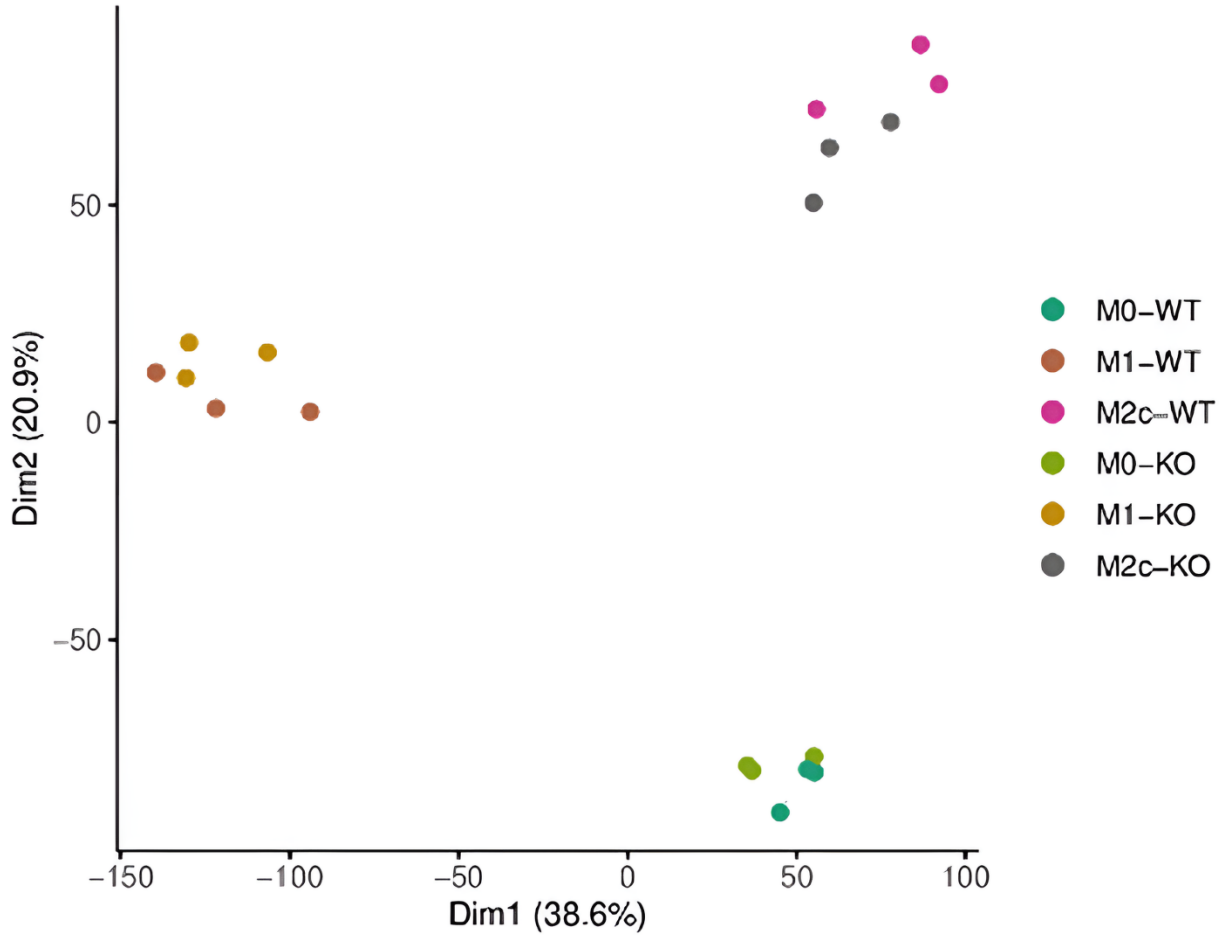

Figure 24. PCA analysis of RNA sequencing data from M0, M1 and M2c macrophages from WT and sEH-/- mice (n=3/each group). PCA plot was generated via an online tool SRPLOT (https://bioinformatics.com.cn).

In sEH$^{-/-}$ M2c macrophages, the most enriched genes were inflammation-related genes such as Cxcl3, Cxcl3, Cx3cr1, Ackr3 Il1b, Nlrp3, and Il16 (Figure 25). String analysis with the most enriched genes in sEH$^{-/-}$ M2c macrophages showed that Il1b was in the

interacting center associated with all the related inflammatory gene expression (Figure 26). GO analysis of most enriched gene showed interleukin-1 production, positive regulation of immune effector process, positive regulation of defense response, cell chemotaxis was most changed pathway (Figure 27). This data further suggested that the deletion of sEH caused the incomplete M2c macrophage polarization. Some of the most significant changed gene for example Tlr2, Mrc1 and Nlrp3 were experimentally verified, via RT-PCR, Western blotting (Figure 28).

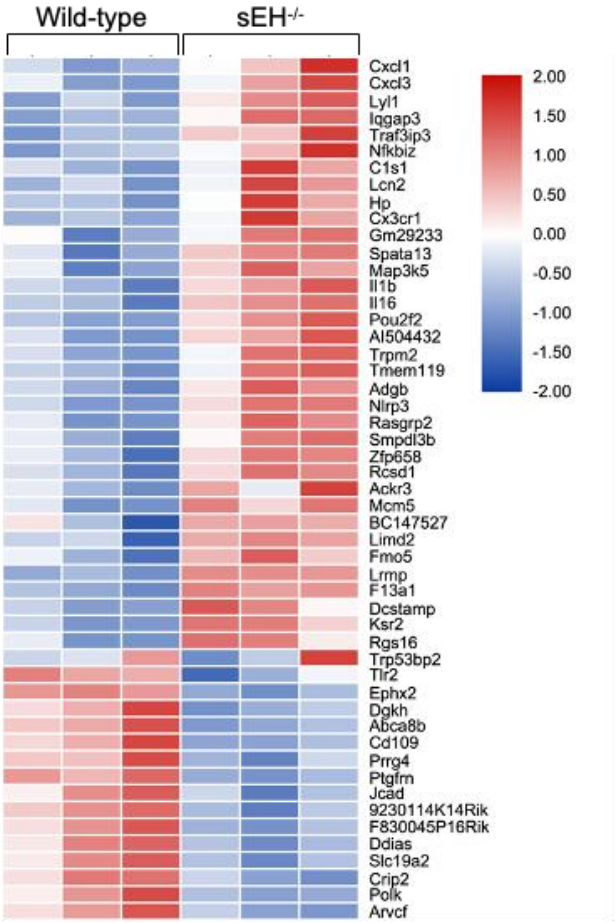

Figure 25. Heatmap showing top 50 most differentially expressed genes in M2c macrophages from wild-type and sEH$^{-/-}$ mice; n=3 mice per group. Heatmap was generated via an online tool SRPLOT (https://bioinformatics.com.cn).

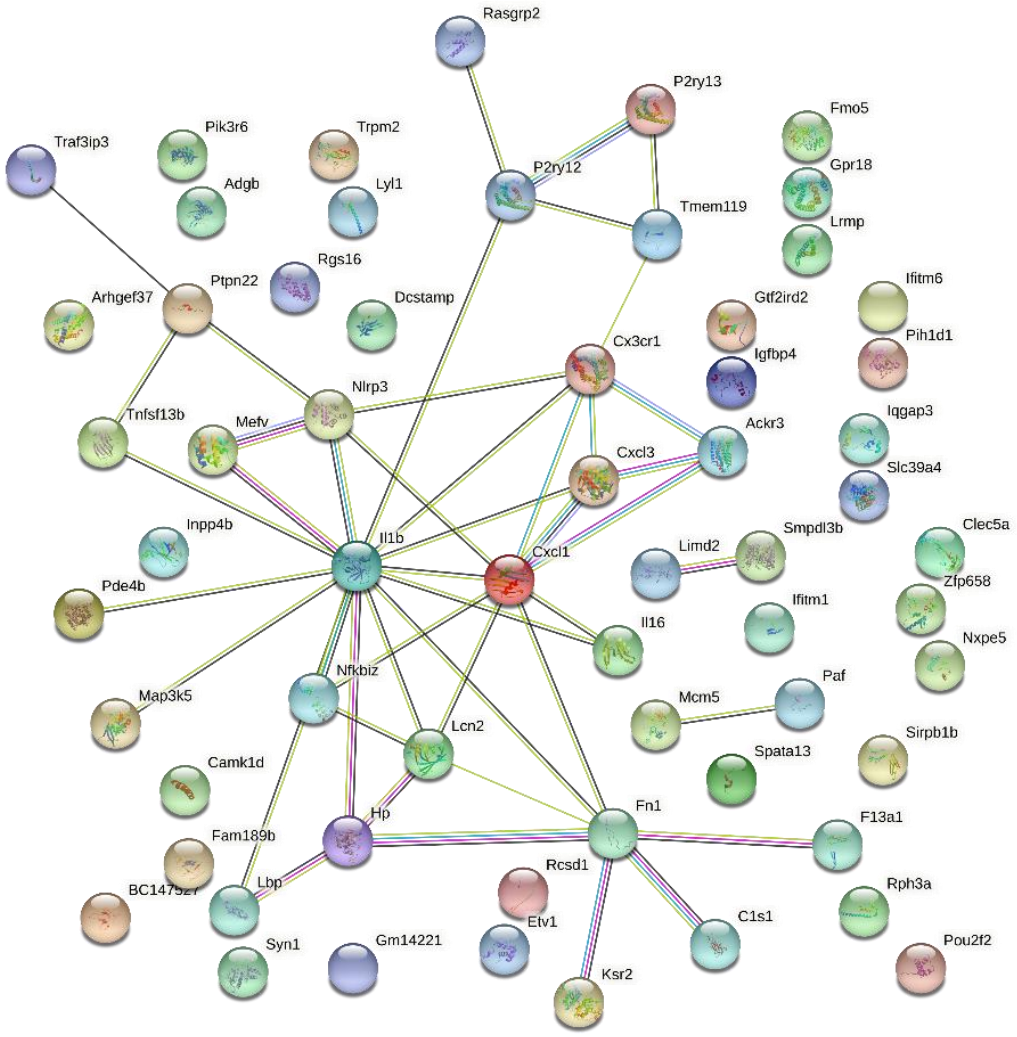

Figure 26. Sting analysis of the gene set (top 30 genes) enriched in M2c macrophages (sEH$^{-/-}$) compared to wild-type. Figure was generated in the string website (STRING: functional protein association networks, string-db.org), Version 11.5) based on the instruction from website.

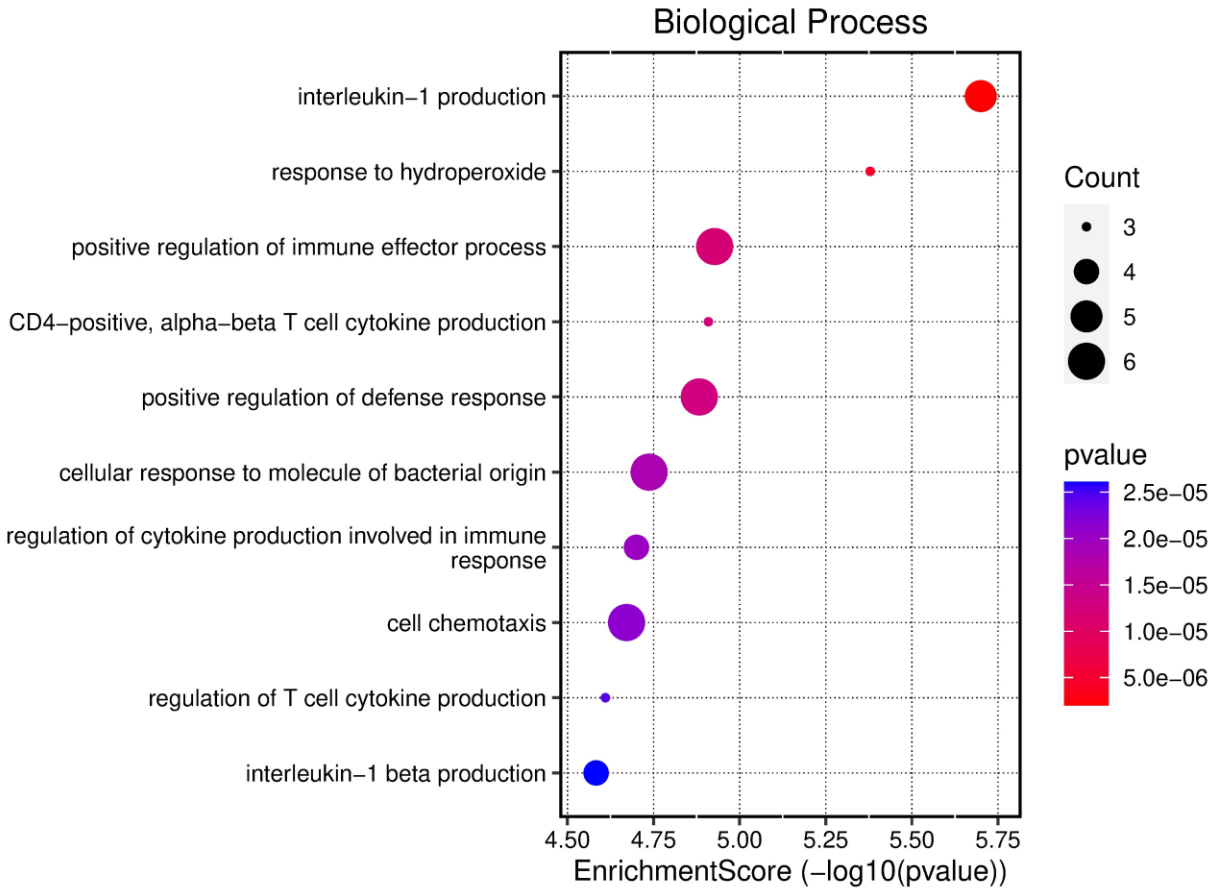

Figure 27. GO pathway gene set enrichment analysis of the most enriched genes from sEH$^{-/-}$ M2c macrophages. GO analysis was generated via an online tool SRPLOT(https://bioinformatics.com.cn). The count of genes was represented by the size of the dots, while the p-value was represented by the color.

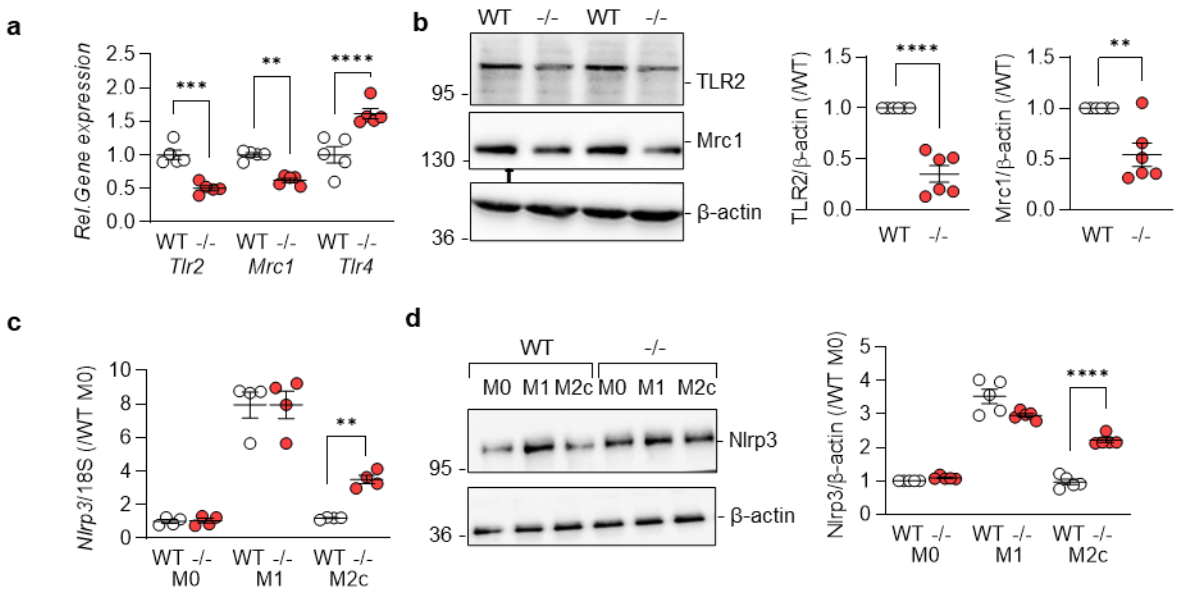

Figure 28. Validation of most significant changed gene from RNA sequencing. (a & b) Expression of Tlr2, Mrc1 and Tlr4 in M2c polarized macrophages from wild-type (WT) and sEH$^{-/-}$ (-/-) mice; n=5-6 mice per group (Student's t-test). (c & d) Expression of Nlrp3 (mRNA & protein) in M0, M1 and M2c macrophages from wild-type (WT) and sEH$^{-/-}$ (-/-) mice (two-way ANOVA followed by Turkey's multiple comparison test). *P<0.05, **P<0.01, ***P<0.001, ****P<0.0001.

Overall, our findings suggest that the sEH is essential for maintaining proper M2c macrophage polarization, which is characterized by elevated expression of phagocytosis-associated receptors Tlr2 and Mrc1, and decreased expression of inflammation-associated Nlrp3 and Il-1β. Our analysis of differential gene expression in peritoneal fluid following zymosan administration further supported this notion, as sEH$^{-/-}$ mice exhibited impaired resolution of inflammation, with decreased expression of resolution-associated makers including Tlr2, Mertk, Cd206, Cd163 and Snai1, and increased expression of inflammation-associated markers such as Il1b, Nos2, Tlr4 and Nlrp3, as shown (Figure 29).

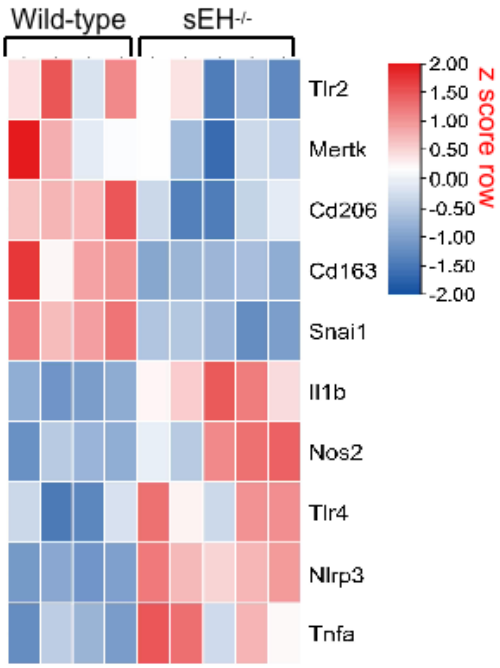

Figure 29. Heatmap showing most differentially regulated transcripts related to the inflammation and resolution of inflammation in cells from peritoneal fluid isolated from 6 days after zymosan administration: n=4-5 mice per group.

4.10 sEH promotes M2c macrophages polarization

To further demonstrate the role of sEH in the polarization of M2c macrophages, we performed loss and gain of function experiments to evaluate the role of sEH in M2c macrophages polarization. We used Tlr2 and Mrc1 expression as readouts for M2c polarization, as other markers associated with phagocytosis and efferocytosis such as Mertk, Cd36 and Dectin were comparable in macrophages from wild-type and sEH$^{-/-}$ mice (Figure 30). Inhibition of sEH with sEH inhibitor resulted in lower expression of Tlr2 and Mrc1 in wild-type macrophages (Figure 31a). Overexpression of sEH rescued Tlr2 and Mrc1 expression in sEH$^{-/-}$ macrophages, while overexpression of the mutant epoxide hydrolase structural domain did not have this effect (Figure 31b), indicating that the sEH-hydrolase domain is responsible for this phenotype and that sEH-derived lipid mediators are involved in M2c macrophage polarization.

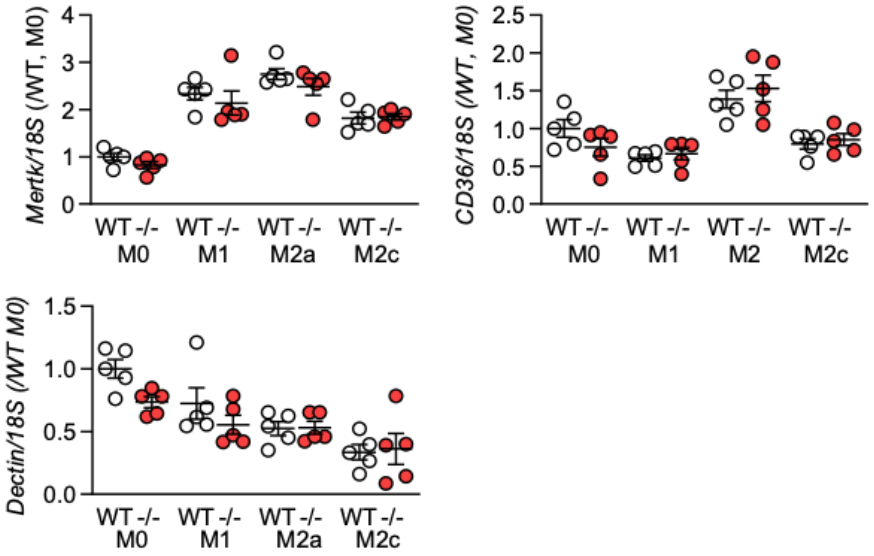

Figure 30. Expression of genes related to phagocytosis and efferocytosis by M0, M1, M2a and M2c macrophages from wild-type (WT) and sEH$^{-/-}$(-/-) mice. n=5-6 mice per group (one way ANOVA followed by Turkey's multiple comparison).

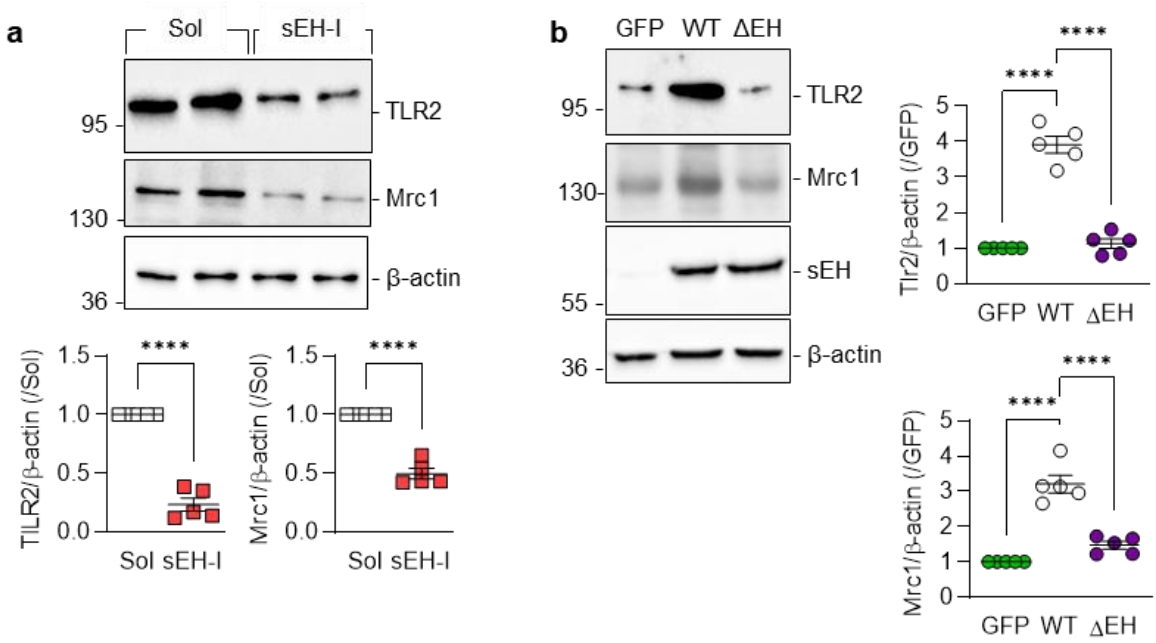

Figure 31. Gain and/or loss of function to validate the effect of sEH on Tlr2 and Mrc1 expression. (a) Expression of Tlr2 and Mrc1 in M2c polarized macrophages from wild-type mice in the presence of solvent (Sol) or the sEH inhibitor (sEH-I); n=5-6 mice per group (Student's t test). (b) Tlr2 and Mrc1 expression in M2c polarized macrophages from sEH-/- mice overexpressing either GFP, the wild-type sEH (WT) or a catalytically inactive sEH mutant (ΔEH); n=5-6 mice per group (one way ANOVA followed by Turkey's multiple comparison). *P<0.05, **P<0.01, ***P<0.001, ****P<0.0001

4.11 Impact of TGF-β-induced macrophage repolarization on PPAR-γ related gene expression

To investigate the potential link between PUFAs and M2c macrophages polarization, we re-analyzed the RNA sequencing data of M0, M1 and M2c only in wild-type mice. The PCA successfully grouped macrophages into three distinct clusters (Figure 32a). Further analysis of differentially expressed genes in M2c versus M1 polarized macrophages revealed significant differences, including the upregulation of 2952 genes and downregulation of 2051 genes induced by TGF-β (Figure 32b). Notably, Pparg was found to be among the genes which are significantly increased in M2c macrophages, and gene set enrichment analysis identified changes in the expression of several targets of the PPAR family of transcription factors (Figure 32 b and c). PPAR-γ is a well-studied receptor associated with lipid action [113], and its upregulation in M2c macrophages suggests a

potential role in macrophages polarization. Additionally, the analysis identified a significant pathway associated with the metabolism of arachidonic acid, further suggesting a potential link between arachidonic acid metabolism and PPAR-γ in the polarization of M2c macrophages (Figure 32b and c).

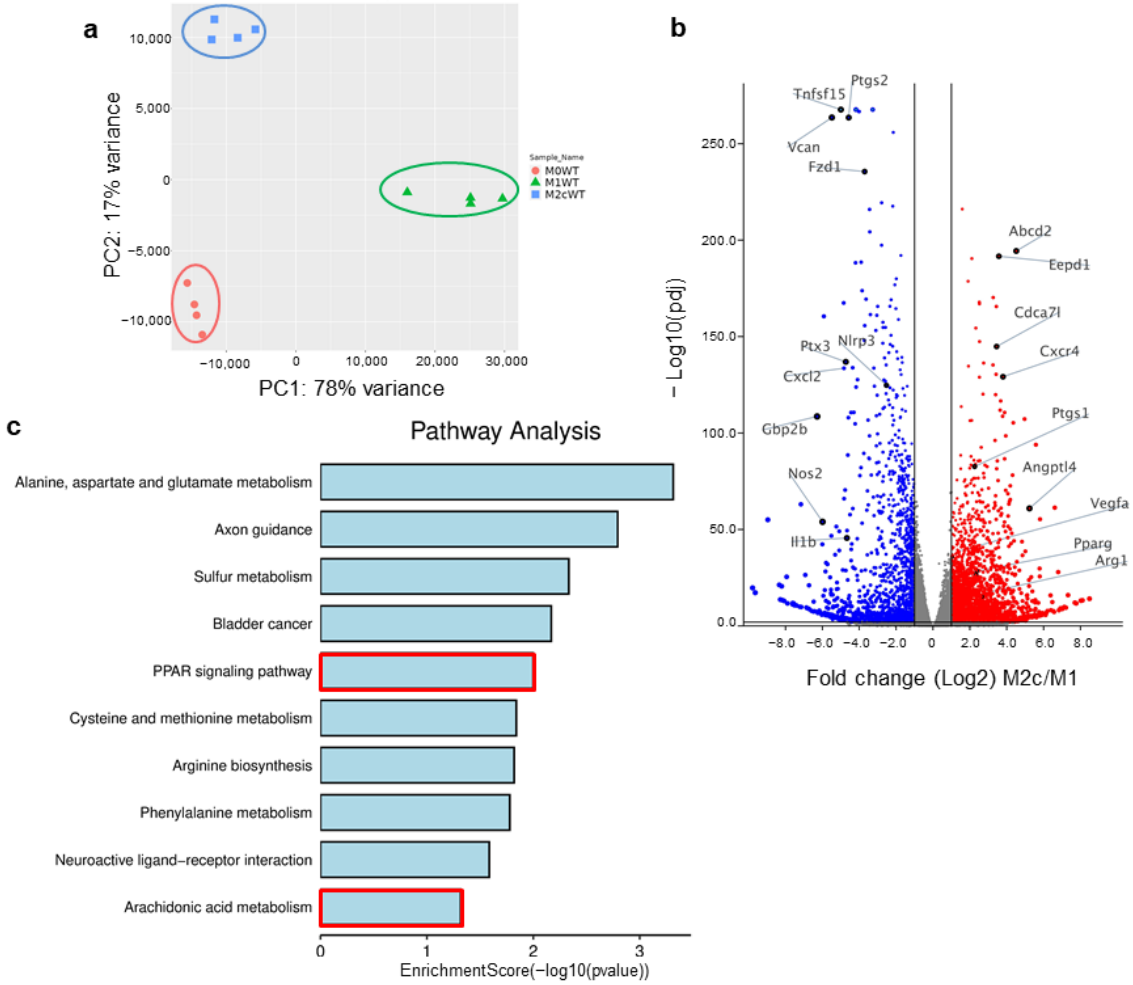

Figure 32. Impact of TGF-β-induced macrophage repolarization on gene expression. (a) Principal component analysis showing the clustering of RNA-seq samples from differentially polarized (M0, M1 and M2c) murine macrophages; n=4/group. (b) Volcano plot showing differentially expressed genes in M1 and M2c polarized. Blue = genes significantly downregulated and red = genes significantly upregulated in M2c versus M1 macrophages. (c) Gene set enrichment analysis of gene expression in M1 and M2c macrophages.

4.12 TGF-β-induced M2c macrophage polarization relies on PPAR-γ and ALK5 activation

To determine the role of PPAR-γ in regulating specific macrophage genes, we examined the impact of the GW9662 (10 µmol/L), a PPAR-γ antagonist, on the expression of Cxcr4 (predominantly expressed in M2c) and Ptgs2 and Ptx3 (both highly expressed in M1). Our results revealed that PPAR-γ antagonism had no significant effect on Cxcr4 expression. However, cells treated with GW9662 led to significantly elevated levels of Ptgs2 and Ptx3 compared to the solvent-treated cells (Figure 33a). This upregulation of pro-inflammatory genes suggests that PPAR-γ activation is involved in the repression of Ptgs2 and Ptx3, which are typically associated with M1 polarization. Notably, the latter cells have the ability to effectively phagocytose cell debris, but particle uptake was clearly reduced in cells treated with the PPAR-γ antagonist (Figure 33b).

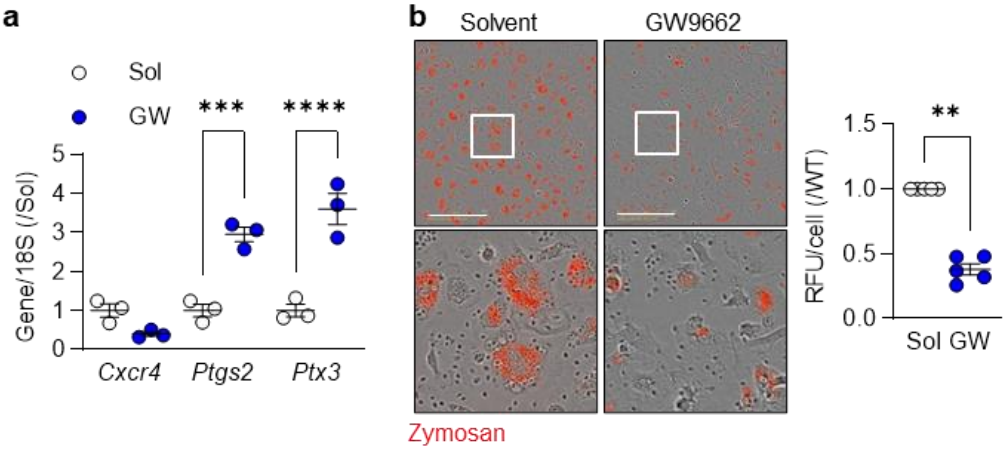

Figure 33. M2c macrophage polarization relies on PPAR-γ activation. (**a**) Expression of Cxcr4, Ptgs2 and Ptx3 in M2c polarized macrophages treated with solvent or the PPAR-γ antagonist; GW9662 (10 µmol/L) 2 hours prior to the addition of TGF-β (n=3 independent experiments, Student's t test). (**b**) Zymosan phagocytosis by M2c macrophages treated as in a. Images were taken 30 minutes after zymosan addition and the white boxes indicate the area magnified in the lower panels; bar = 200 µm (n=5/group, Kruskal-Wallis rank sum test). ***P<0.001, ****P<0.0001.

We also observed a significant increase in PPAR-γ expression in M2c compared to M1 or M0 macrophages (Figure 34a). As M2c polarization was induced by adding TGF-β to M1 polarized macrophages, we investigated which TGF-β type I receptor ALK1 or ALK5, mediated the TGF-β-induced increase in PPAR-γ levels. We found that neither solvent

nor the ALK1 inhibitor LDN193189 (100 nmol/L), prevented TGF-β-induced increase in PPAR-γ levels (Figure 34b). However, in macrophages pretreated with the ALK5 inhibitor, SD208 (500 nmol/L), the response was abolished (Figure 34b).

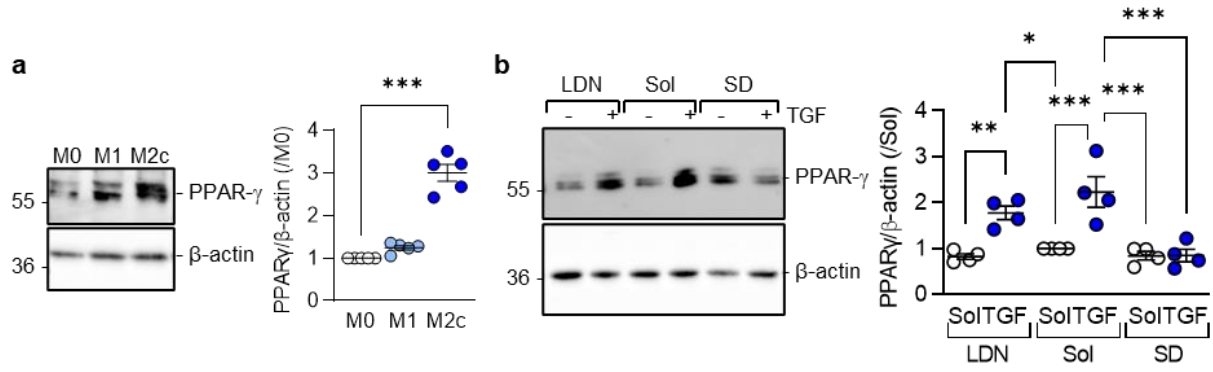

Figure 34. TGF-β-regulated PPAR-γ expression depends on the activation of ALK5. (a) Expression of PPAR-γ in M0, M1 and M2c polarized murine macrophages; n=5/group (Kruskal-Wallis test followed and Dunn's multiple comparison test). (b) Expression of PPAR-γ in M1 polarized murine macrophages treated with solvent, the ALK1 inhibitor; LDN193189 (100 nmol/L), or the ALK5 inhibitor; SD208 (500 nmol/L) for 2 hours prior to the addition of TGF-β for M2c polarization; n=4/group (two-way ANOVA and Sidak's multiple comparisons test). *P<0.05, **P<0.01, ***P<0.001.

The evidence above indicated the potential role of PPAR-γ in M2c macrophages polarization. To further investigate this, we applied the PPAR-γ inhibitor to check if it affects the polarization of M2c macrophages. Indeed, inhibition of PPAR-γ attenuated the effects of TGF-β on polarization of M2c macrophages, which replicated the effects of sEH inhibition, as demonstrated by changes in marker expression of Tlr2, Mrc1, and Nlrp3 (Figure 35).

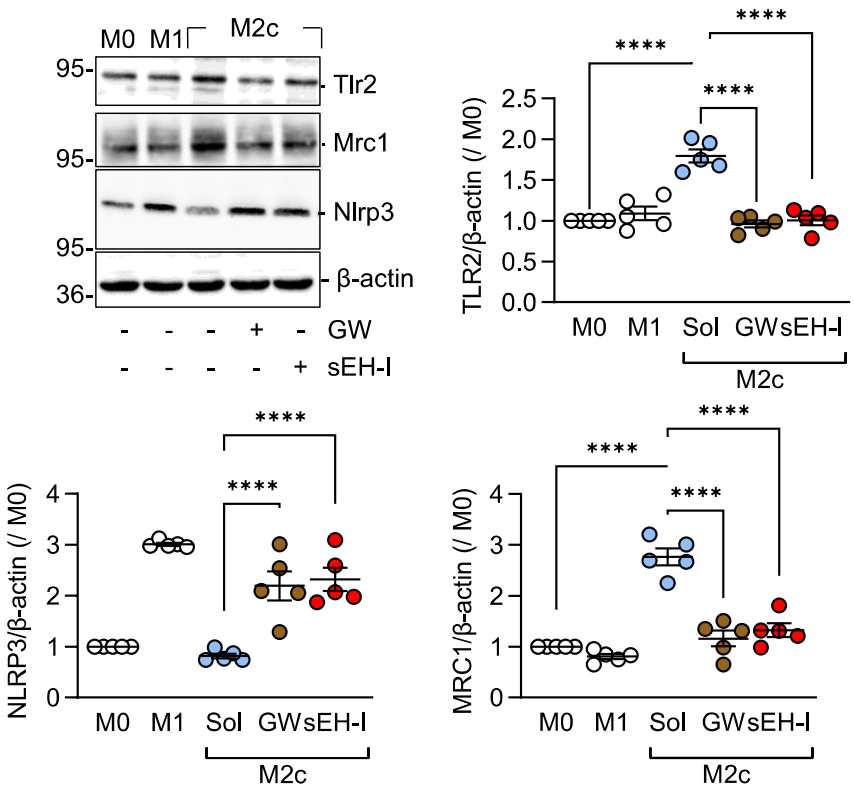

Figure 35. Effects of PPAR-γ antagonist and sEH inhibitor on M2c macrophages polarization. Impact of of solvent (Sol, 0.1% DMSO) and PPAR antagonist (10 µmol/L, 30 min prior to 10 ng/ml TGF-β) and sEH inhibitor (sEH-I, 10 µmol/L, 30 min prior to 10 ng/ml TGF-β) on the expression of Tlr2, Mrc1 and Nlrp3 (n=5 independent experiments, Krusakal-Wallis test followed by Dunn's multiple comparison test). ****P<0.001

4.13 Fatty acid profile

To determine which lipids were altered during polarization of M2c macrophages, we generated lipid profiles from human M1 and M2c macrophages group treated with either solvent and sEH inhibitor (t-AUCB). There is a clear cluster difference in M1 and M2c macrophages profile as shown in (Figure 36a). The polarization of M1 to M2c macrophages resulted in a shift from sEH substrates such as 11, 12-EET, 14,15-EET, 9, 10-EpoME, 16,17-EpDPE to sEH products, including 11, 12-DHET, 14, 15-DHET, 9, 10-DiHOME, which suggests an increase in sEH expression during M1 to M2c polarization (Figure 36b). Figure 36b shows that there is a clear cluster difference in the M2c macrophages profiles between the solvent and sEH inhibitor-treated groups. Inhibition of

sEH revealed that sEH products (9,10-DiHOME, 11,12-DHET, 14,15-DHET) were enriched in the solvent group, whereas sEH substrates (14,15-EET, 11,12-EET, 9,10-EpoME) were enriched in the sEH inhibitor-treated group of M2c macrophages (Figure 36d).

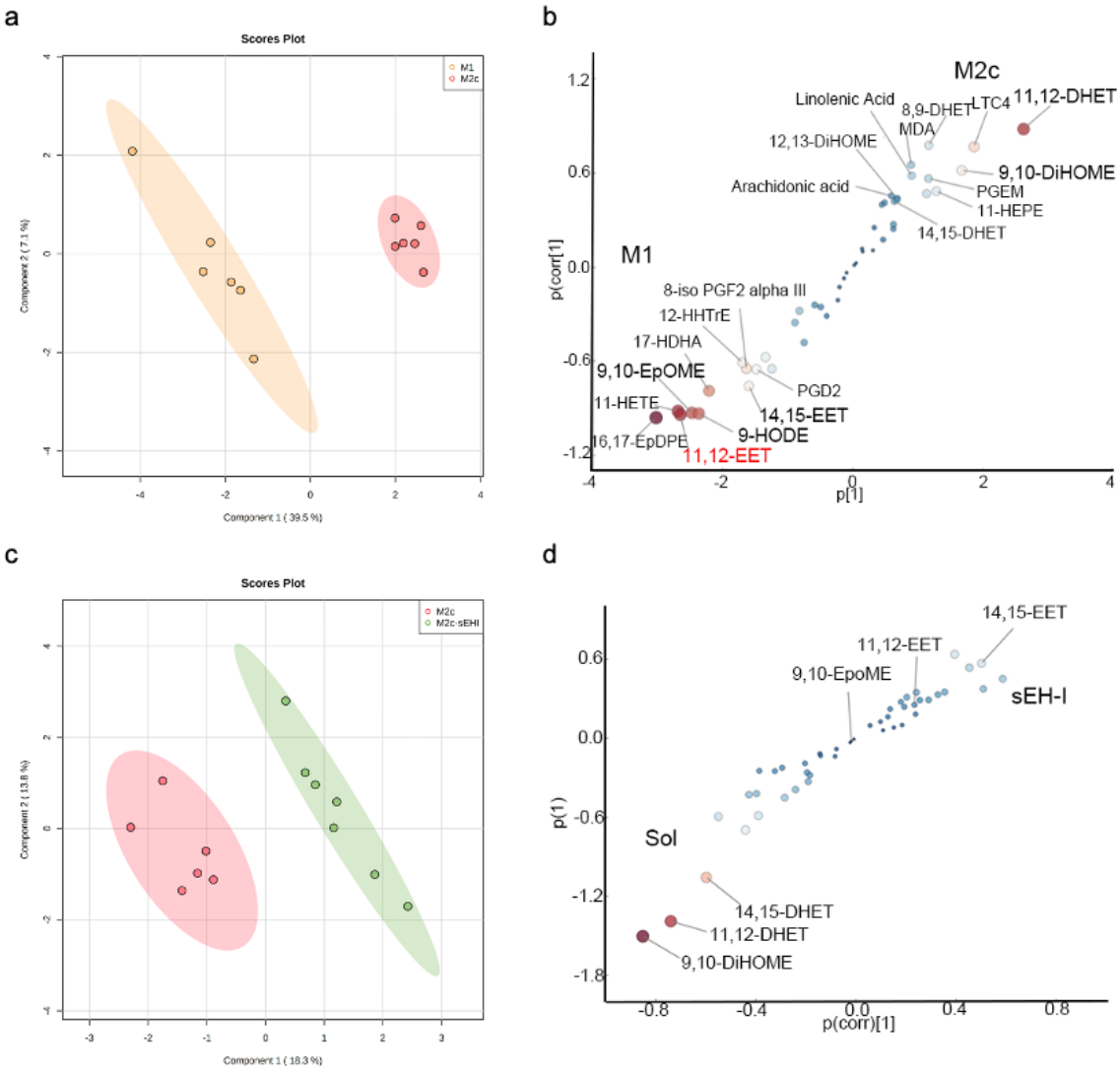

Figure 36. lipid profile analysis of human M1 and M2c macrophages, as well as M2c macrophages treated with sEH inhibitor or solvent. (a) PCA of lipid profile data from human M1 and M2c macrophages. (b) S-plot comparison showing the most significant changed fatty acids in M1 and M2c macrophages from human. (c) PCA of lipid profile data from M2c macrophages treated with solvent (0.1%DMSO) and t-AUCB (10 μmol/L). (d) S-plot comparing the most significant changed fatty acids in M2c macrophages from solvent (Sol) and sEH inhibitor (sEH-I) treated group.

4.14 Effects of lipids on M2c macrophage polarization

Next, we investigated the influence of the AA epoxide 11,12-EET and the linoleic acid (LA) epoxide 9,10-EpOME as well as their corresponding diols on M2c macrophage polarization. Among those significantly changed lipids, 11,12-EET was found to notably inhibited the polarization of M2c macrophages, as evidenced by reduced levels of Tlr2 and increased levels of Nlrp3 (Figure 37a). Importantly, we also observed that the impact of 11,12-EET on the expression of Tlr2 and Nlrp3 was further attenuated by the EET antagonist14,15-epoxyeicosa-5(Z)-enoic acid (EEZE) (Figure 37b). These data imply that the action of 11,12-EET relied on a yet to be defined 11,12-EET-related receptors.

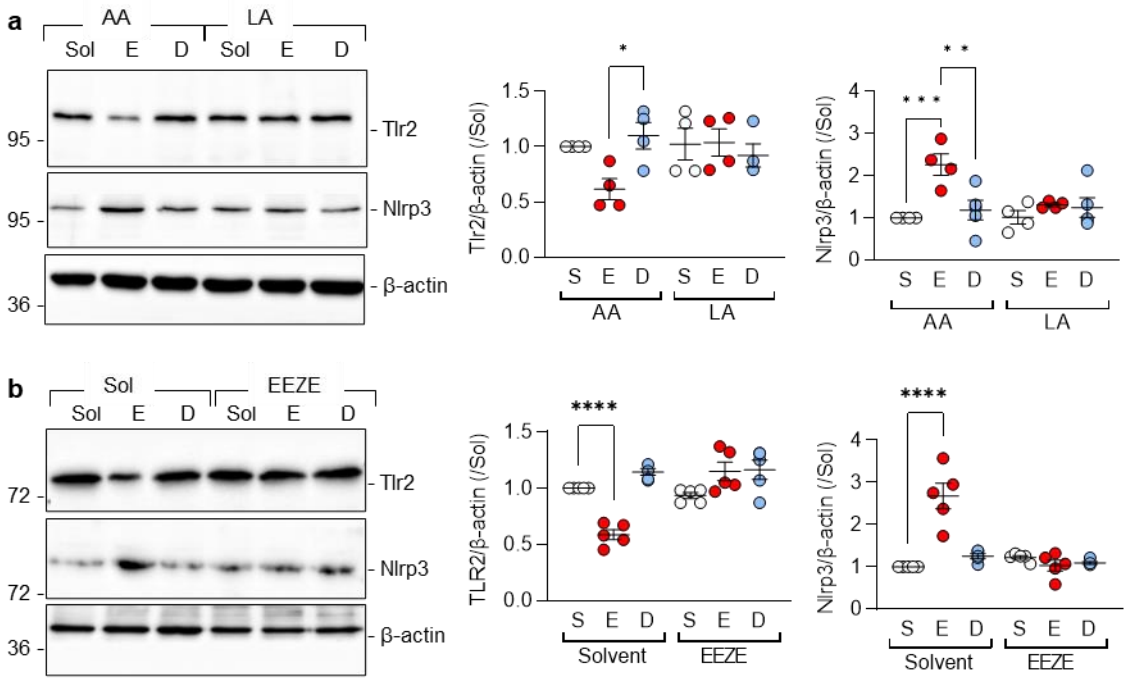

Figure 37. Effects of altered PUFA epoxides and diols on Tlr2 and Nlrp3 expression in human macrophages. (a) The expression of Tlr2 and Nlrp3 was assessed in polarized M1 macrophages treated with 11,12-EET (1 µmol/L), 11,12-DHET (1 µmol/L), 9,10-EpOME (1 µmol/L), and 9,10-DiHOME (1 µmol/L) for 48 hours (n=4 independent experiments). (b) The expression of Tlr2 and Nlrp3 was examined in polarized M1 macrophages treated with 11,12-EET (1 µmol/L), 11,12-DHET (1 µM), in the presence of solvent (Sol) or the EET antagonist, EEZE (3 µmol/L, administered 30 minutes before adding EET/DHET), for 48 hours (n=4 independent experiments). Statistical analysis was conducted using two-way ANOVA followed by Sidak's multiple comparison test. (*P<0.05, **P<0.01, ***P<0.001, ****P<0.0001).

4.15 PPAR-γ activity in differentially polarized macrophages from wild-type and sEH-/- mice

We aimed to investigate whether mediators known to regulate PPAR-γ were implicated in the TGF-β-regulation of PPAR-γ levels and gene expression. We focused on the role of sEH, metabolizes the PPAR-γ activator; 11,12-EET, into its less active diol; 11,12-DHET, given that arachidonic acid metabolism was one of the pathways altered by TGF-β (see Figure 38c), and sEH inhibition prevents the development of atherosclerosis in animal models [114,115]. To this end, a luciferase construct containing three PPAR-γ responsive elements was expressed in macrophages from wild-type mice that were then polarized to the M0, M1 and M2c phenotypes. Consistent with the increase in PPAR-γ protein levels, luciferase activity was significantly increased in the M2c macrophages from wild-type mice (Figure 38a). Deletion of the sEH significantly blunted the latter response and was reflected in the differential expression of PPAR-γ-regulated genes in M2c macrophages from the two genotypes (Figure 38c). Indeed, the well characterized PPAR-γ-regulated genes Gipr, Vldlr and Rbp1 were all expressed at significantly lower levels in M2c macrophages from sEH-/- versus wild-type mice. The levels of a series of fatty acid epoxides are metabolized by the sEH but it was possible to demonstrate higher 11,12-EET and lower 11,12-DHET levels in M2c polarized macrophages from sEH-/- versus wild-type mice (Figure 38c). Furthermore, treatment of M1 polarized macrophages from wild-type mice with 11,12-EET (1 µmol/L) prior to the repolarization with TGF-β, also decreased PPAR-γ activity (Figure 38d).

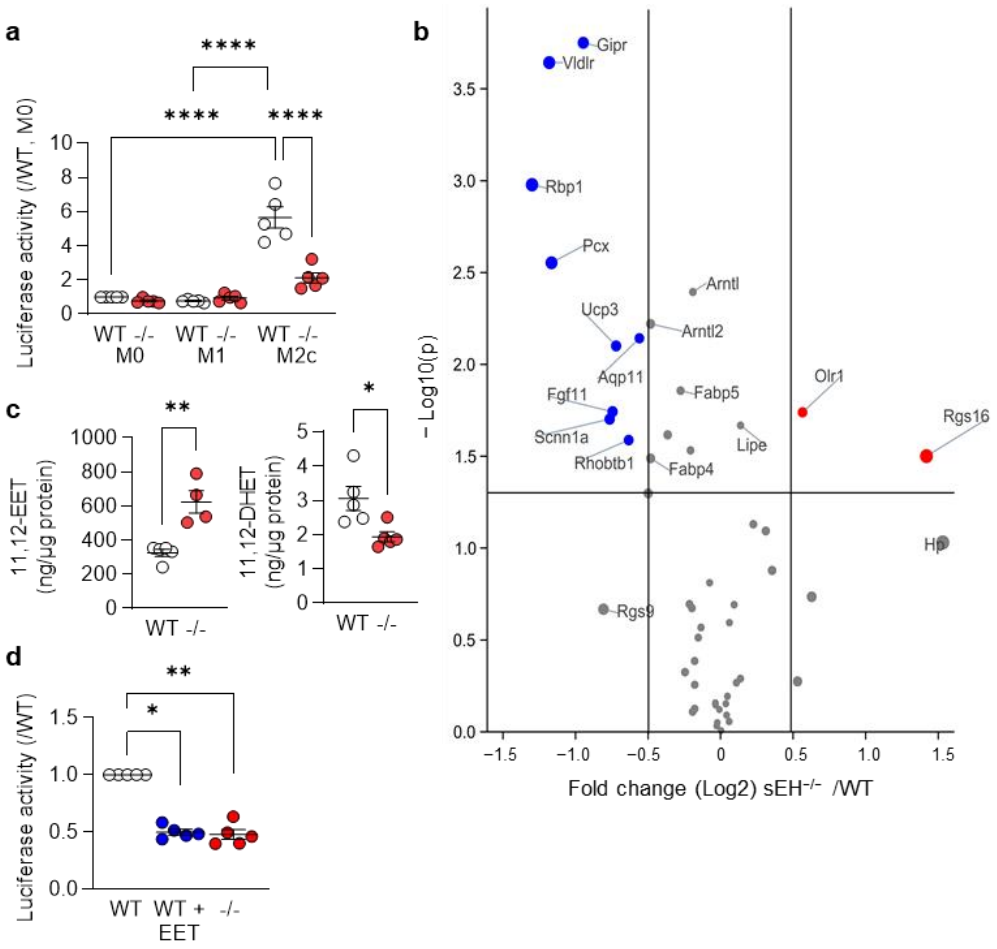

Figure 38. PPAR-γ activity in differentially polarized macrophages from wild-type and sEH-/- mice. (a) Activity of a PPAR-γ-luciferase construct in M0, M1 and M2c macrophages from wild-type (WT) and sEH-/- mice; n=5/group (two-way ANOVA and Tukey's multiple comparisons test). (b) Volcano plot showing the expression of known PPAR-γ-regulated genes in M2c macrophages from wild-type (WT) and sEH-/- mice. Dataset as in Figure. 1; n=4/group. Blue = genes significantly downregulated and red = genes significantly upregulated in sEH-/- mice versus wild-type. Grey indicates no significant alteration. (c) 11,12-EET and 11,12-DHET levels in M2c macrophages from wild type and sEH-/- (-/-) mice (n=5/group; Student's t test). (d) PPAR-γ activity in M2c polarized macrophages from wild-type mice with solvent or 11,12-EET (1 µmol/L, 30 min prior to TGF-β). Solvent-treated cells from sEH-/- mice were included as control; n=5/group (Kruskal-Wallis test followed and Dunn's multiple comparison test). *P<0.05, **P<0.01, ****P<0.0001.

4.16 Regulation of PPAR-γ levels by 11,12-EET

The sEH substrate, 11,12-EET, effectively prevented the TGF-β-induced elevation in PPAR-γ protein levels in murine macrophages (Figure 39a), whereas the sEH product, 11,12-DHET, demonstrated no impact. Interestingly, 11,12-EET induced alteration of PPAR-γ protein levels without affecting Pparg gene expression (Figure 39b), indicating a potential effect on the stability of the PPAR-γ protein. Previous studies in adipocytes have revealed that ligand-dependent PPAR-γ activation is associated with its subsequent proteasomal degradation [116]. Th, we performed experiments in the absence and present of the proteasome inhibitor MG132 (2 µmol/L) to determine whether 11,12-EET decreased PPAR-γ levels by stimulating its proteasomal degradation. 11,12-EET, but not 11,12-DHET, decreased PPAR-γ protein levels in M2c polarized macrophages, and proteasome inhibition prevented the effect (Figure 39c).

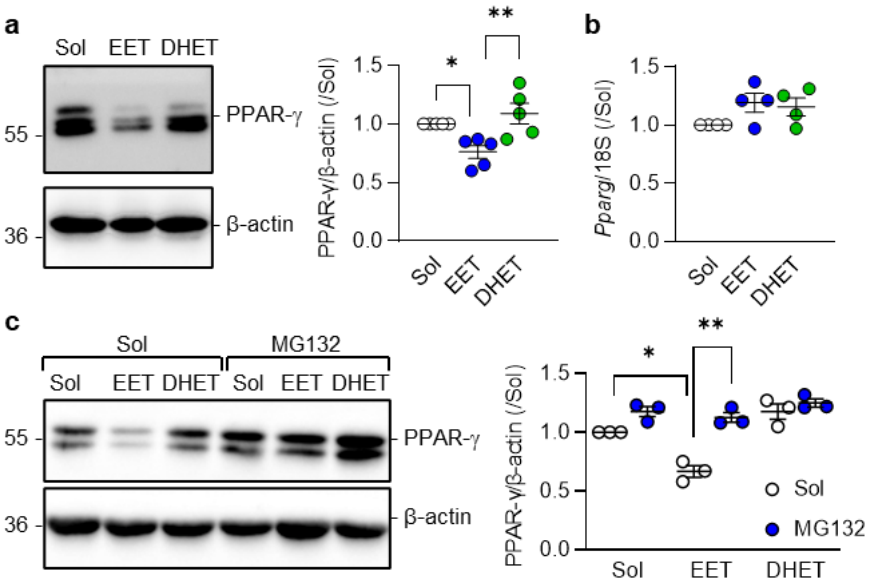

Figure 39. Regulation of PPAR-γ levels by 11,12-EET and 11,12-DHET in M2c polarized macrophages. (a) Impact of solvent (Sol, 0.1% DMSO), 11,12-EET or 11,12-DHET (both 1 µmol/L; 30 minutes prior to TGF-β) on the expression of PPAR-γ in M2c polarized macrophages (n=5 independent experiments, Kruskal-Wallis test followed and Dunn's multiple comparison test). (b) PPAR-γ mRNA levels in cells treated with solvent, 11,12-EET and 11,12-DHET as in panel a (n=4/group, one way ANOVA and Tukey's multiple comparisons test). (c) Consequence of inhibiting protein degradation using MG132 (2 µmol/L) on PPAR-γ protein stability in M2c polarized macrophages treated with solvent (Sol, 0.1% DMSO), 11,12-EET or 11,12-DHET (both 1 µmol/L) prior to the addition of TGF-β (n=3/group, two way ANOVA and Sidak's multiple comparisons test). *P<0.05, **P<0.01.

Our findings differ from those of previous studies regarding the activation of PPAR-γ by 11,12-EET [117–120]. To gain a better understanding, additional investigation is necessary to determine whether the effects of 11,12-EET on PPAR-γ stability or activity are time-dependent. To examine this, HEK293 cells expressing PPAR-γ reporter constructs were treated with 11,12-EET (1 µmol/L) or a solvent control to evaluate PPAR-γ activity on such conditions. The control group exhibited no significant changes over time, while the pioglitazone-treated group showed increased PPAR-γ activity after 12 hours, that was sustained for an additional 24 hours (Figure 40). 11,12-EET, on the other hand, initially increased PPAR-γ activity after 12 hours, but the levels subsequently decreased over the next 36 hours (Figure 40). These findings suggests that 11,12-EET may initially

bind to and activate PPAR-γ and subsequently reduce its expression through proteasomal degradation.

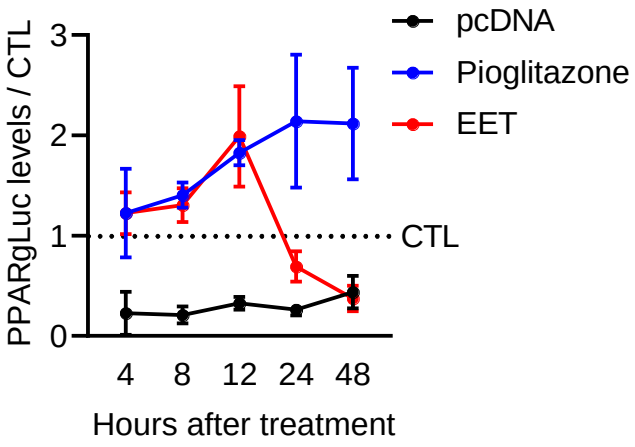

Figure 40. Impact of 11,12-EET on PPAR-γ activity in HEK cells. HEK cells were transfected with a PPAR-γ luciferase constructs. After 24 hours, HEK cells were treated with solvent (0.1% DMSO), 11,12-EET (1 μmol/L), or the PPAR-γ agonist (pioglitazone, 10 μmol/L) for indicated time (n=3 independent experiments). The luciferase activity was the measured based on the manual provide as described as Figure 20

Taken together, our study investigated the role of sEH in regulating the resolution of inflammation through macrophage polarization. We found that TGF-β1 plays a critical role in resolving inflammation by increasing sEH expression in macrophages. Depleting sEH led to reduced phagocytic capacity, delayed resolution of inflammation by decreasing the expression of phagocytic receptors Mrc1 and Tlr2, and increased expression of inflammatory markers Il1b and Nlrp3. Repolarization from M1 to M2c macrophages depended on elevated expression and activation of PPAR-γ. In vivo studies using a zymosan-induced sterile resolving peritonitis model showed that the absence of sEH significantly hindered phagocytic capacity, preventing the upregulation of scavenger receptor expression necessary for phagocytosis and efferocytosis, ultimately leading to delayed resolution of inflammation. Interestingly, we observed that 11,12-EET specifically attenuated M2c macrophages by suppressing Tlr2 expression while increasing Nlrp3 expression. The potential mechanism involves short-term activation of PPAR-γ by the

sEH substrate 11,12-EET, followed by reduced long-term activation, possibly due to proteasomal degradation.

4.17 Astrocyte isolation and verification

Given that macrophage and astrocyte share similar functions, we decided to determine whether TGF-β Like macrophages, astrocytes can be categorized into distinct phenotypes, including A0, A1, and A2, which exhibit non-reactive, reactive, and protective effects, respectively.

Astrocytes were isolated from postnatal pups younger than 7 days, and further purification was performed using a Percoll gradient. The resulting cell gradient was obtained, with microglia at the bottom, astrocytes in the middle, and myelin layers at the top Figure 41. To verify the purity of the astrocytes obtained, the cells were stained with astrocytes-specific markers GFAP and ALDH1L1, as well as microglia marker F4/80 (Figure 42). The majority of the cells isolated were GFAP and ALDH1L1 positive, while F4/80 staining was mostly negative indicating sufficient astrocytes purity for subsequent experiments.

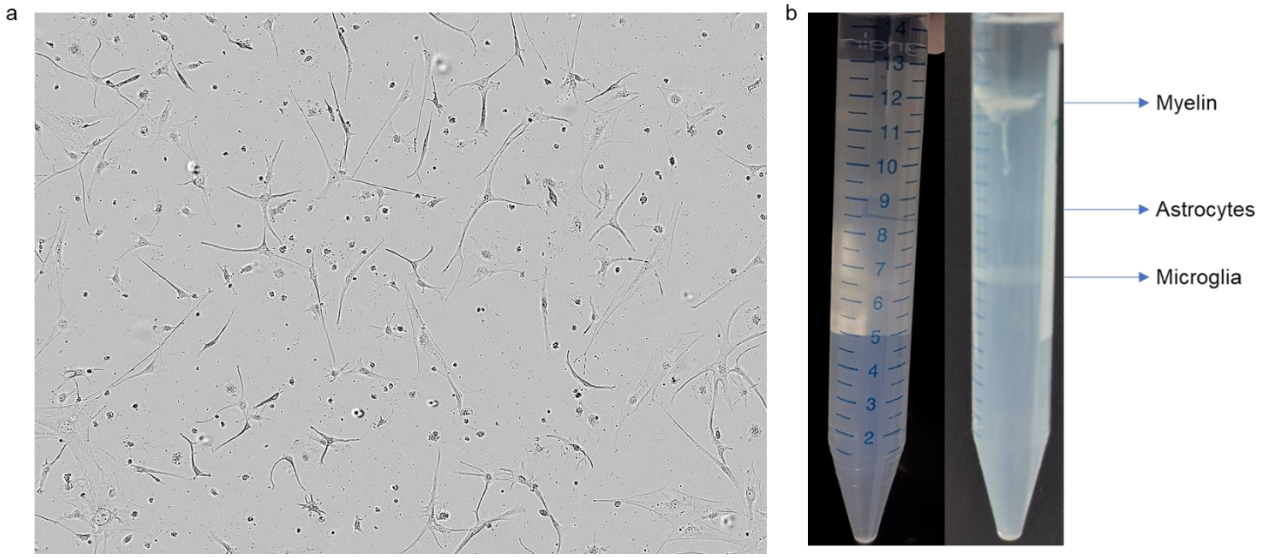

Figure 41. Isolation and primary cultured astrocytes. (a) Cultured astrocytes seen through light micro. (b) Isolation of astrocytes using the Percoll gradient centrifugation. from top to bottom is myelin, astrocytes and microglia. The gradient is composed of, from bottom to top, 6 ml 70% Percoll, 3 ml 50% Percoll, 3 ml 35% Percoll and 2 ml 1XPBS in 15 ml Falcon tube.

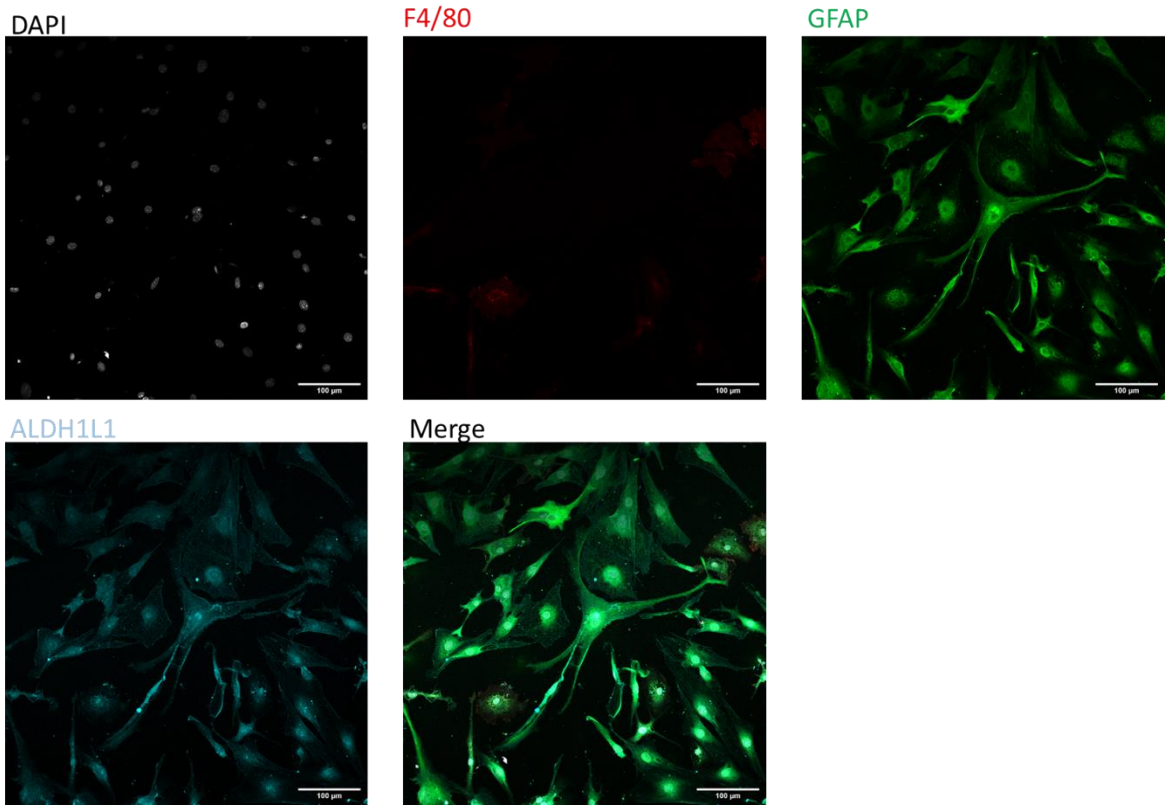

Figure 42. Immunostaining of astrocytes after Percoll purification, cells were stained with DAPI, F4/80, GFAP and ALDH1L1. Astrocytes (P1) were seeded in ibidi cell culture slides. After 36 hours, the cells were blocked with 3% BSA in PBS for 2 hours and stained with F4/80, GFAP, and ALDH1L1 antibodies overnight at 4 degrees on a shaker. The cells were then washed with PBS and incubated with corresponding secondary antibodies and DAPI (1:200) for 2 hours at room temperature before visualizing the cells under a microscope. Comparable results were obtained in the additional cell batches

4.18 TGF-β increases sEH expression in astrocytes

sEH is reported to be highly expressed in astrocytes [84–86], however as the expression stability in culture was not clear. Therefore, we assessed the sEH levels in astrocytes under basal cultural conditions and following treatment with TGF-β1. We found that sEH was highly expressed in cultured astrocytes and that TGF-β1 treatment led to a significant increase in sEH expression in a dose-dependent manner (Figure 43a and b). Similar to macrophages, TGF-β stimulation of astrocytes resulted in the upregulation of the ALK5/pSMAD2 target gene Snail, while the level of ALK1/pSMAD1/5 target gene Id3 remained unchanged (Figure 43 c and d). Furthermore, we found that the upregulation of

sEH was Alk5-dependent, as inhibition of Alk5 completely attenuated the effects of TGF-β on sEH expression (Figure 43e). The inhibition of ALK1 had no effect (Figure 43e).

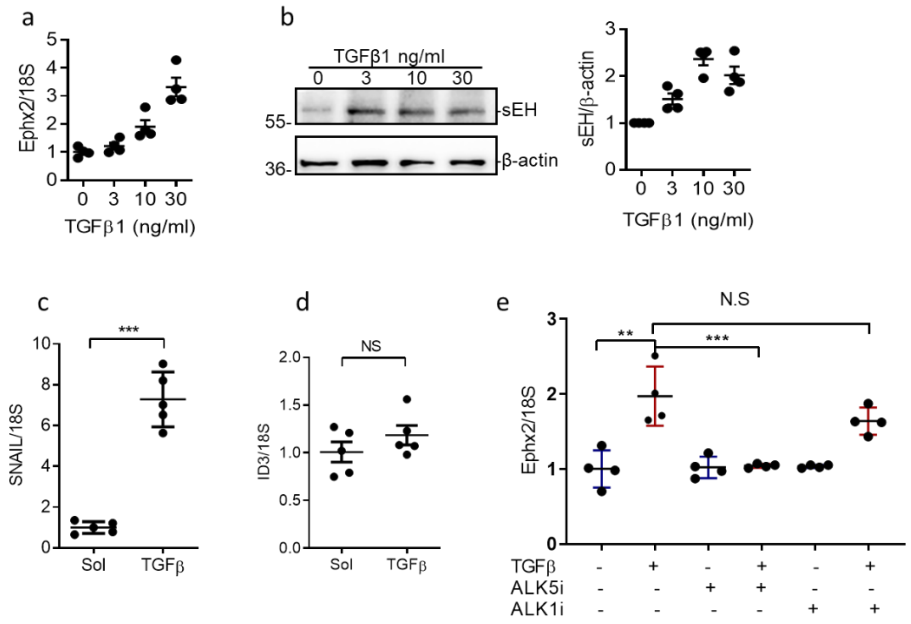

Figure 43. Consequences of TGF-β1 on sEH expression in cultured astrocytes. (a&b) Effect of TGF-β1 on sEH expression in astrocytes, astrocytes were exposed to solvent or different concentration of TGF-β1 (0-30 ng/ml) in mRNA (a, n=4 independent experiments) and protein level (b, n=4 independent experiments) in 24 hours. (c&d) Effects of TGF-β1 on Snail and Id3 expression in astrocytes treated with 10 ng/ml TGF-β1 for 24 hours (n=5, independent experiments). (e) Effects of Alk5 and Alk1 inhibition on TGF-β1-induced sEH expression (n=4, independent experiments, one-way ANOVA followed by Turkey's multiple comparison). *P<0.05, **P<0.01, ***P<0.001, ****P<0.0001.

4.18 sEH deletion attenuated the activation of A1 astrocytes in vitro and in vivo

TGF-β is involved in the transition from a neurotoxic A1 astrocyte to an inactivate A0 astrocytes (101). In astrocytes from wild-type mice, TGF-β attenuated the expression of the pan-reactive astrocyte marker Gfap, as well as A1-specific markers such as Ligp1, Serping1, Amigo2, H2d1, H2t23, and C3d (Figure 44a). However, it had no effect on the A2 astrocyte markers such as Emp2, S100a10, and Ptx3 (Figure 44a). Importantly, inhibition or deletion of sEH reduced the expression of GFAP and A1-specific markers in vitro (Figure 44a). Interestingly, the combination of sEH inhibitor and TGF-β further increased the expression of A2 astrocyte markers, including Emp2, S100a10, and Ptx3

(Figure 44a). This suggests that sEH deficiency attenuates A1 astrocyte activation and enhances A2 astrocyte activation (Figure 44b). The TGF-β induced expression of the sEH blocked the transition from A0 astrocytes to A2 astrocytes (Figure 44b). The protein level of C3d, a marker of A1 astrocytes, was significantly lower in astrocytes from $sEH^{-/-}$ mice (Figure 44c). We observed a similar phenotype in the brain cortex of wild-type and $sEH^{-/-}$ mice, with lower expression of A1 markers and higher expression of A2 markers at the mRNA level (Figure 45a). Protein level analysis was performed for pan-reactive marker GFAP, ALDH1L1, and A1 marker C3d (Figure 45b), revealing significantly lower expression of these markers in the cortex of $sEH^{-/-}$ mice.

To further investigate this phenomenon, we examined the phagocytic activity of astrocytes. Previous studies have demonstrated that A1 astrocytes exhibit reduced phagocytic activity, and we observed a similar trend in sEH-deleted astrocytes, which displayed enhanced uptake of Aβ42, Aβ40, ox-LDL, zymosan, E. coli (bacterial), and zymosan particles (Figure 46).

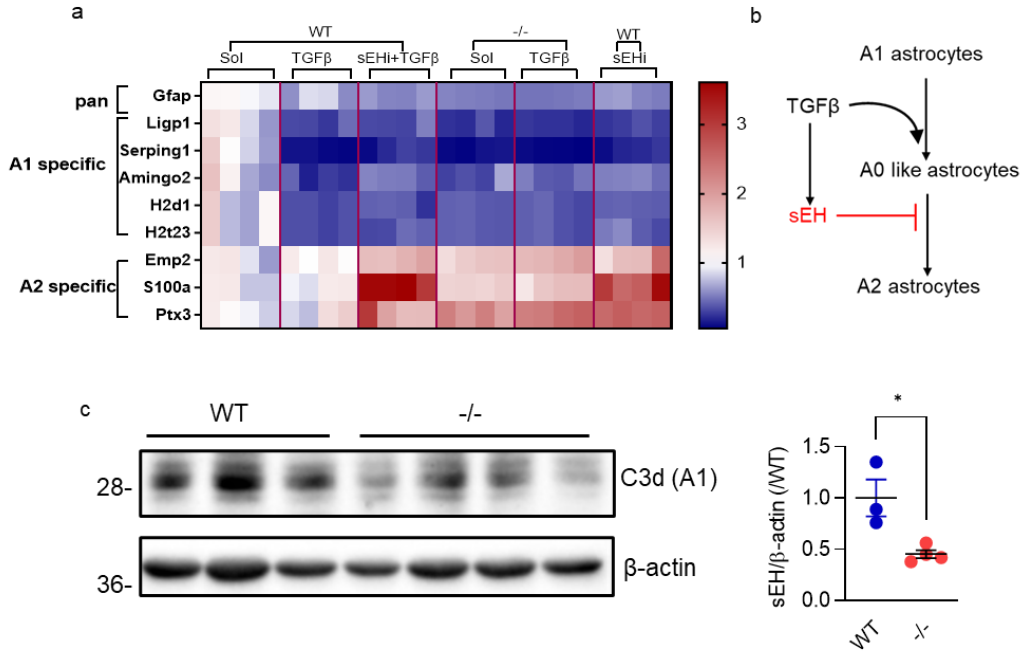

Figure 44. Effect of sEH and TGF-β1 on astrocyte polarization in vitro. (a) effects of TGF-β1 (10 ng/ml, 24 hours), sEH knockout and sEH inhibitor (t-AUCB, 10 μM, 24 hours) on the expression of pan-reactive astrocytes marker (Gfap), A1 specific markers (Ligp1, Serping1, Amigo2, H2d1, H2t23), and A2 specific markers (Emp2, S100a, Ptx3) expression. (b) Proposed mechanism of the role of sEH in astrocytes heterogeneity. (c) effects of sEH deletion on the expression of A1 specific marker C3d expression (n=3-4 independent experiments, Student's test). *P<0.05

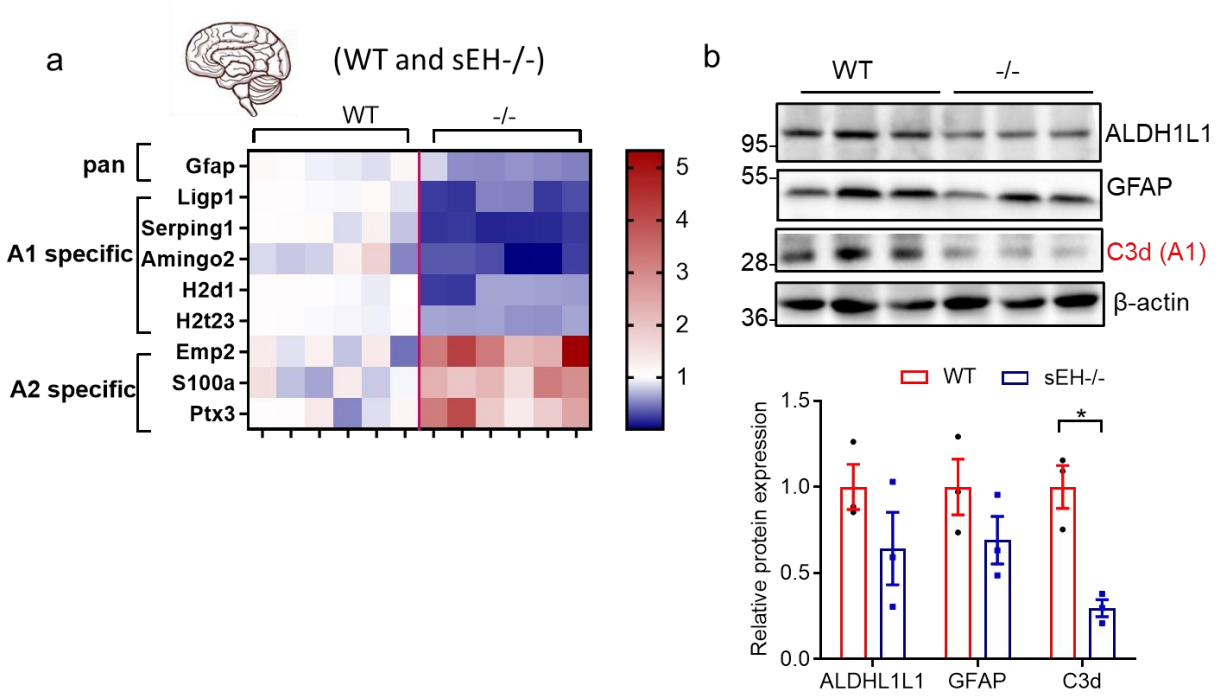

Figure 45. Effects of sEH on astrocyte marker expression in the brain tissue. (a) Expression of pan-reactive, A1-specific and A2-specific markers in the cortex from wild-type and sEHKO mice (8-10 week-old) which was generated by qRT-PCR (n=6 independent experiments). (b) Western blot analysis of astrocytes-specific markers in the cortex from wild-type and $sEH^{-/-}$ mice at 10 week-old (n=3 independent experiments, Student's test). *P<0.05.

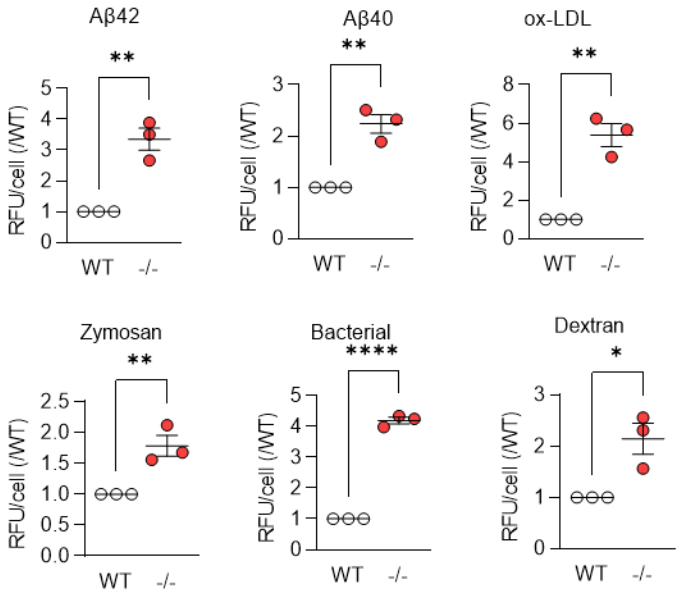

Figure 46. Effects of sEH knockout on the phagocytosis functions. Uptake of Aβ42, Aβ40, ox-LDL, Zymosan, Bacterila (E. coli, 10 μg/mL) and Dextran in the isolated astrocytes from wild-type (WT) and $sEH^{-/-}$ (-/-) mice. The isolated cells were applied for florescent labelled Aβ42 (10 μM), Aβ40 (10 μM), ox-LDL (2 μg/ml), bacterial (E.coli, 10 μg/mL) and zymosan (10 μg/mL), dextan (2 μmol/L) for 30 min and measured in florescent plate reader. (n=3 independent experiments, Student's test). *P<0.05, **P<0.01, ****P<0.001

4.20 sEH expression is increased in APP/PS1 mice around the plaque

Given our findings on the altered uptake of Aβ42 and Aβ40 by astrocytes, we set out to explore the potential involvement of sEH in Alzheimer's diseases. At 6 months of age, APP/PS1 mice display amyloid plaque formation, a marker of Alzheimer's disease development (Figure 47a). Significantly, we observed increased expression of sEH in the vicinity of the amyloid plaque area, accompanied by highly reactive astrocytes, as indicated by elevated levels of GFAP (Figure 47a). Western blotting assays further confirmed the elevated expression of sEH (Figure 47b). Interestingly, we also identified the phosphorylation of SMAD2 and a decrease in PPAR-γ expression in the cortex of 6-month-old APP/PS1 mice (Figure 48).

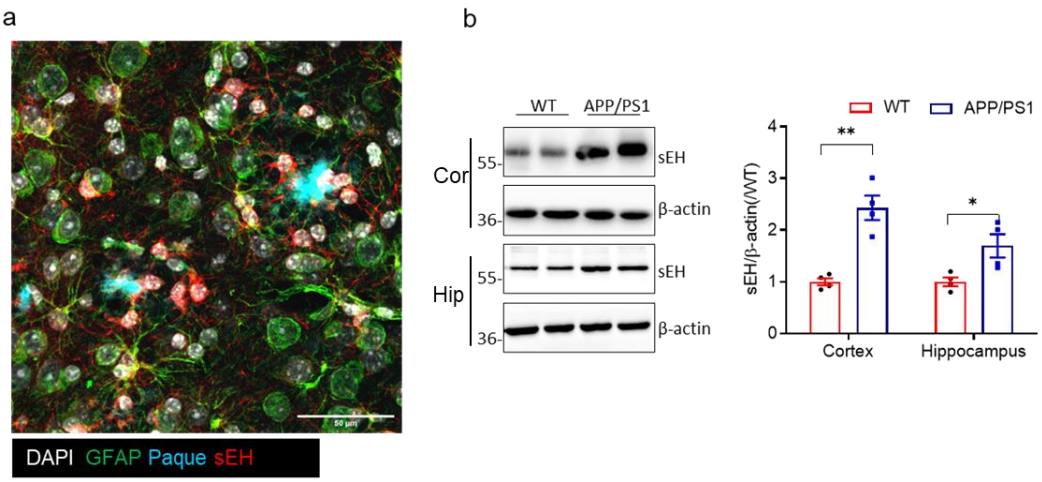

Figure 47. Expression of sEH in APP/PS1 mice. a) Immunol staining of the brain paraffin slides from 6-months-old, GFAP indicates the reactive astrocytes, Plaque was visualized with Congo red and Sudan Black staining. b) Western blotting analysis of the expression of sEH in the cortex (Cor, upper panel) and hippocampus (Hip, lower panel) from 6-month-old female mice.

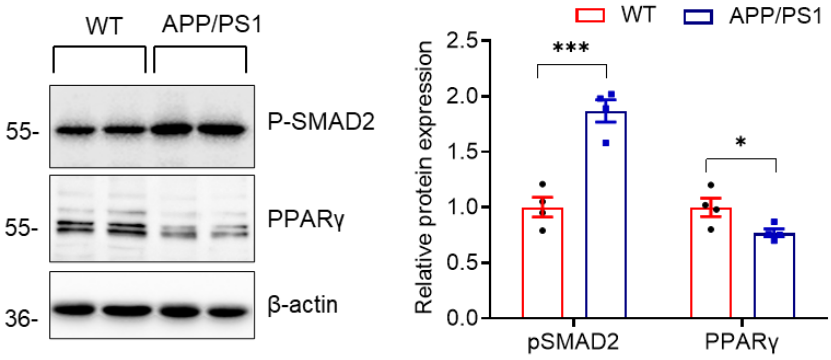

Figure 48. Expression of pSMAD2 and PPAR-γ in the cortex from APP/PS1 mice at 6-month-old from female mice. n=4 for each group and Student's test was used to compare the difference between each group. *P<0.05, ***P<0.001

Taken together, our findings revealed the crucial involvement of TGF-β1 in astrocyte activation, as it upregulates sEH expression by activating the Alk5 receptor and Smad2/3/4 to the sEH promoter. Inhibiting or deleting sEH promotes the transition of A1 astrocytes to A0 and subsequently to A2 astrocytes, indicating the protective functions associated with sEH inhibition or deletion. Lower sEH levels enhance astrocytes phagocytosis, leading to increased uptake of various substances. Additionally, we observed elevated sEH expression in a murine model of Alzheimer's diseases, along with increased pSMAD2 expression and reduced PPAR-γ levels, aligning with our findings in macrophages.

5. Discussion

5.1 sEH in macrophages

The results of this investigation revealed that TGF-β1 is critical for resolution of inflammation by upregulating sEH expression in macrophages. This upregulation of sEH expression occurs through activation of the Alk5 receptor and binding of Smad2/3/4 to the sEH promoter. Depletion of sEH resulted in reduced phagocytic capacity, delayed resolution of inflammation, decreased expression of phagocytic receptors Mrc1 and Tlr2, and increased expression of inflammatory markers Il1b and Nlrp3. In addition, we found that the repolarization of M1 to M2c macrophages relies on increased expression and activation of PPAR-γ. Inhibition of PPAR-γ had similar effects to sEH inhibition in attenuating M2c macrophage polarization. Furthermore, PPAR-γ expression is dependent on the activation of TGF-β signaling. In vivo studies using a sterile resolving peritonitis model (zymosan-induced) showed that the absence of sEH significantly reduced phagocytic capacity by preventing the upregulation of scavenger receptor expression necessary for phagocytosis and efferocytosis, ultimately leading to delayed resolution of inflammation. Lipid profile analysis showed that M1 to M2c macrophage polarization is associated with decreased levels of sEH substrates (e.g., 11,12-EET,14,15-EET, 9,10-EpOME) and increased levels of sEH products (e.g., 11,12-DHET, 14.15-DHET, 9,10-DiHOME). Interestingly, we only observed that 11,12-EET attenuated M2c macrophages by suppressing the expression of the M2c macrophage marker Tlr2 while increasing the expression of Nlrp3. We discovered that the mechanism involves short-term activation of PPAR-γ by the sEH substrate 11,12-EET, followed by reduced long-term activation, possibly due to proteasomal degradation.

Numerous studies have investigated the anti-inflammatory effects of EETs and sEH inhibition in various inflamed tissues [52,53,54,55]. In the zymosan-induced peritonitis model, neutrophilia serves as a crucial marker for initiating acute inflammatory responses, followed by a gradual decrease in neutrophil numbers during inflammation resolution [121]. In our research, we found that the mice lacking show a slight reduction in neutrophil infiltration on day 1, indicating that inhibiting or deleting sEH attenuates the inflammatory

response. This finding is consistent with observations in a mouse model of hypertoxic acute lung injury and other models [138,124]. Furthermore, our in vitro study demonstrated that sEH deficiency diminishes M1 macrophage polarization, leading to decreased expression of pro-inflammatory markers like Tnfa, Il1b, and Nos2. This anti-inflammatory effect is likely mediated by increased activation of PPAR-γ or inhibition of NF-κB signaling due to elevated epoxide levels, which suppress the expression of pro-inflammatory genes such as VCAM, iNOS, and COX2 [122]. One recent study also indicated that EETs inhibit activation of Nlrp3 inflammation in murine macrophages and attenuated the production of IL-1β [123]. Additionally, the deficiency of sEH may also reduce reactive oxygen species (ROS) generation, a pivotal factor in the development of inflammatory disorders, which therefore attenuates mice hyperoxic acute lung injury [108]. ROS generated by polymorphonuclear neutrophils at inflammatory sites cause tissue injury and endothelial dysfunction [124].

Inhibition of CYP enzymes, that are upstream of sEH, can hinder the resolution of inflammation by disrupting Ly6c+ monocyte infiltration, thus affecting the pro-resolving phenotype of monocyte lineage cells and reducing macrophage efferocytosis [125]. Conversely, the absent of sEH exhibited the opposite effect, highlighting the anti-inflammatory properties associated with sEH deficiency [127]. Importantly, a more pronounced effect was observed in later stages, as sEH-deficient mice exhibited incomplete or delayed resolution of inflammation in vivo in our study. This was evidenced by a reduction in resident macrophages, recruited macrophages, dendritic cells levels as well as reduced expression of phagocytic and efferocytosis markers such as Mrc1, Tlr2 and Mertk which serve as key mediators in the resolution of inflammation phases.

Alternatively activated M2 macrophages play a crucial role in attenuating inflammation responses, clearing apoptotic cells and promoting tissue repair [126,127]. Although the classification and definition of macrophage subtypes is continuously evolving, M2c macrophages induced by TGF-β, characterized by specific gene expression profiles, are particularly important for resolution of inflammation due to their phagocytic and efferocytosis [58]. In our study, we employed RNA-seq to investigate the gene expression profile of M2c macrophages and examine the influence of sEH activity. The absence of sEH resulted in elevated levels of Nlrp3, iNos, Tnfα, and IL-1β, which are components

associated with inflammasome activation and pro-inflammatory responses. Conversely, the expression of several scavenger receptors essential for phagocytosis and efferocytosis (Tlr2, Cd206/Mrc1, Cd163, Mertk) was reduced. Comparable effects on Tlr2 and Mrc1 protein expression were observed in macrophages from wild-type mice treated with an sEH inhibitor. Furthermore, M2c macrophages derived from sEH-deficient mice exhibited increased levels of Tlr2 and Mrc1 upon overexpression of wild-type sEH but not an enzymatically inactive mutant. Consistent with the delayed resolution phenotype observed in vivo, sEH-deficient macrophages displayed decreased efficiency in phagocytosing zymosan and ox-LDL compared to wild-type cells.

A more recent study has demonstrated that the sEH promoted macrophages phagocytosis and clearance of Streptococcus pneumoniae through the regulation of Tlr2 and peptidoglycan recognition protein 1 (PGLYRP1) expression [128]. Similar to our observation, we also found that sEH is required for M2c macrophages polarization and resolution of inflammation by regulating the expression of Tlr2 and Mrc1. The difference regarding the receptors involved in clearance of Streptococcus pneumoniae and our zymosan-induced peritonitis model is probably due to the different expression level of corresponding receptors in these tissues.

sEH expression has been reported to be regulated at physiological and pathological conditions such as increased blood pressure and diabetic retinopathy [98], Alzheimer's disease etc. [77,84], however, the underlying mechanisms are poorly understood. Previous studies have suggested the involvement of SP1 in enhancing Ephx2 reporter activity and the regulation of sEH levels through AP-1 activation in angiotensin II (Ang II)-treated endothelial cells and rat hearts following ischemia-reperfusion [129]. Gender differences in sEH also has been addressed in our study, male mice expressing higher sEH levels and experiencing blood pressure reduction upon sEH inhibition [130]. Female-specific down-regulation of sEH expression is linked to estrogen-dependent methylation of the Ephx2 gene, leading to reduced binding of Sp1, AP-1, and NF-κB to the promoter [101]. We also observed that the macrophages from female mice are more sensitive to TGF-β stimulation at least as for expression of sEH.

In our study, we demonstrated that TGF-β1 signaling and pSmad2, rather than Sp1, significantly regulate sEH expression in macrophages. In addition, sEH expression is also regulated by Ang II in human umbilical vein endothelial cells (HUVECs) and bovine aortic endothelial cells (BAECs) via an AP-1-dependent mechanism [131]. Activation of the ALK5/pSMAD2 pathway by Ang II and homocysteine also has been observed in some studies [132] . Leading to the hypothesis that Ang II and homocysteine upregulates the expression of sEH is partially attributed to the activation of pSMAD2 and therefore enhance the transcription of sEH.

To gain a better understanding of the functional implications of sEH deletion in macrophages, we conducted an investigation to detect the levels of specific epoxides and diols in human macrophages that were polarized into M1 and M2c phenotypes. Notably, we observed changes in the levels of 11,12-EET/DHET, 14,15-EET/DHET, and 9,10-EpOME/DiHOME. Interestingly, among these compounds, only 11,12-EET exhibited the ability to downregulate Tlr2 expression and upregulate Nlrp3 expression, exhibiting similarities to the effects observed in M1 polarized macrophages lacking sEH. However, the precise receptor responsible for mediating this process remains unclear.

PPAR-γ, a member of the nuclear receptor superfamily, plays an important role in cell differentiation, maintenance, and function [133]. Serval studies have identified PUFAs as ligands for PPAR-γ [134,135]. Inhibition or deletion of the sEH enzyme results in elevated levels of EETs. In our study, we also observed increased expression of PPAR-γ in M2c macrophages, which was attenuated by ALK5 inhibitor. Moreover, TGF-β-stimulated macrophages from $sEH^{-/-}$ mice exhibited reduced PPAR-γ activity. Our findings, along with the decreased levels of PPAR-γ protein in sEH-deficient macrophages, suggest that 11,12-EET induces a transient increase in PPAR-γ activity, followed by a pathway triggered by EETs that leads to PPAR-γ degradation. This mechanism was confirmed in cells treated with MG132, where PPAR-γ levels remained unaffected by 11,12-EET. This suggests that 11,12-EET may induce proteasomal degradation of PPAR-γ. In adipocytes, PPAR-γ is rapidly degraded through the ubiquitin proteasome pathway, both under basal and ligand-activated conditions [136]. Inhibition of the proteasome enhances PPAR-γ activity, indicating that the ubiquitin proteasome system regulates PPAR-γ activity through its degradation [137]. Although the specific ubiquitin ligase activated by 11,12-EET was

not investigated, there is indirect evidence linking 11,12-EET to increased ubiquitination. For example, overexpression of CYP2J2, an enzyme generating 11,12-EET, in cardiomyocytes has been shown to promote the ubiquitination of the pattern recognition receptor NLRX1 [138].

Taken together, our findings demonstrate that sEH expression and activity are required to promote the resolution of inflammation by regulating the expression of stability of PPAR -γ and thus the gene reprogramming of macrophages induced by TGF-β1. Additionally, our results indicate that the levels of the sEH substrate 11,12-EET in macrophages can influence macrophage polarization by TGF-β, partially through promoting the ubiquitination and degradation of PPAR-γ. Further investigation is still needed to determine the extent to which changes in PPAR-γ expression contribute to the observed phenotype, considering the role of sEH inhibition in preventing atherosclerosis development in mice and the importance of converting inflammatory macrophages to the M2 phenotype in driving atherosclerosis regression.

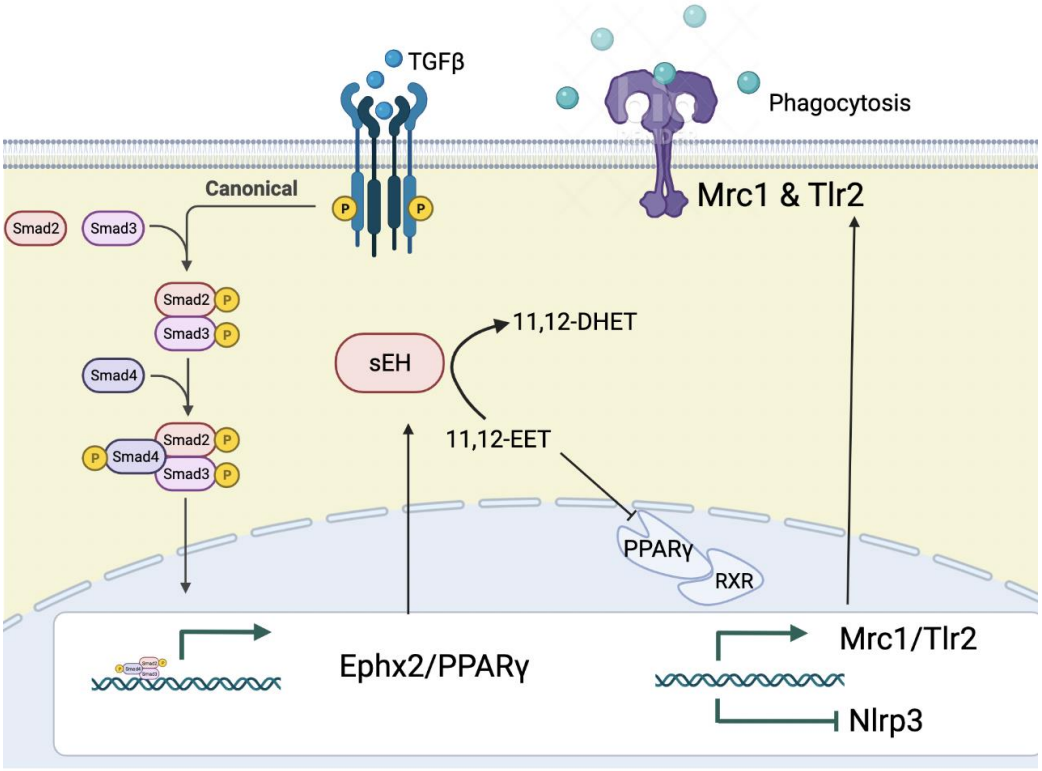

Figure 49. Proposed mechanisms for current studies. TGF-β increases sEH expression via activating Alk5/pSmad2 pathway, therefore increases the transcription of Ephx2 and PPAR-γ. The increased expression of sEH metabolized epoxide like 11,12-EET to 11,12-DHET. 11,12-EET first binds to PPAR-γ but then increased the degradation of PPAR-γ protein by regulating phagocytic receptors Mrc1 and Tlr2, and inflammatory markers Il1b and Nlrp3 expression. The figure was generated via Biorender (https://www.biorender.com/).

5.2 sEH in astrocyte

In our study, we explored the role of sEH in astrocyte activation and polarization. Our findings highlight the critical involvement of TGF-β1 in astrocyte activation, demonstrated by its ability to upregulate sEH expression in astrocytes through the activation of the ALK5 receptor and the binding of SMAD2/3/4 to the sEH promoter. Notably, inhibiting or deleting sEH promotes the transition of A1 astrocytes to A0 and further to A2 astrocytes, indicating the protective functions associated with sEH inhibition or deletion. These findings are consistent with the functional properties of astrocyte, as lower levels of sEH enhance their phagocytic functions, as evidenced by increased uptake of Aβ42, Aβ40, ox-LDL, Zymosan, Bacterial, and Dextran. This suggests that decreased sEH levels align astrocyte functions more closely with the A0 or A2 phenotype. Furthermore, our investigation of Alzheimer's disease (AD) mice and previous studies collectively demonstrate elevated sEH expression in AD mice compared to wild-type mice. Interestingly, these AD mice also exhibit increased pSMAD2 expression and reduced PPAR-γ levels, which are consistent with our findings in macrophages. The activation of the ALK5/pSMAD2 pathway induces sEH expression in astrocytes, both under normal physiological conditions and in pathological contexts.

sEH is an enzyme involved in fatty acid metabolism. Its upregulation in the brain of AD patients suggests its potential involvement in the disease [77,84,88]. Studies have shown that sEH is upregulated in the brains of AD patients and that endocannabinoid metabolism serves as an adaptive response to neuroinflammation [84]. These findings suggest a possible link between sEH and AD pathology. Furthermore, research has indicated that inhibiting sEH could be a novel therapeutic approach for AD [77,84,88]. Genetic deletion of sEH has been demonstrated to delay the progression of the disease, highlighting its potential as a therapeutic target. Additionally, pharmacological inhibition of sEH has shown promise as a therapy for AD [84]. In mouse models of AD, sEH inhibition reduces neuroinflammation, a prominent feature of AD pathology [84].

The upregulation of sEH in the brain of Alzheimer's disease (AD) patients suggests a potential connection between sEH and the disease [77,84,88]. Studies have consistently shown that sEH is elevated in the brains of AD patients, and this upregulation is believed

to be an adaptive response to neuroinflammation through endocannabinoid metabolism [97]. These findings highlight the possibility of sEH's involvement in the pathology of AD. Furthermore, research indicates that targeting sEH could be a promising therapeutic approach for AD [84]. Several studies have investigated the role of sEH in AD and have demonstrated that genetic deletion of sEH can delay the progression of the disease, indicating its potential as a therapeutic target [97]. Additionally, pharmacological inhibition of sEH has shown promise in reducing neuroinflammation, a prominent feature of AD pathology, in mouse models [97]. The upregulation of sEH in the brains of AD patients, its involvement in endocannabinoid metabolism, and the potential benefits of inhibiting sEH through genetic or pharmacological means provide compelling evidence for exploring sEH as a therapeutic target for AD. Further research in this area holds promise for developing novel treatments that can effectively address the neuroinflammatory processes associated with AD.

TGF-β1 has been shown to promote microglia-mediated neuroprotective action of targeting and clearing Aβ plaques through phagocytosis, while its role in blocking clustering of microglia and perpetuation of subsequent inflammation towards Aβ deposits has also been reported [139]. TGF-β1/SMAD signaling is reduced in aging and chronic inflammation, facilitating cytotoxic activation of microglia and microglia-mediated neurodegeneration [139,140]. However, it has also been observed that TGF-β1 induces the expression of sEH in astrocytes. In addition, increased pSmad2 levels have been observed in the AD mice model (APP/PS1), which is different and contradictory to the findings mentioned above. The underlying mechanisms are not clear, but it is possible that this is due to the different time point that we check the activation of pSMAD2 and sEH in the APP/PS1 mouse model [140].

In conclusion, our study elucidates the regulatory role of sEH in astrocyte activation and polarization. The upregulation of sEH by TGF-β1 through ALK5/pSMAD2 activation highlights the complex interplay between signaling pathways and astrocyte function. The observed transitions of astrocytes and the enhanced phagocytic abilities associated with sEH inhibition or deletion provide insights into potential therapeutic strategies for modulating astrocyte phenotypes. Moreover, our findings in AD mice support the relevance of sEH in neurodegenerative diseases. Further investigations are warranted to

fully unravel the underlying mechanisms and to explore the therapeutic potential of targeting the sEH pathway in astrocyte-mediated neuroinflammatory conditions, including Alzheimer's disease.

6. Summary

sEH inhibition has emerged as a promising therapeutic approach with demonstrated benefits in inflammation, pain, chronic obstructive pulmonary disease (COPD), and neural degenerative disease [84,141]. Small molecule inhibitors specifically designed to target sEH have been effective in stabilizing endogenous epoxide levels, modulating their biological activity, and providing relief in preclinical pain models [141,142]. This highlights the potential roles of sEH inhibition in managing pain-related disorders and suggests its utility in mitigating neuroinflammation associated with neurological diseases [141,142]. Efforts to optimize sEH inhibitors have facilitated their use as valuable experimental tools, aiding in the understanding of sEH's role in pathological processes and enabling the development of more precise therapeutic strategies.

Even the role of sEH in the inflammation-associated diseases is relatively clear, its expression regulation remains largely unclear. Immunoblotting and RNA sequencing analysis confirmed the higher level of sEH mRNA and protein in macrophages and astrocytes. TGF-β1 upregulates sEH expression in both cell types which all relied on the activation of the ALK5 receptor and SMAD2/3/4 binding to the sEH promoter increased sEH expression. Depletion of sEH in macrophages resulted in reduced phagocytic capacity, delayed resolution of inflammation, altered expression of phagocytic receptors, and increased inflammatory markers. Elevated sEH expression was also observed in the AD mouse model, aligning with findings in macrophages and suggesting its involvement in neurodegenerative diseases. This indicates the different roles of sEH in different phases of inflammation. In acute inflammation phases, sEH inhibition has contributed to anti-inflammation effects while in the resolution of inflammation inhibition of sEH delayed the resolution of inflammation. This unexpected effect is attributed to elevated levels of 11,12-EET, an sEH substrate, which inhibits the pro-resolving polarization of M2c macrophages by promoting the degradation of the lipid mediator receptor PPAR-γ. The precise mechanism is not fully understood, but it is likely that 11,12-EET initially activates PPAR-γ before inducing its degradation. These findings raise concerns regarding the therapeutic potential of sustained sEH inhibition in conditions where the resolution phase of inflammation is critical, such as Alzheimer's disease, Parkinson's disease, and neural

pain. Prolonged or excessive sEH inhibition may hinder inflammation resolution due to the inhibitory effects of 11,12-EET on pro-resolving M2c macrophage polarization. It challenges the notion that sEH inhibition would be uniformly beneficial throughout all stages of inflammation.

Further research is needed to comprehensively understand the intricate mechanisms underlying the interplay between sEH, 11,12-EET, and inflammation resolution. Specifically, elucidating how 11,12-EET influences PPAR-γ degradation will be crucial for developing targeted therapeutic strategies that balance the anti-inflammatory benefits of sEH inhibition with the resolution-promoting requirements of specific inflammatory conditions. These concerns underscore the importance of carefully evaluating the potential risks and benefits of sEH inhibition as a therapeutic approach in different disease contexts.

7. Zusammenfassung

Die Hemmung von sEH hat sich als vielversprechender therapeutischer Ansatz erwiesen, der nachweislich bei Entzündungen, Schmerzen, chronisch obstruktiven Lungenerkrankungen (COPD) und degenerativen Nervenerkrankungen hilft [84,141]. Kleinmolekulare Inhibitoren, die speziell auf sEH abzielen, haben sich als wirksam erwiesen, indem sie den Gehalt an endogenen Epoxiden stabilisieren, ihre biologische Aktivität modulieren und in präklinischen Schmerzmodellen Linderung verschaffen [141,142]. Dies unterstreicht die potenzielle Rolle der sEH-Hemmung bei der Behandlung schmerzbedingter Erkrankungen und deutet auf ihren Nutzen bei der Abschwächung von Neuroinflammation im Zusammenhang mit neurologischen Erkrankungen hin [141,142]. Die Bemühungen um die Optimierung von sEH-Inhibitoren haben ihre Verwendung als wertvolle experimentelle Werkzeuge erleichtert, was zum Verständnis der Rolle von sEH bei pathologischen Prozessen beiträgt und die Entwicklung präziserer therapeutischer Strategien ermöglicht.

Auch wenn die Rolle von sEH bei entzündungsbedingten Krankheiten relativ klar ist, bleibt die Regulation seiner Expression weitgehend unklar. Immunoblotting- und RNA-Sequenzierungsanalysen bestätigten das höhere Niveau von sEH mRNA und Protein in Makrophagen und Astrozyten. TGF-β1 erhöht die sEH-Expression in beiden Zelltypen, die alle auf die Aktivierung des ALK5-Rezeptors angewiesen sind, und die Bindung von SMAD2/3/4 an den sEH-Promotor erhöht die sEH-Expression. Die Abreicherung von sEH in Makrophagen führte zu einer verringerten phagozytischen Kapazität, einer verzögerten Auflösung der Entzündung, einer veränderten Expression von phagozytischen Rezeptoren und erhöhten Entzündungsmarkern. Eine erhöhte sEH-Expression wurde auch im AD-Mausmodell beobachtet, was mit den Ergebnissen in Makrophagen übereinstimmt und auf eine Beteiligung von sEH an neurodegenerativen Erkrankungen hindeutet. Dies weist auf die unterschiedliche Rolle von sEH in verschiedenen Entzündungsphasen hin. In akuten Entzündungsphasen hat die Hemmung von sEH zu entzündungshemmenden Effekten beigetragen, während die Hemmung von sEH bei der Auflösung der Entzündung die Auflösung der Entzündung verzögerte. Dieser unerwartete Effekt wird auf erhöhte Spiegel von 11,12-EET, einem sEH-Substrat, zurückgeführt, das

die auflösungsfördernde Polarisierung von M2c-Makrophagen hemmt, indem es den Abbau des Lipidmediatorrezeptors PPAR-γ fördert. Der genaue Mechanismus ist noch nicht vollständig geklärt, aber es ist wahrscheinlich, dass 11,12-EET zunächst PPAR-γ aktiviert, bevor es seinen Abbau einleitet. Diese Ergebnisse geben Anlass zu Bedenken hinsichtlich des therapeutischen Potenzials einer anhaltenden sEH-Hemmung bei Erkrankungen, bei denen die Auflösungsphase der Entzündung entscheidend ist, wie z. B. bei der Alzheimer-Krankheit, der Parkinson-Krankheit und Nervenschmerzen. Eine verlängerte oder übermäßige Hemmung von sEH könnte die Auflösung der Entzündung aufgrund der hemmenden Wirkung von 11,12-EET auf die auflösungsfördernde M2c-Makrophagenpolarisation behindern. Dies stellt die Vorstellung in Frage, dass eine sEH-Hemmung in allen Phasen der Entzündung gleichmäßig vorteilhaft wäre.

Weitere Forschungsarbeiten sind erforderlich, um die komplexen Mechanismen zu verstehen, die dem Zusammenspiel zwischen sEH, 11,12-EET und der Entzündungshemmung zugrunde liegen. Insbesondere die Klärung der Frage, wie 11,12-EET den PPAR-γ-Abbau beeinflusst, wird für die Entwicklung gezielter therapeutischer Strategien entscheidend sein, die den entzündungshemmenden Nutzen der sEH-Hemmung mit den auflösungsfördernden Anforderungen spezifischer Entzündungszustände in Einklang bringen. Diese Bedenken unterstreichen, wie wichtig es ist, die potenziellen Risiken und Vorteile der sEH-Hemmung als therapeutischen Ansatz in verschiedenen Krankheitskontexten sorgfältig abzuwägen.

References

1. Ruxton, C.H.S.; Reed, S.C.; Simpson, M.J.A.; Millington, K.J. The health benefits of omega-3 polyunsaturated fatty acids: a review of the evidence. *J. Hum. Nutr. Diet.* **2004**, *17*, 449–459, doi:10.1111/j.1365-277X.2004.00552.x.

2. Simopoulos, A.P. The importance of the ratio of omega-6/omega-3 essential fatty acids. *Biomed. Pharmacother.* **2002**, *56*, 365–379, doi:10.1016/s0753-3322(02)00253-6.

3. Wang, D.; Dubois, R.N. Eicosanoids and cancer. *Nat. Rev. Cancer* **2010**, *10*, 181–193, doi:10.1038/nrc2809.

4. Bahia, M.S.; Katare, Y.K.; Silakari, O.; Vyas, B.; Silakari, P. Inhibitors of microsomal prostaglandin E2 synthase-1 enzyme as emerging anti-inflammatory candidates. *Med. Res. Rev.* **2014**, *34*, 825–855, doi:10.1002/med.21306.

5. Capra, V.; Bäck, M.; Barbieri, S.S.; Camera, M.; Tremoli, E.; Rovati, G.E. Eicosanoids and their drugs in cardiovascular diseases: focus on atherosclerosis and stroke. *Med. Res. Rev.* **2013**, *33*, 364–438, doi:10.1002/med.21251.

6. Grosser, T.; Ricciotti, E.; FitzGerald, G.A. The Cardiovascular Pharmacology of Nonsteroidal Anti-Inflammatory Drugs. *Trends Pharmacol. Sci.* **2017**, *38*, 733–748, doi:10.1016/j.tips.2017.05.008.

7. Patrignani, P.; Patrono, C. Aspirin and Cancer. *J. Am. Coll. Cardiol.* **2016**, *68*, 967–976, doi:10.1016/j.jacc.2016.05.083.

8. Sala, A.; Proschak, E.; Steinhilber, D.; Rovati, G.E. Two-pronged approach to anti-inflammatory therapy through the modulation of the arachidonic acid cascade. *Biochem. Pharmacol.* **2018**, *158*, 161–173, doi:10.1016/j.bcp.2018.10.007.

9. Wang, B.; Wu, L.; Chen, J.; Dong, L.; Chen, C.; Wen, Z.; Hu, J.; Fleming, I.; Wang, D.W. Metabolism pathways of arachidonic acids: mechanisms and potential therapeutic targets. *Signal Transduct. Target. Ther.* **2021**, *6*, 94, doi:10.1038/s41392-020-00443-w.

10. Tallima, H.; El Ridi, R. Arachidonic acid: Physiological roles and potential health benefits - A review. *J. Adv. Res.* **2018**, *11*, 33–41, doi:10.1016/j.jare.2017.11.004.

11. Morteau, O. Prostaglandins and inflammation: the cyclooxygenase controversy. *Arch. Immunol. Ther. Exp. (Warsz)* **2000**, *48*, 473–480.

12. Panigrahy, D.; Kaipainen, A.; Greene, E.R.; Huang, S. Cytochrome P450-derived eicosanoids: the neglected pathway in cancer. *Cancer Metastasis Rev.* **2010**, *29*, 723–735, doi:10.1007/s10555-010-9264-x.

13. Tsai, M.-J.; Chang, W.-A.; Tsai, P.-H.; Wu, C.-Y.; Ho, Y.-W.; Yen, M.-C.; Lin, Y.-S.; Kuo, P.-L.; Hsu, Y.-L. Montelukast Induces Apoptosis-Inducing Factor-Mediated Cell Death of Lung Cancer Cells. *Int. J. Mol. Sci.* **2017**, *18*, doi:10.3390/ijms18071353.

14. Martinez, J.A.; Yang, J.; Wertheim, B.C.; Roe, D.J.; Schriewer, A.; Lance, P.; Alberts, D.S.; Hammock, B.D.; Thompson, P.A. Celecoxib use and circulating oxylipins in a colon polyp prevention trial. *PLoS One* **2018**, *13*, e0196398, doi:10.1371/journal.pone.0196398.

15. Zhou, Y.; Khan, H.; Xiao, J.; Cheang, W.S. Effects of Arachidonic Acid Metabolites on Cardiovascular Health and Disease. *Int. J. Mol. Sci.* **2021**, *22*, doi:10.3390/ijms222112029.

16. Deng, Y.; Theken, K.N.; Lee, C.R. Cytochrome P450 epoxygenases, soluble epoxide hydrolase, and the regulation of cardiovascular inflammation. *Journal of Molecular and Cellular Cardiology* **2010**, *48*, 331–341, doi:10.1016/j.yjmcc.2009.10.022.

17. Ni, K.-D.; Liu, J.-Y. The Functions of Cytochrome P450 ω-hydroxylases and the Associated Eicosanoids in Inflammation-Related Diseases. *Front. Pharmacol.* **2021**, *12*, 716801, doi:10.3389/fphar.2021.716801.

18. Michaelis, U.R.; Falck, J.R.; Schmidt, R.; Busse, R.; Fleming, I. Cytochrome P4502C9-derived epoxyeicosatrienoic acids induce the expression of cyclooxygenase-2 in endothelial cells. *Arterioscler. Thromb. Vasc. Biol.* **2005**, *25*, 321–326, doi:10.1161/01.ATV.0000151648.58516.eb.

19. Node, K.; Huo, Y.; Ruan, X.; Yang, B.; Spiecker, M.; Ley, K.; Zeldin, D.C.; Liao, J.K. Anti-inflammatory properties of cytochrome P450 epoxygenase-derived eicosanoids. *Science* **1999**, *285*, 1276–1279, doi:10.1126/science.285.5431.1276.

20. Fleming, I. Cytochrome p450 and vascular homeostasis. *Circ. Res.* **2001**, *89*, 753–762, doi:10.1161/hh2101.099268.

21. Medhora, M.; Daniels, J.; Mundey, K.; Fisslthaler, B.; Busse, R.; Jacobs, E.R.; Harder, D.R. Epoxygenase-driven angiogenesis in human lung microvascular endothelial cells. *Am. J. Physiol. Heart Circ. Physiol.* **2003**, *284*, H215-24, doi:10.1152/ajpheart.01118.2001.

22. Vriens, J.; Owsianik, G.; Fisslthaler, B.; Suzuki, M.; Janssens, A.; Voets, T.; Morisseau, C.; Hammock, B.D.; Fleming, I.; Busse, R.; et al. Modulation of the Ca2 permeable cation channel TRPV4 by cytochrome P450 epoxygenases in vascular endothelium. *Circ. Res.* **2005**, *97*, 908–915, doi:10.1161/01.RES.0000187474.47805.30.

23. Sun, J.; Sui, X.; Bradbury, J.A.; Zeldin, D.C.; Conte, M.S.; Liao, J.K. Inhibition of vascular smooth muscle cell migration by cytochrome p450 epoxygenase-derived eicosanoids. *Circ. Res.* **2002**, *90*, 1020–1027, doi:10.1161/01.res.0000017727.35930.33.

24. Yang, L.; Mäki-Petäjä, K.; Cheriyan, J.; McEniery, C.; Wilkinson, I.B. The role of epoxyeicosatrienoic acids in the cardiovascular system. *Br. J. Clin. Pharmacol.* **2015**, *80*, 28–44, doi:10.1111/bcp.12603.

25. Fleming, I.; Busse, R. Endothelium-derived epoxyeicosatrienoic acids and vascular function. *Hypertension* **2006**, *47*, 629–633, doi:10.1161/01.HYP.0000208597.87957.89.

26. Chen, J.; Capdevila, J.H.; Zeldin, D.C.; Rosenberg, R.L. Inhibition of cardiac L-type calcium channels by epoxyeicosatrienoic acids. *Mol. Pharmacol.* **1999**, *55*, 288–295, doi:10.1124/mol.55.2.288.

27. Chen, J.K.; Capdevila, J.; Harris, R.C. Overexpression of C-terminal Src kinase blocks 14, 15-epoxyeicosatrienoic acid-induced tyrosine phosphorylation and mitogenesis. *J. Biol. Chem.* **2000**, *275*, 13789–13792, doi:10.1074/jbc.275.18.13789.

28. Chen, J.K.; Capdevila, J.; Harris, R.C. Cytochrome p450 epoxygenase metabolism of arachidonic acid inhibits apoptosis. *Mol. Cell. Biol.* **2001**, *21*, 6322–6331, doi:10.1128/MCB.21.18.6322-6331.2001.

29. Blanco, V.M.; Stern, J.E.; Filosa, J.A. Tone-dependent vascular responses to astrocyte-derived signals. *Am. J. Physiol. Heart Circ. Physiol.* **2008**, *294*, H2855-63, doi:10.1152/ajpheart.91451.2007.

30. Potente, M.; Fisslthaler, B.; Busse, R.; Fleming, I. 11,12-Epoxyeicosatrienoic acid-induced inhibition of FOXO factors promotes endothelial proliferation by down-regulating p27Kip1. *J. Biol. Chem.* **2003**, *278*, 29619–29625, doi:10.1074/jbc.M305385200.

31. Webler, A.C.; Michaelis, U.R.; Popp, R.; Barbosa-Sicard, E.; Murugan, A.; Falck, J.R.; Fisslthaler, B.; Fleming, I. Epoxyeicosatrienoic acids are part of the VEGF-activated signaling cascade leading to angiogenesis. *Am. J. Physiol. Cell Physiol.* **2008**, *295*, C1292-301, doi:10.1152/ajpcell.00230.2008.

32. Imig, J.D.; Dimitropoulou, C.; Reddy, D.S.; White, R.E.; Falck, J.R. Afferent arteriolar dilation to 11, 12-EET analogs involves PP2A activity and Ca2+-activated K+ Channels. *Microcirculation* **2008**, *15*, 137–150, doi:10.1080/10739680701456960.

33. Michaelis, U.R.; Fleming, I. From endothelium-derived hyperpolarizing factor (EDHF) to angiogenesis: Epoxyeicosatrienoic acids (EETs) and cell signaling. *Pharmacol. Ther.* **2006**, *111*, 584–595, doi:10.1016/j.pharmthera.2005.11.003.

34. Popp, R.; Brandes, R.P.; Ott, G.; Busse, R.; Fleming, I. Dynamic modulation of interendothelial gap junctional communication by 11,12-epoxyeicosatrienoic acid. *Circ. Res.* **2002**, *90*, 800–806, doi:10.1161/01.res.0000015328.20581.d6.

35. Campbell, W.B.; Gebremedhin, D.; Pratt, P.F.; Harder, D.R. Identification of epoxyeicosatrienoic acids as endothelium-derived hyperpolarizing factors. *Circ. Res.* **1996**, *78*, 415–423, doi:10.1161/01.res.78.3.415.

36. Fisslthaler, B.; Popp, R.; Kiss, L.; Potente, M.; Harder, D.R.; Fleming, I.; Busse, R. Cytochrome P450 2C is an EDHF synthase in coronary arteries. *Nature* **1999**, *401*, 493–497, doi:10.1038/46816.

37. Fleming, I. The factor in EDHF: Cytochrome P450 derived lipid mediators and vascular signaling. *Vascul. Pharmacol.* **2016**, *86*, 31–40, doi:10.1016/j.vph.2016.03.001.

38. Fleming, I. The pharmacology of the cytochrome P450 epoxygenase/soluble epoxide hydrolase axis in the vasculature and cardiovascular disease. *Pharmacol. Rev.* **2014**, *66*, 1106–1140, doi:10.1124/pr.113.007781.

39. Harris, T.R.; Hammock, B.D. Soluble epoxide hydrolase: gene structure, expression and deletion. *Gene* **2013**, *526*, 61–74, doi:10.1016/j.gene.2013.05.008.

40. Morisseau, C.; Hammock, B.D. Impact of soluble epoxide hydrolase and epoxyeicosanoids on human health. *Annu. Rev. Pharmacol. Toxicol.* **2013**, *53*, 37–58, doi:10.1146/annurev-pharmtox-011112-140244.

41. Sura, P.; Sura, R.; Enayetallah, A.E.; Grant, D.F. Distribution and expression of soluble epoxide hydrolase in human brain. *J. Histochem. Cytochem.* **2008**, *56*, 551–559, doi:10.1369/jhc.2008.950659.

42. Chen, L.; Deng, H.; Cui, H.; Fang, J.; Zuo, Z.; Deng, J.; Li, Y.; Wang, X.; Zhao, L. Inflammatory responses and inflammation-associated diseases in organs. *Oncotarget* **2018**, *9*, 7204–7218, doi:10.18632/oncotarget.23208.

43. Fullerton, J.N.; Gilroy, D.W. Resolution of inflammation: a new therapeutic frontier. *Nat. Rev. Drug Discov.* **2016**, *15*, 551–567, doi:10.1038/nrd.2016.39.

44. Liu, J.; Cao, X. Cellular and molecular regulation of innate inflammatory responses. *Cell. Mol. Immunol.* **2016**, *13*, 711–721, doi:10.1038/cmi.2016.58.

45. Serhan, C.N.; Brain, S.D.; Buckley, C.D.; Gilroy, D.W.; Haslett, C.; O'Neill, L.A.J.; Perretti, M.; Rossi, A.G.; Wallace, J.L. Resolution of inflammation: state of the art, definitions and terms. *FASEB J.* **2007**, *21*, 325–332, doi:10.1096/fj.06-7227rev.

46. Sansbury, B.E.; Spite, M. Resolution of Acute Inflammation and the Role of Resolvins in Immunity, Thrombosis, and Vascular Biology. *Circ. Res.* **2016**, *119*, 113–130, doi:10.1161/CIRCRESAHA.116.307308.

47. Gautier, E.L.; Ivanov, S.; Lesnik, P.; Randolph, G.J. Local apoptosis mediates clearance of macrophages from resolving inflammation in mice. *Blood* **2013**, *122*, 2714–2722, doi:10.1182/blood-2013-01-478206.

48. Schett, G.; Neurath, M.F. Resolution of chronic inflammatory disease: universal and tissue-specific concepts. *Nat. Commun.* **2018**, *9*, 3261, doi:10.1038/s41467-018-05800-6.

49. Hirayama, D.; Iida, T.; Nakase, H. The Phagocytic Function of Macrophage-Enforcing Innate Immunity and Tissue Homeostasis. *Int. J. Mol. Sci.* **2017**, *19*, doi:10.3390/ijms19010092.

50. Mosser, D.M.; Hamidzadeh, K.; Goncalves, R. Macrophages and the maintenance of homeostasis. *Cell. Mol. Immunol.* **2020**, *18*, 579–587, doi:10.1038/s41423-020-00541-3.

51. Mu, X.; Li, Y.; Fan, G.-C. Tissue-Resident Macrophages in the Control of Infection and Resolution of Inflammation. *Shock* **2021**, *55*, 14–23, doi:10.1097/SHK.0000000000001601.

52. Ma, R.-Y.; Black, A.; Qian, B.-Z. Macrophage diversity in cancer revisited in the era of single-cell omics. *Trends Immunol.* **2022**, *43*, 546–563, doi:10.1016/j.it.2022.04.008.

53. Yang, Q.; Zhang, H.; Wei, T.; Lin, A.; Sun, Y.; Luo, P.; Zhang, J. Single-Cell RNA Sequencing Reveals the Heterogeneity of Tumor-Associated Macrophage in Non-Small Cell Lung Cancer and Differences Between Sexes. *Front. Immunol.* **2021**, *12*, 756722, doi:10.3389/fimmu.2021.756722.

54. Chávez-Galán, L.; Olleros, M.L.; Vesin, D.; Garcia, I. Much More than M1 and M2 Macrophages, There are also CD169(+) and TCR(+) Macrophages. *Front. Immunol.* **2015**, *6*, 263, doi:10.3389/fimmu.2015.00263.

55. Colin, S.; Chinetti-Gbaguidi, G.; Staels, B. Macrophage phenotypes in atherosclerosis. *Immunol. Rev.* **2014**, *262*, 153–166, doi:10.1111/imr.12218.

56. Martinez, F.O.; Sica, A.; Mantovani, A.; Locati, M. Macrophage activation and polarization. *Front. Biosci.* **2008**, *13*, 453–461, doi:10.2741/2692.

57. Wang, L.-X.; Zhang, S.-X.; Wu, H.-J.; Rong, X.-L.; Guo, J. M2b macrophage polarization and its roles in diseases. *J. Leukoc. Biol.* **2019**, *106*, 345–358, doi:10.1002/JLB.3RU1018-378RR.

58. Zhang, F.; Wang, H.; Wang, X.; Jiang, G.; Liu, H.; Zhang, G.; Wang, H.; Fang, R.; Bu, X.; Cai, S.; et al. TGF-β induces M2-like macrophage polarization via SNAIL-mediated suppression of a pro-inflammatory phenotype. *Oncotarget* **2016**, *7*, 52294–52306, doi:10.18632/oncotarget.10561.

59. Meng, X.-M.; Tang, P.M.-K.; Li, J.; Lan, H.Y. TGF-β/Smad signaling in renal fibrosis. *Front. Physiol.* **2015**, *6*, 82, doi:10.3389/fphys.2015.00082.

60. Massagué, J. TGFβ signalling in context. *Nat. Rev. Mol. Cell Biol.* **2012**, *13*, 616–630, doi:10.1038/nrm3434.

61. Akhurst, R.J.; Hata, A. Targeting the TGFβ signalling pathway in disease. *Nat. Rev. Drug Discov.* **2012**, *11*, 790–811, doi:10.1038/nrd3810.

62. Shi, Y.; Massagué, J. Mechanisms of TGF-beta signaling from cell membrane to the nucleus. *Cell* **2003**, *113*, 685–700, doi:10.1016/s0092-8674(03)00432-x.

63. López-Casillas, F.; Cheifetz, S.; Doody, J.; Andres, J.L.; Lane, W.S.; Massagué, J. Structure and expression of the membrane proteoglycan betaglycan, a component of the TGF-beta receptor system. *Cell* **1991**, *67*, 785–795, doi:10.1016/0092-8674(91)90073-8.

64. Dijke, P. ten; Goumans, M.-J.; Pardali, E. Endoglin in angiogenesis and vascular diseases. *Angiogenesis* **2008**, *11*, 79–89, doi:10.1007/s10456-008-9101-9.

65. Chen, Y.G.; Hata, A.; Lo, R.S.; Wotton, D.; Shi, Y.; Pavletich, N.; Massagué, J. Determinants of specificity in TGF-beta signal transduction. *Genes Dev.* **1998**, *12*, 2144–2152, doi:10.1101/gad.12.14.2144.

66. Macías-Silva, M.; Abdollah, S.; Hoodless, P.A.; Pirone, R.; Attisano, L.; Wrana, J.L. MADR2 is a substrate of the TGFbeta receptor and its phosphorylation is required for nuclear accumulation and signaling. *Cell* **1996**, *87*, 1215–1224, doi:10.1016/s0092-8674(00)81817-6.

67. Wong, C.; Rougier-Chapman, E.M.; Frederick, J.P.; Datto, M.B.; Liberati, N.T.; Li, J.M.; Wang, X.F. Smad3-Smad4 and AP-1 complexes synergize in transcriptional activation of the c-Jun promoter by transforming growth factor beta. *Mol. Cell. Biol.* **1999**, *19*, 1821–1830, doi:10.1128/mcb.19.3.1821.

68. Hill, C.S. Transcriptional Control by the SMADs. *Cold Spring Harb. Perspect. Biol.* **2016**, *8*, doi:10.1101/cshperspect.a022079.

69. Hata, A.; Chen, Y.-G. TGF-β Signaling from Receptors to Smads. *Cold Spring Harb. Perspect. Biol.* **2016**, *8*, doi:10.1101/cshperspect.a022061.

70. Nomura, T.; Khan, M.M.; Kaul, S.C.; Dong, H.D.; Wadhwa, R.; Colmenares, C.; Kohno, I.; Ishii, S. Ski is a component of the histone deacetylase complex required for transcriptional repression by Mad and thyroid hormone receptor. *Genes Dev.* **1999**, *13*, 412–423, doi:10.1101/gad.13.4.412.

71. Koh, B.; Hufford, M.M.; Pham, D.; Olson, M.R.; Wu, T.; Jabeen, R.; Sun, X.; Kaplan, M.H. The ETS Family Transcription Factors Etv5 and PU.1 Function in Parallel To Promote Th9 Cell Development. *J. Immunol.* **2016**, *197*, 2465–2472, doi:10.4049/jimmunol.1502383.

72. Qin, Z.; Xia, W.; Fisher, G.J.; Voorhees, J.J.; Quan, T. YAP/TAZ regulates TGF-β/Smad3 signaling by induction of Smad7 via AP-1 in human skin dermal fibroblasts. *Cell Commun. Signal.* **2018**, *16*, 18, doi:10.1186/s12964-018-0232-3.

73. Oberheim, N.A.; Goldman, S.A.; Nedergaard, M. Heterogeneity of astrocytic form and function. *Methods Mol. Biol.* **2012**, *814*, 23–45, doi:10.1007/978-1-61779-452-0_3.

74. Ries, M.; Sastre, M. Mechanisms of Aβ Clearance and Degradation by Glial Cells. *Front. Aging Neurosci.* **2016**, *8*, 160, doi:10.3389/fnagi.2016.00160.

75. Frost, G.R.; Li, Y.-M. The role of astrocytes in amyloid production and Alzheimer's disease. *Open Biol.* **2017**, *7*, doi:10.1098/rsob.170228.

76. Murphy, M.P.; LeVine, H. Alzheimer's disease and the amyloid-beta peptide. *J. Alzheimers. Dis.* **2010**, *19*, 311–323, doi:10.3233/JAD-2010-1221.

77. Hung, C.-C.; Lee, Y.-H.; Kuo, Y.-M.; Hsu, P.-C.; Tsay, H.-J.; Hsu, Y.-T.; Lee, C.-C.; Liang, J.-J.; Shie, F.-S. Soluble epoxide hydrolase modulates immune responses in activated astrocytes involving regulation of STAT3 activity. *J. Neuroinflammation* **2019**, *16*, 123, doi:10.1186/s12974-019-1508-2.

78. Brandebura, A.N.; Paumier, A.; Onur, T.S.; Allen, N.J. Astrocyte contribution to dysfunction, risk and progression in neurodegenerative disorders. *Nat. Rev. Neurosci.* **2023**, *24*, 23–39, doi:10.1038/s41583-022-00641-1.

79. Alberini, C.M.; Cruz, E.; Descalzi, G.; Bessières, B.; Gao, V. Astrocyte glycogen and lactate: New insights into learning and memory mechanisms. *Glia* **2018**, *66*, 1244–1262, doi:10.1002/glia.23250.

80. Liddelow, S.A.; Guttenplan, K.A.; Clarke, L.E.; Bennett, F.C.; Bohlen, C.J.; Schirmer, L.; Bennett, M.L.; Münch, A.E.; Chung, W.-S.; Peterson, T.C.; et al. Neurotoxic reactive astrocytes are induced by activated microglia. *Nature* **2017**, *541*, 481–487, doi:10.1038/nature21029.

81. Linnerbauer, M.; Rothhammer, V. Protective Functions of Reactive Astrocytes Following Central Nervous System Insult. *Front. Immunol.* **2020**, *11*, 573256, doi:10.3389/fimmu.2020.573256.

82. Escartin, C.; Galea, E.; Lakatos, A.; O'Callaghan, J.P.; Petzold, G.C.; Serrano-Pozo, A.; Steinhäuser, C.; Volterra, A.; Carmignoto, G.; Agarwal, A.; et al. Reactive astrocyte nomenclature, definitions, and future directions. *Nat. Neurosci.* **2021**, *24*, 312–325, doi:10.1038/s41593-020-00783-4.

83. Guttenplan, K.A.; Weigel, M.K.; Prakash, P.; Wijewardhane, P.R.; Hasel, P.; Rufen-Blanchette, U.; Münch, A.E.; Blum, J.A.; Fine, J.; Neal, M.C.; et al. Neurotoxic reactive astrocytes induce cell death via saturated lipids. *Nature* **2021**, *599*, 102–107, doi:10.1038/s41586-021-03960-y.

84. Ghosh, A.; Comerota, M.M.; Wan, D.; Chen, F.; Propson, N.E.; Hwang, S.H.; Hammock, B.D.; Zheng, H. An epoxide hydrolase inhibitor reduces neuroinflammation in a mouse model of Alzheimer's disease. *Sci. Transl. Med.* **2020**, *12*, doi:10.1126/scitranslmed.abb1206.

85. Hu, J.; Bibli, S.-I.; Wittig, J.; Zukunft, S.; Lin, J.; Hammes, H.-P.; Popp, R.; Fleming, I. Soluble epoxide hydrolase promotes astrocyte survival in retinopathy of prematurity. *J. Clin. Invest.* **2019**, *129*, 5204–5218, doi:10.1172/JCI123835.

86. Kuo, Y.-M.; Hsu, P.-C.; Hung, C.-C.; Hu, Y.-Y.; Huang, Y.-J.; Gan, Y.-L.; Lin, C.-H.; Shie, F.-S.; Chang, W.-K.; Kao, L.-S.; et al. Soluble Epoxide Hydrolase Inhibition Attenuates Excitotoxicity Involving 14,15-Epoxyeicosatrienoic Acid-Mediated Astrocytic Survival and Plasticity to Preserve Glutamate Homeostasis. *Mol. Neurobiol.* **2019**, *56*, 8451–8474, doi:10.1007/s12035-019-01669-8.

87. Baldwin, K.T.; Eroglu, C. Molecular mechanisms of astrocyte-induced synaptogenesis. *Curr. Opin. Neurobiol.* **2017**, *45*, 113–120, doi:10.1016/j.conb.2017.05.006.

88. Lee, H.-T.; Lee, K.-I.; Chen, C.-H.; Lee, T.-S. Genetic deletion of soluble epoxide hydrolase delays the progression of Alzheimer's disease. *J. Neuroinflammation* **2019**, *16*, 267, doi:10.1186/s12974-019-1635-9.

89. Hampel, H.; Hardy, J.; Blennow, K.; Chen, C.; Perry, G.; Kim, S.H.; Villemagne, V.L.; Aisen, P.; Vendruscolo, M.; Iwatsubo, T.; et al. The Amyloid-β Pathway in Alzheimer's Disease. *Mol. Psychiatry* **2021**, *26*, 5481–5503, doi:10.1038/s41380-021-01249-0.

90. Knopman, D.S.; Amieva, H.; Petersen, R.C.; Chételat, G.; Holtzman, D.M.; Hyman, B.T.; Nixon, R.A.; Jones, D.T. Alzheimer disease. *Nat. Rev. Dis. Primers* **2021**, *7*, 33, doi:10.1038/s41572-021-00269-y.

91. Reiserer, R.S.; Harrison, F.E.; Syverud, D.C.; McDonald, M.P. Impaired spatial learning in the APPSwe + PSEN1DeltaE9 bigenic mouse model of Alzheimer's disease. *Genes Brain Behav.* **2007**, *6*, 54–65, doi:10.1111/j.1601-183X.2006.00221.x.

92. Jankowsky, J.L.; Fadale, D.J.; Anderson, J.; Xu, G.M.; Gonzales, V.; Jenkins, N.A.; Copeland, N.G.; Lee, M.K.; Younkin, L.H.; Wagner, S.L.; et al. Mutant presenilins specifically elevate the levels of the 42 residue beta-amyloid peptide in vivo: evidence for augmentation of a 42-specific gamma secretase. *Hum. Mol. Genet.* **2004**, *13*, 159–170, doi:10.1093/hmg/ddh019.

93. Lok, K.; Zhao, H.; Shen, H.; Wang, Z.; Gao, X.; Zhao, W.; Yin, M. Characterization of the APP/PS1 mouse model of Alzheimer's disease in senescence accelerated background. *Neurosci. Lett.* **2013**, *557 Pt B*, 84–89, doi:10.1016/j.neulet.2013.10.051.

94. Qiu, T.; Liu, Q.; Chen, Y.-X.; Zhao, Y.-F.; Li, Y.-M. Aβ42 and Aβ40: similarities and differences. *J. Pept. Sci.* **2015**, *21*, 522–529, doi:10.1002/psc.2789.

95. Maxeiner, H.; Husemann, J.; Thomas, C.A.; Loike, J.D.; El Khoury, J.; Silverstein, S.C. Complementary roles for scavenger receptor A and CD36 of human monocyte-derived macrophages in adhesion to surfaces coated with oxidized low-density lipoproteins and in secretion of H_2O_2. *J Exp Med* **1998**, *188*, 2257–2265, doi:10.1084/jem.188.12.2257.

96. Li, X.; Kempf, S.; Günther, S.; Hu, J.; Fleming, I. 11,12-EET Regulates PPAR-γ Expression to Modulate TGF-β-Mediated Macrophage Polarization. *Cells* **2023**, *12*, doi:10.3390/cells12050700.

97. Kim, J.B.; Wright, H.M.; Wright, M.; Spiegelman, B.M. ADD1/SREBP1 activates PPARgamma through the production of endogenous ligand. *Proc. Natl. Acad. Sci. U. S. A.* **1998**, *95*, 4333–4337, doi:10.1073/pnas.95.8.4333.

98. Hu, J.; Dziumbla, S.; Lin, J.; Bibli, S.-I.; Zukunft, S.; Mos, J. de; Awwad, K.; Frömel, T.; Jungmann, A.; Devraj, K.; et al. Inhibition of soluble epoxide hydrolase prevents diabetic retinopathy. *Nature* **2017**, *552*, 248–252, doi:10.1038/nature25013.

99. Schildge, S.; Bohrer, C.; Beck, K.; Schachtrup, C. Isolation and culture of mouse cortical astrocytes. *J. Vis. Exp.* **2013**, doi:10.3791/50079.

100. Harris, T.R.; Hammock, B.D. Soluble epoxide hydrolase: Gene structure, expression and deletion. *Gene* **2013**, *526*, 61–74, doi:10.1016/j.gene.2013.05.008.

101. Yang, Y.-M.; Sun, D.; Kandhi, S.; Froogh, G.; Zhuge, J.; Huang, W.; Hammock, B.D.; Huang, A. Estrogen-dependent epigenetic regulation of soluble epoxide hydrolase via DNA methylation. *Proc. Natl. Acad. Sci. U. S. A.* **2018**, *115*, 613–618, doi:10.1073/pnas.1716016115.

102. Gupta, N.C.; Davis, C.M.; Nelson, J.W.; Young, J.M.; Alkayed, N.J. Soluble epoxide hydrolase: sex differences and role in endothelial cell survival. *Arterioscler. Thromb. Vasc. Biol.* **2012**, *32*, 1936–1942, doi:10.1161/ATVBAHA.112.251520.

103. Jamieson, K.L.; Keshavarz-Bahaghighat, H.; Darwesh, A.M.; Sosnowski, D.K.; Seubert, J.M. Age and Sex Differences in Hearts of Soluble Epoxide Hydrolase Null Mice. *Front. Physiol.* **2020**, *11*, 48, doi:10.3389/fphys.2020.00048.

104. Awwad, K.; Hu, J.; Shi, L.; Mangels, N.; Abdel Malik, R.; Zippel, N.; Fisslthaler, B.; Eble, J.A.; Pfeilschifter, J.; Popp, R.; et al. Role of secreted modular calcium-binding protein 1 (SMOC1) in transforming growth factor β signalling and angiogenesis. *Cardiovasc. Res.* **2015**, *106*, 284–294, doi:10.1093/cvr/cvv098.

105. Tanaka, H.; Kamita, S.G.; Wolf, N.M.; Harris, T.R.; Wu, Z.; Morisseau, C.; Hammock, B.D. Transcriptional regulation of the human soluble epoxide hydrolase gene EPHX2. *Biochim. Biophys. Acta* **2008**, *1779*, 17–27, doi:10.1016/j.bbagrm.2007.11.005.

106. Jones, R.D.; Liao, J.; Tong, X.; Xu, D.; Sun, L.; Li, H.; Yang, G.-Y. Epoxy-Oxylipins and Soluble Epoxide Hydrolase Metabolic Pathway as Targets for NSAID-Induced Gastroenteropathy and Inflammation-Associated Carcinogenesis. *Front. Pharmacol.* **2019**, *10*, 731, doi:10.3389/fphar.2019.00731.

107. Lai, Y.-S.; Putra, R.B.D.S.; Aui, S.-P.; Chang, K.-T. M2C Polarization by Baicalin Enhances Efferocytosis via Upregulation of MERTK Receptor. *Am. J. Chin. Med.* **2018**, *46*, 1899–1914, doi:10.1142/S0192415X18500957.

108. Liu, L.-P.; Li, B.; Shuai, T.-K.; Zhu, L.; Li, Y.-M. Deletion of soluble epoxide hydrolase attenuates mice Hyperoxic acute lung injury. *BMC Anesthesiol.* **2018**, *18*, 48, doi:10.1186/s12871-018-0490-z.

109. Cybulsky, M.I.; Cheong, C.; Robbins, C.S. Macrophages and Dendritic Cells: Partners in Atherogenesis. *Circ. Res.* **2016**, *118*, 637–652, doi:10.1161/CIRCRESAHA.115.306542.

110. Kawakami, T.; Lichtnekert, J.; Thompson, L.J.; Karna, P.; Bouabe, H.; Hohl, T.M.; Heinecke, J.W.; Ziegler, S.F.; Nelson, P.J.; Duffield, J.S. Resident renal mononuclear phagocytes comprise five discrete populations with distinct phenotypes and functions. *J. Immunol.* **2013**, *191*, 3358–3372, doi:10.4049/jimmunol.1300342.

111. Taghavie-Moghadam, P.L.; Butcher, M.J.; Galkina, E.V. The dynamic lives of macrophage and dendritic cell subsets in atherosclerosis. *Ann. N. Y. Acad. Sci.* **2014**, *1319*, 19–37, doi:10.1111/nyas.12392.

112. Wacleche, V.S.; Tremblay, C.L.; Routy, J.-P.; Ancuta, P. The Biology of Monocytes and Dendritic Cells: Contribution to HIV Pathogenesis. *Viruses* **2018**, *10*, doi:10.3390/v10020065.

113. Han, L.; Shen, W.-J.; Bittner, S.; Kraemer, F.B.; Azhar, S. PPARs: regulators of metabolism and as therapeutic targets in cardiovascular disease. Part II: PPAR-β/δ and PPAR-γ. *Future Cardiol.* **2017**, *13*, 279–296, doi:10.2217/fca-2017-0019.

114. Zhang, L.-N.; Vincelette, J.; Cheng, Y.; Mehra, U.; Chen, D.; Anandan, S.-K.; Gless, R.; Webb, H.K.; Wang, Y.-X.J. Inhibition of soluble epoxide hydrolase attenuated atherosclerosis, abdominal aortic aneurysm formation, and dyslipidemia. *Arterioscler Thromb Vasc Biol* **2009**, *29*, 1265–1270, doi:10.1161/atvbaha.109.186064.

115. Ulu, A.; Davis, B.B.; Tsai, H.-J.; Kim, I.-H.; Morisseau, C.; Inceoglu, B.; Fiehn, O.; Hammock, B.D.; Weiss, R.H. Soluble epoxide hydrolase inhibitors reduce the development of atherosclerosis in apolipoprotein e-knockout mouse model. *J Cardiovasc Pharmacol* **2008**, *52*, 314–323, doi:10.1097/fjc.0b013e318185fa3c.

116. Li, J.J.; Wang, R.; Lama, R.; Wang, X.; Floyd, Z.E.; Park, E.A.; Liao, F.-F. Ubiquitin Ligase NEDD4 Regulates PPARγ Stability and Adipocyte Differentiation in 3T3-L1 Cells. *Sci. Rep.* **2016**, *6*, 38550, doi:10.1038/srep38550.

117. Dai, M.; Wu, L.; He, Z.; Zhang, S.; Chen, C.; Xu, X.; Wang, P.; Gruzdev, A.; Zeldin, D.C.; Wang, D.W. Epoxyeicosatrienoic acids regulate macrophage polarization and prevent LPS-induced cardiac dysfunction. *J. Cell. Physiol.* **2015**, *230*, 2108–2119, doi:10.1002/jcp.24939.

118. Lai, J.; Chen, C. The Role of Epoxyeicosatrienoic Acids in Cardiac Remodeling. *Front. Physiol.* **2021**, *12*, 642470, doi:10.3389/fphys.2021.642470.

119. Ricote, M.; Glass, C.K. PPARs and molecular mechanisms of transrepression. *Biochim. Biophys. Acta* **2007**, *1771*, 926–935, doi:10.1016/j.bbalip.2007.02.013.

120. Zhao, G.; Wang, J.; Xu, X.; Jing, Y.; Tu, L.; Li, X.; Chen, C.; Cianflone, K.; Wang, P.; Dackor, R.T.; et al. Epoxyeicosatrienoic acids protect rat hearts against tumor necrosis factor-α-induced injury. *J. Lipid Res.* **2012**, *53*, 456–466, doi:10.1194/jlr.M017319.

121. Cash, J.L.; White, G.E.; Greaves, D.R. Chapter 17. Zymosan-induced peritonitis as a simple experimental system for the study of inflammation. *Methods Enzymol.* **2009**, *461*, 379–396, doi:10.1016/S0076-6879(09)05417-2.

122. Das Mahapatra, A.; Choubey, R.; Datta, B. Small molecule soluble epoxide hydrolase inhibitors in multitarget and combination therapies for inflammation and cancer. *Molecules* **2020**, *25*, doi:10.3390/molecules25235488.

123. Luo, X.-Q.; Duan, J.-X.; Yang, H.-H.; Zhang, C.-Y.; Sun, C.-C.; Guan, X.-X.; Xiong, J.-B.; Zu, C.; Tao, J.-H.; Zhou, Y.; et al. Epoxyeicosatrienoic acids inhibit the activation of NLRP3 inflammasome in murine macrophages. *J. Cell. Physiol.* **2020**, *235*, 9910–9921, doi:10.1002/jcp.29806.

124. Mittal, M.; Siddiqui, M.R.; Tran, K.; Reddy, S.P.; Malik, A.B. Reactive oxygen species in inflammation and tissue injury. *Antioxid. Redox Signal.* **2014**, *20*, 1126–1167, doi:10.1089/ars.2012.5149.

125. Gilroy, D.W.; Edin, M.L.; Maeyer, R.P.H. de; Bystrom, J.; Newson, J.; Lih, F.B.; Stables, M.; Zeldin, D.C.; Bishop-Bailey, D. CYP450-derived oxylipins mediate inflammatory resolution. *Proc. Natl. Acad. Sci. U. S. A.* **2016**, *113*, E3240-9, doi:10.1073/pnas.1521453113.

126. Mantovani, A.; Sica, A.; Sozzani, S.; Allavena, P.; Vecchi, A.; Locati, M. The chemokine system in diverse forms of macrophage activation and polarization. *Trends Immunol.* **2004**, *25*, 677–686, doi:10.1016/j.it.2004.09.015.

127. Martinez, F.O.; Gordon, S. The M1 and M2 paradigm of macrophage activation: time for reassessment. *F1000Prime Rep.* **2014**, *6*, 13, doi:10.12703/P6-13.

128. Li, H.; Bradbury, J.A.; Edin, M.L.; Graves, J.P.; Gruzdev, A.; Cheng, J.; Hoopes, S.L.; DeGraff, L.M.; Fessler, M.B.; Garantziotis, S.; et al. sEH promotes macrophage phagocytosis and lung clearance of Streptococcus pneumoniae. *J. Clin. Invest.* **2021**, *131*, doi:10.1172/JCI129679.

129. Xue, H.-M.; Sun, W.-T.; Chen, H.-X.; He, G.-W.; Yang, Q. Targeting IRE1α-JNK-c-Jun/AP-1-sEH Signaling Pathway Improves Myocardial and Coronary Endothelial Function Following Global Myocardial Ischemia/Reperfusion. *Int. J. Med. Sci.* **2022**, *19*, 1460–1472, doi:10.7150/ijms.74533.

130. Ren, Q.; Ma, M.; Ishima, T.; Morisseau, C.; Yang, J.; Wagner, K.M.; Zhang, J.-C.; Yang, C.; Yao, W.; Dong, C.; et al. Gene deficiency and pharmacological inhibition of soluble epoxide hydrolase confers resilience to repeated social defeat stress. *Proc. Natl. Acad. Sci. U. S. A.* **2016**, *113*, E1944-52, doi:10.1073/pnas.1601532113.

131. Ai, D.; Fu, Y.; Guo, D.; Tanaka, H.; Wang, N.; Tang, C.; Hammock, B.D.; Shyy, J.Y.-J.; Zhu, Y. Angiotensin II up-regulates soluble epoxide hydrolase in vascular endothelium in vitro and in vivo. *Proc. Natl. Acad. Sci. U. S. A.* **2007**, *104*, 9018–9023, doi:10.1073/pnas.0703229104.

132. Zhang, D.; Xie, X.; Chen, Y.; Hammock, B.D.; Kong, W.; Zhu, Y. Homocysteine upregulates soluble epoxide hydrolase in vascular endothelium in vitro and in vivo. *Circ. Res.* **2012**, *110*, 808–817, doi:10.1161/CIRCRESAHA.111.259325.

133. Evans, R.M.; Barish, G.D.; Wang, Y.-X. PPARs and the complex journey to obesity. *Nat. Med.* **2004**, *10*, 355–361, doi:10.1038/nm1025.

134. Bordoni, A.; Di Nunzio, M.; Danesi, F.; Biagi, P.L. Polyunsaturated fatty acids: from diet to binding to ppars and other nuclear receptors. *Genes Nutr.* **2006**, *1*, 95–106, doi:10.1007/BF02829951.

135. Edwards, I.J.; O'Flaherty, J.T. Omega-3 Fatty Acids and PPAR-γ in Cancer. *PPAR Res.* **2008**, *2008*, 358052, doi:10.1155/2008/358052.

136. Kilroy, G.E.; Zhang, X.; Floyd, Z.E. PPAR-gamma AF-2 domain functions as a component of a ubiquitin-dependent degradation signal. *Obesity (Silver Spring)* **2009**, *17*, 665–673, doi:10.1038/oby.2008.616.

137. Yin, L.; Wang, L.; Shi, Z.; Ji, X.; Liu, L. The Role of Peroxisome Proliferator-Activated Receptor Gamma and Atherosclerosis: Post-translational Modification and Selective Modulators. *Front. Physiol.* **2022**, *13*, 826811, doi:10.3389/fphys.2022.826811.

138. He, Z.; Zhang, X.; Chen, C.; Wen, Z.; Hoopes, S.L.; Zeldin, D.C.; Wang, D.W. Cardiomyocyte-specific expression of CYP2J2 prevents development of cardiac remodelling induced by angiotensin II. *Cardiovasc. Res.* **2015**, *105*, 304–317, doi:10.1093/cvr/cvv018.

139. Kapoor, M.; Chinnathambi, S. TGF-β1 signalling in Alzheimer's pathology and cytoskeletal reorganization: a specialized Tau perspective. *J. Neuroinflammation* **2023**, *20*, 72, doi:10.1186/s12974-023-02751-8.

140. Tichauer, J.E.; Flores, B.; Soler, B.; Eugenín-von Bernhardi, L.; Ramírez, G.; Bernhardi, R. von. Age-dependent changes on TGFβ1 Smad3 pathway modify the pattern of microglial cell activation. *Brain Behav. Immun.* **2014**, *37*, 187–196, doi:10.1016/j.bbi.2013.12.018.

141. Wagner, K.M.; McReynolds, C.B.; Schmidt, W.K.; Hammock, B.D. Soluble epoxide hydrolase as a therapeutic target for pain, inflammatory and neurodegenerative diseases. *Pharmacol. Ther.* **2017**, *180*, 62–76, doi:10.1016/j.pharmthera.2017.06.006.

142. Zarriello, S.; Tuazon, J.P.; Corey, S.; Schimmel, S.; Rajani, M.; Gorsky, A.; Incontri, D.; Hammock, B.D.; Borlongan, C.V. Humble beginnings with big goals: small molecule soluble epoxide hydrolase inhibitors for treating CNS disorders. *Prog. Neurobiol.* **2019**, *172*, 23–39, doi:10.1016/j.pneurobio.2018.11.001.

8. Acknowledgements

I take this opportunity to thank the people who made this trip possible. Firstly, I would like to express my sincere gratitude to Prof Dr Ingrid Fleming. She has given me the opportunity to study and be part of this great team. I am grateful for her continuous support, patience and scientific guidance.

Apart from my supervisor, I am grateful to Prof. Dr. Jiong Hu and Sebastian Kempf for being great mentors throughout. I owe them a lot for their unwavering support, both scientifically and emotionally.

I would also like to thank Janina Wittig, Zumer Naeem, Maria Drekolia, Xiaozhu Zhou, Ürün Ukan, Dr. Fredy Delgado-Lagos, Dr. Anastasia Kyselova, Giorgia Ciliberti, Dr. Laila Santos and Dr. Daniel Suida for all the great scientific discussions over coffee breaks and, most importantly, for their companies for these four years PhD period. I am grateful to have such great friends and colleagues who have made this place my home.

I would also like to thank Dr Sofia-Iris Bibli, Dr Rüdiger Popp, Dr Timo Frömel, Dr Stephan Klatt, Dr Seven Zukunft, Dr Andreas Weigert and Dr Beate Fisslthaler for sharing their scientific expertise with me. Beate, in particular, has been a great support to me in difficult moments.

I would also like to thank all the technicians in the lab for their support and professional assistance. Special thanks to Isabel Winter, Mechthild Piepenbrock, Katharina Bruch, Ingrid Kempter, Katharina Herbig and Oliver Haun to their technical support.

Finally, I would like to thank my family - my parents, my wife and my son - for believing in me and supporting me throughout my journey, even when it meant living on another continent.

9. Corriculum vitae

Geburtsdatum

Geburtsort

Email

Ausbildung

2018-

Dissertation Goethe Universität Frankfurt am Main

2015-2018

Musterstudium MSc. Biological Chemistry and Molecular Biology

, South China Agricultural University, Guangzhou, China

2010-2015

Bachelorstudium BSc. Pharmaceutical Engineering, Nanchang University, Nanchang China

Publications:

1. Li, Xiaoming; Kempf, Sebastian; Günther, Stefan; Hu, Jiong; Fleming, Ingrid (2023): 11,12-EET Regulates PPAR-γ Expression to Modulate TGF-β-Mediated Macrophage Polarization. In Cells 12 (5). DOI: 10.3390/cells12050700.

2. Li, Xiaoming; Mu, Peiqiang; Qiao, Han; Wen, Jikai; Deng, Yiqun (2018): JNK-AKT-NF-κB controls P-glycoprotein expression to attenuate the cytotoxicity of deoxynivalenol in mammalian cells. In Biochemical Pharmacology 156, pp. 120–134. DOI: 10.1016/j.bcp.2018.08.020.

3. Li, Xiaoming; Mu, Peiqiang; Wen, Jikai; Deng, Yiqun (2017): Carrier-Mediated and Energy-Dependent Uptake and Efflux of Deoxynivalenol in Mammalian Cells. In Scientific reports 7 (1), p. 5889. DOI: 10.1038/s41598-017-06199-8.

4. Li, Xiaoming; Kempf, Sebastian; Delgado-Lagos, Fredy; Ukan, Ürün; Günther, Stefan; Weigert, Andreas; Hu, Jiong; Fleming, Ingrid: Soluble Epoxide Hydrolase is Required for the Resolution of Inflammation. In Preparation

Code and Data reproducibility

---
title: 'RNA analysis for PPARG'
author: Xiaoming Li
date: Fri Jan 20 06:06:39 2023
output: html_document

```{r setup, include=FALSE}
knitr::opts_chunk$set(echo = TRUE)
knitr::opts_chunk$set(fig.width=6, fig.height=5, fig.align = 'center')
```

Load the libraries

```{r}
library(edgeR)
library(limma)
library(Glimma)
library(org.Mm.eg.db)
library(gplots)
library(RColorBrewer)
library(NMF)
library(tidyverse)
```

Load the data

```{r, message=FALSE  }
 inputFile <- '~/Downloaded_Converted_Data.csv'  # Expression matrix
 sampleInfoFile <- NULL
 geneInfoFile <- 'Mouse__mmusculus_gene_ensembl_GeneInfo.csv' #Gene symbols, location etc.
 geneSetFile <- 'Mouse__mmusculus_gene_ensembl.db'  # pathway database in SQL; can be GMT format
 STRING10_speciesFile <- 'https://raw.githubusercontent.com/iDEP-SDSU/idep/master/shinyapps/idep/STRING10_species.csv'
```

Parameters for reading data

```{r, message=FALSE  }
 input_missingValue <- 'geneMedian'      #Missing values imputation method
 input_dataFileFormat <- 1 #1- read counts, 2 FKPM/RPKM or DNA microarray
 input_minCounts <- 0.5     #Min counts
 input_NminSamples <- 1   #Minimum number of samples
 input_countsLogStart <- 4 #Pseudo count for log CPM
 input_CountsTransform <- 1        #Methods for data transformation of counts. 1-EdgeR's logCPM 2-VST, 3-rlog
```

```{r, message=FALSE  }
 readData.out <- readData(inputFile)
 library(knitr)   #  install if needed. for showing tables with kable
 kable( head(readData.out$data) )    # show the first few rows of data
```

```{r, message=FALSE  }
```

```
 readSampleInfo.out <- NULL
```

```{r, message=FALSE  }
 input_selectOrg ="NEW"
 input_selectGO <- 'GOBP'#Gene set category
 input_noIDConversion = TRUE
 allGeneInfo.out <- geneInfo(geneInfoFile)
 converted.out = NULL
 convertedData.out <- convertedData()
 nGenesFilter()
 convertedCounts.out <- convertedCounts()  # converted counts, just for compatibility
```

Pre-process
```{r, message=FALSE  }
# Read counts per library
 parDefault = par()
 par(mar=c(12,4,2,2))
 # barplot of total read counts
 x <- readData.out$rawCounts
 groups = as.factor( detectGroups(colnames(x ) ) )
 if(nlevels(groups)<=1 | nlevels(groups) >20 )
  col1 = 'green'  else
  col1 = rainbow(nlevels(groups))[ groups ]

 barplot( colSums(x)/1e6,
                  col=col1,las=3, main="Total read counts (millions)")
 readCountsBias()  # detecting bias in sequencing depth
```
```{r, message=FALSE  }
```

```
 # Box plot
 x = readData.out$data
 boxplot(x, las = 2, col=col1,
    ylab='Transformed expression levels',
    main='Distribution of transformed data')
```

```{r, message=FALSE  }

 #Density plot
 par(parDefault)
 densityPlot()
```

```{r, message=FALSE  }

 # Scatter plot of the first two samples
 plot(x[,1:2],xlab=colnames(x)[1],ylab=colnames(x)[2],
    main='Scatter plot of first two samples')
```

```{r, message=FALSE  }

 ####plot gene or gene family
 input_selectOrg ="BestMatch"
 input_geneSearch <- 'SNCA;Robo3;GAPDH'    #Gene ID for searching
 genePlot()
```

```{r, message=FALSE  }
 input_useSD <- 'FALSE'    #Use standard deviation instead of standard error in error bar?
 geneBarPlotError()
```

```

## PCA and beyond

```{r, message=FALSE  }
 input_selectFactors <- 'Sample_Name'
 input_selectFactors2 <- 'Sample_Name'
 input_tsneSeed2 <- 0        #Random seed for t-SNE
 #PCA, MDS and t-SNE plots
 PCAplot()
```

```{r, message=FALSE  }
 MDSplot()
```

```{r, message=FALSE  }
 tSNEplot()
```

```{r, message=FALSE  }

 #Read gene sets for pathway analysis using PGSEA on principal components
 input_selectGO6 <- 'GOBP'
 GeneSets.out <-readGeneSets( geneSetFile,
    convertedData.out, input_selectGO6,input_selectOrg,
    c(input_minSetSize, input_maxSetSize)  )
 PCApathway() # Run PGSEA analysis
```

```{r, message=FALSE  }
 cat( PCA2factor() )   #The correlation between PCs with factors
```

DEG1
```

```{r, message=FALSE  }
 input_CountsDEGMethod <- 3     #DESeq2= 3,limma-voom=2,limma-trend=1
 input_limmaPval <- 0.1      #FDR cutoff
 input_limmaFC <- 2          #Fold-change cutoff
 input_selectModelComprions <- NULL   #Selected comparisons
 input_selectFactorsModel <- NULL        #Selected comparisons
 input_selectInteractions <- NULL          #Selected comparisons
 input_selectBlockFactorsModel <- NULL          #Selected comparisons
 factorReferenceLevels.out <- NULL

 limma.out <- limma()
 DEG.data.out <- DEG.data()
 limma.out$comparisons
```
```{r, message=FALSE  }
 input_selectComparisonsVenn = limma.out$comparisons[1:3] # use first three
comparisons
 input_UpDownRegulated <- FALSE       #Split up and down regulated genes
 vennPlot() # Venn diagram
```
```{r, message=FALSE  }
  sigGeneStats() # number of DEGs as figure
```
```{r, message=FALSE  }
  sigGeneStatsTable() # number of DEGs as table
```

Schriftliche Erklärung

Ich erkläre ehrenwörtlich, dass ich die dem Fachbereich Medizin der Johann Wolfgang Goethe-Universität Frankfurt am Main zur Prüfung eingereichte Thesis mit dem Titel

The Role of Soluble Epoxide Hydrolase in Macrophage and Astrocyte Polarization

am Zentrum der Molekularen Medizin, am Institut für Vaskuläre Signaltransduktion (Vascular Signalling) unter Betreuung und Anleitung von Prof. Dr. Ingrid Fleming mit Unterstützung durch Prof. Dr. Jiong Hu ohne sonstige Hilfe selbst durchgeführt und bei der Abfassung der Arbeit keine anderen als die in der Thesis angeführten Hilfsmittel benutzt habe. Darüber hinaus versichere ich, nicht die Hilfe einer kommerziellen Promotionsvermittlung in Anspruch genommen zu haben.

Ich habe bisher an keiner in- oder ausländischen Universität ein Gesuch um Zulassung zur Promotion oder zu einem PhD-Verfahren eingereicht*. Die vorliegende Arbeit wurde bisher nicht als Thesis oder Dissertation eingereicht.

Die Grundsätze der Johann Wolfgang Goethe-Universität Frankfurt am Main zur Sicherung guter wissenschaftlicher Praxis in ihrer gültigen Form liegen mir vor und wurden bei der wissenschaftlichen Arbeit eingehalten.

Vorliegende Ergebnisse der Arbeit wurden (oder werden) in folgendem Publikationsorgan veröffentlicht:

- [Auflistung aller Autoren der Reihenfolge nach, Titel, Zeitschrift, Band, Seite, Veröffentlichungsjahr]

Frankfurt (Main) _____ _____

(Ort, Datum) (Unterschrift)

*) im Falle des Nichtzutreffens streichen